

UNIVERSITY OF BOLOGNA

---

ADVANCED RESEARCH CENTER ON ELECTRONIC SYSTEMS FOR  
INFORMATION AND COMMUNICATION TECHNOLOGIES

XXVI Ph.D. Course in Information Technologies

ING-INF/03, 09/F2

**Interference Management and Energy Efficiency  
in Satellite Communications**

by

**Francesco Lombardo**

Coordinator:

Prof. **Claudio Fiegna**

Advisors:

Prof. **Alessandro Vanelli-Coralli**

Prof. **Giovanni E. Corazza**

---

March 2014



*To Beatrice  
and to my family*



# Contents

<b>Introduction</b>	<b>1</b>
<b>I Part I: Interference Management in SatCom Systems</b>	<b>9</b>
<b>1 Interference Management in SatCom Systems: Return Link</b>	<b>13</b>
1.1 Scenarios and Parameters . . . . .	14
1.2 System model . . . . .	16
1.3 Return Link Interference Analysis . . . . .	19
1.4 System Capacity upper and lower bounds . . . . .	21
1.4.1 Simulation Results . . . . .	24
1.5 Interference cancellation strategies . . . . .	30
1.5.1 Interference Cancellation: Performance Analysis . . . . .	31
1.5.1.1 System Throughput . . . . .	31
1.5.1.2 System Availability . . . . .	40
1.5.1.3 Decoding and Cancellation Order Analysis . . . . .	43
1.6 Results Summary . . . . .	46
<b>2 Interference Management in SatCom Systems: Forward Link</b>	<b>49</b>
2.1 Forward Link Scenario and System Model . . . . .	50
2.2 Decodability Analysis: $E_s/(N_0 + I_0)$ vs. $E_s/N_0$ . . . . .	52
2.3 Performance evaluation . . . . .	57
2.3.1 Baseline Performance without Interference Cancellation . . . . .	57
2.3.2 Interference Cancellation at the Terminal . . . . .	60
2.3.2.1 Conventional Interference Cancellation . . . . .	60

2.3.2.2	Interference Cancellation Based on ModCod Unbalance	61
2.4	Results Summary	63
<b>3</b>	<b>Interference Management for the TT&amp;C component of a SatCom System: Receiver Design for a BFSK-FFH Control Channel</b>	<b>65</b>
3.1	System Model	66
3.2	Double-Threshold Demodulator	68
3.2.1	Clipped-Linear Combining	69
3.2.2	Double-Threshold approach	70
3.3	Performance Analysis	72
3.4	Results Summary	77
<b>II</b>	<b>Part II: Waveform Energy Efficiency for SatCom Systems</b>	<b>79</b>
<b>4</b>	<b>Mesh SatCom Networks</b>	<b>83</b>
4.1	Satellite Mesh Solutions	84
4.2	Trade-offs in Mesh SatCom Networks topologies	86
<b>5</b>	<b>Waveform trade-offs in Mesh SatCom Systems</b>	<b>87</b>
5.1	Reference Scenario	88
5.2	Waveform Solutions	89
5.2.1	Linear Modulation Waveforms	89
5.2.2	Continuous Phase Modulation Waveforms	91
5.3	Performance Analysis	93
5.4	Results Summary	96
<b>6</b>	<b>Energy Efficient CPM Waveform Design for SatCom Mesh Systems</b>	<b>99</b>
6.1	CPM Scheme Selection	100
6.2	Code Selection	105
6.3	Performance Analysis	106
6.4	Results Summary	109
<b>A</b>	<b>Satellite Communications: an Introduction</b>	<b>111</b>
A.1	Satellite Communications Systems Architecture	111
A.2	Beam Forming in Satellite Systems	113
A.3	Multi-Beam Satellite Scenario	115

<b>Contents</b>	<b>iii</b>
<hr/>	
<b>Conclusions</b>	<b>123</b>
<b>Personal Publications and Contributions</b>	<b>127</b>
<b>Bibliography</b>	<b>131</b>
<b>Acknowledgements</b>	<b>139</b>



# List of Figures

1.1	Traditional chessboard colour reuse scheme, $FR = 4$ . . . . .	16
1.2	Uniform colour reuse scheme, $FR = 4$ . . . . .	17
1.3	The FSS 245 beams antenna pattern. The triple point is 4.3 dB. . .	18
1.4	The FSS 61 beams Supernational antenna pattern. . . . .	19
1.5	The FSS 61 beams Supernational antenna pattern. . . . .	20
1.6	$C/I$ , $C/N$ and $C/(N + I)$ distributions for scenario 1.a at EIRP=45 dBW . . . . .	23
1.7	$C/I$ , $C/N$ and $C/(N + I)$ distributions for scenario 1.b at EIRP=45 dBW . . . . .	24
1.8	$C/I$ , $C/N$ and $C/(N + I)$ distributions for scenario 1.c at EIRP=45 dBW . . . . .	25
1.9	$C/I$ , $C/N$ and $C/(N + I)$ distributions for scenario 2.a at EIRP=45 dBW . . . . .	25
1.10	$C/I$ , $C/N$ and $C/(N + I)$ distributions for scenario 2.b at EIRP=45 dBW . . . . .	26
1.11	Upper bound on spectral efficiency in scenario 1.a, including zoom around EIRP=45dBW. . . . .	26
1.12	Upper bound on spectral efficiency in scenario 1.b, including zoom around EIRP=45dBW. . . . .	27
1.13	Upper bound on spectral efficiency in scenario 1.c, including zoom around EIRP=45dBW. . . . .	27
1.14	Upper bound on throughput in scenario 1.a, including zoom around EIRP=45dBW. . . . .	28

1.15	Upper bound on throughput in scenario 1.b, including zoom around EIRP=45dBW. . . . .	28
1.16	Upper bound on throughput in scenario 1.c, including zoom around EIRP=45dBW. . . . .	29
1.17	Upper bound on spectral efficiency and throughput in scenario 2.a . . . . .	29
1.18	Upper bound on spectral efficiency and throughput in scenario 2.b . . . . .	29
1.19	IC Techniques Performance Average System Throughput vs. EIRP [dBW] - Scenario 1.a AWGN and AWGN with Rain Fading . . . . .	32
1.20	IC Techniques Performance Average System Throughput vs. EIRP [dBW] - Scenario 1.b AWGN and AWGN with Rain Fading . . . . .	33
1.21	IC Techniques Performance Average System Throughput vs. EIRP [dBW] - Scenario 1.c AWGN and AWGN with Rain Fading . . . . .	33
1.22	IC Techniques Performance Average System Throughput vs. EIRP [dBW] - Scenario 2.a AWGN and AWGN with Rain Fading . . . . .	34
1.23	IC Techniques Performance Average System Throughput vs. EIRP [dBW] - Scenario 2.b AWGN and AWGN with Rain Fading . . . . .	34
1.24	IC Techniques Performance Average System Throughput vs. EIRP [dBW] - Scenario 1.a AWGN and AWGN with Non-Ideal Cancellation ( $\beta = 0.99$ ) . . . . .	35
1.25	IC Techniques Performance Average System Throughput vs. EIRP [dBW] - Scenario 1.b AWGN and AWGN with Non-Ideal Cancellation ( $\beta = 0.99$ ) . . . . .	35
1.26	IC Techniques Performance Average System Throughput vs. EIRP [dBW] - Scenario 1.c AWGN and AWGN with Non-Ideal Cancellation ( $\beta = 0.99$ ) . . . . .	36
1.27	IC Techniques Performance Average System Throughput vs. EIRP [dBW] - Scenario 2.a AWGN and AWGN with Non-Ideal Cancellation ( $\beta = 0.99$ ) . . . . .	36
1.28	IC Techniques Performance Average System Throughput vs. EIRP [dBW] - Scenario 2.b AWGN and AWGN with Non-Ideal Cancellation ( $\beta = 0.99$ ) . . . . .	37
1.29	IC Techniques Performance Average System Throughput vs. EIRP [dBW] - Scenario 1.a AWGN, Rain Fading, and Non-Ideal Cancellation ( $\beta = 0.99$ ) . . . . .	37

1.30	IC Techniques Performance Average System Throughput vs. EIRP [dBW] - Scenario 1.b AWGN, Rain Fading, and Non-Ideal Cancellation ( $\beta = 0.99$ ) . . . . .	38
1.31	IC Techniques Performance Average System Throughput vs. EIRP [dBW] - Scenario 1.c AWGN, Rain Fading, and Non-Ideal Cancellation ( $\beta = 0.99$ ) . . . . .	38
1.32	IC Techniques Performance Average System Throughput vs. EIRP [dBW] - Scenario 2.a AWGN, Rain Fading, and Non-Ideal Cancellation ( $\beta = 0.99$ ) . . . . .	39
1.33	IC Techniques Performance Average System Throughput vs. EIRP [dBW] - Scenario 2.b AWGN, Rain Fading, and Non-Ideal Cancellation ( $\beta = 0.99$ ) . . . . .	39
1.34	Availability for L1 and S10 Waveforms from the DVB-RCS2 standard - Scenario 2.a . . . . .	41
1.35	Availability for L1 and S10 Waveforms from the DVB-RCS2 standard - Scenario 2.b . . . . .	42
1.36	SINR PDF and CDF: fixed vs. maximum SINR based cancellation ordering at EIRP=45dBW - Scenario 1.a . . . . .	44
1.37	SINR PDF and CDF: fixed vs. maximum SINR based cancellation ordering at EIRP=45dBW - Scenario 1.b . . . . .	44
1.38	SINR PDF and CDF: fixed vs. maximum SINR based cancellation ordering at EIRP=45dBW - Scenario 1.c . . . . .	44
1.39	SINR PDF and CDF: fixed vs. maximum SINR based cancellation ordering at EIRP=45dBW - Scenario 2.a . . . . .	45
1.40	SINR PDF and CDF: fixed vs. maximum SINR based cancellation ordering at EIRP=45dBW - Scenario 2.b . . . . .	45
2.1	General Block Diagram for the considered Scenario . . . . .	51
2.2	$E_s/(N_0 + I_0)$ analysis for Case 1 . . . . .	54
2.3	$E_s/(N_0 + I_0)$ analysis for Case 2 . . . . .	55
2.4	Histograms plot for interferer, noise, and interferer plus noise . . . . .	55
2.5	Block diagram of the simulation chain for the considered scenario without IC . . . . .	57
2.6	BER performance Case 1 without IC/MUD: QPSK 1/2 MODCOD . . . . .	58
2.7	$E_s/(N_0 + I_0)$ analysis for Case 1 for extended set of MODCODs . . . . .	59
2.8	BER performance for Case 1 without IC/MUD . . . . .	60

2.9	BER performance for Case 1 using different MODCOD for Reference Signal and Interferers . . . . .	62
3.1	Clipper Demodulator . . . . .	69
3.2	Double-Threshold Demodulator . . . . .	71
3.3	BER performance with 5 interference tones, 5 hops per symbol, 20 frequency bins, and J/S = 20 dB . . . . .	73
3.4	BER performance with 5 interference tones, 5 hops per symbol, 20 frequency bins, and J/S = 3 dB . . . . .	74
3.5	Clipper Demodulator Behaviour: Full Range Analysis . . . . .	75
3.6	Double Threshold Demodulator Behaviour: Full Range Analysis . . . . .	76
4.1	Mesh System Scenario . . . . .	84
5.1	Total Degradation analysis for LM waveform 8: 8PSK 2/3 . . . . .	91
5.2	Block Diagram of the LM receiver . . . . .	91
5.3	Block Diagram of the CPM receiver . . . . .	92
5.4	PER comparison: LM vs. CPM, RCS2 waveform ID = 3, considering phase noise (PN), frequency errors (FE), and ACI . . . . .	93
5.5	PER comparison: LM vs. CPM, RCS2 waveform ID = 8, considering phase noise (PN), frequency errors (FE), and ACI . . . . .	94
5.6	CPM waveforms comparison . . . . .	95
5.7	Spectral Efficiency: CPM vs. LM comparison . . . . .	96
6.1	Maximum achievable spectral efficiency as a function of $E_b/N_0$ for different CPM formats. . . . .	101
6.2	EXIT Chart for the two selected CC-CPM schemes with code rate 1/4. . . . .	103
6.3	Performance comparison between CPM waveforms at $\eta = 0.5$ b/s/Hz and $\eta = 0.25$ b/s/Hz in AWGN Channel and AWGN+ACI (PER vs. $E_b/N_0$ ), Short Traffic Burst (k=400 bits). . . . .	104
6.4	Performance comparison between CPM waveforms at $\eta = 0.5$ b/s/Hz with and without Burst Repetition and $\eta = 0.25$ b/s/Hz with different convolutional codes (PER vs. $E_b/N_0$ ). . . . .	107
6.5	Performance comparison between CPM waveforms at $\eta = 0.5$ b/s/Hz with and without Burst Repetition and $\eta = 0.25$ b/s/Hz with different convolutional codes (PER vs. $C/N$ ). . . . .	108

---

6.6	Performance comparison between CPM waveforms at $\eta = 0.5$ b/s/Hz with and without Burst Repetition and $\eta = 0.25$ b/s/Hz in presence of impairments (PER vs. $C/N$ ). . . . .	109
A.1	Reference Satellite Communications System Architecture . . . . .	112
A.2	Radiation Pattern of a single satellite antenna feed . . . . .	116
A.3	Radiation Pattern of all the 155 antenna feeds (No Beam Forming) . . . . .	116
A.4	Radiation Pattern of a single Beam . . . . .	117
A.5	Radiation Pattern of al the 100 beams . . . . .	118
A.6	Distribution of the C/I over the coverage region without beam forming	118
A.7	Distribution of the C/I over the coverage region with beam forming	119



# List of Tables

1.1	User link system parameters for the Return Link . . . . .	21
1.2	Return Link Single Beam Link Budget in Clear Sky Conditions . . .	22
1.3	Supernational System (61 beams): results summary - Scenario 2.a (with DVB-RCS2 ModCods) . . . . .	47
1.4	Supernational System (61 beams): results summary - Scenario 2.b (with DVB-RCS2 ModCods) . . . . .	48
3.1	Description of the Logic Unit of the Double-Threshold Demodulator	72
3.2	Simulation scenario . . . . .	72
5.1	Linear Modulation Waveform Parameters . . . . .	89
5.2	CPM Modulation Waveform Parameters . . . . .	92
6.1	Selected CPM modulation formats . . . . .	102



# List of Acronyms

<b>3GPP</b>	3rd Generation Partnership Project
<b>4G</b>	4th Generation
<b>AWGN</b>	Additive White Gaussian Noise
<b>BER</b>	Bit Error Rate
<b>BFSK</b>	Binary Frequency Shift Keying
<b>BS</b>	Base Station
<b>CC</b>	Convolutional Code
<b>CDF</b>	Cumulative Distribution Function
<b>CDMA</b>	Code Division Multiple Access
<b>CP</b>	Centralized Processing
<b>CPM</b>	Continuous Phase Modulation
<b>CW</b>	Continuous Wave
<b>DVB</b>	Digital Video Broadcasting
<b>EIRP</b>	Effective Isotropic Radiated Power
<b>ESA</b>	European Space Agency
<b>FDMA</b>	Frequency Division Multiple Access
<b>FFH</b>	Fast Frequency Hopping

<b>FSS</b>	Fixed Satellite Services
<b>GEO</b>	Geostationary Earth Orbit
<b>HPA</b>	High Power Amplifier
<b>IBO</b>	Input Back Off
<b>IC</b>	Interference Cancellation
<b>IM</b>	Interference Management
<b>LEO</b>	Low Earth Orbit
<b>LM</b>	Linear Modulation
<b>LTE</b>	Long Term Evolution
<b>M2M</b>	Machine to Machine
<b>MAP</b>	Maximum a Posteriori
<b>MEO</b>	Medium Earth Orbit
<b>MF</b>	Matched Filter
<b>MF-TDMA</b>	Multiple Frequency Time Division Multiple Access
<b>MIMO</b>	Multiple Input Multiple Output
<b>ML</b>	Maximum Likelihood
<b>MMSE</b>	Minimum Mean Squared Error
<b>MUD</b>	Multi User Detection
<b>OBO</b>	Output Back Off
<b>OFDM</b>	Orthogonal Frequency Division Multiplexing
<b>pdf</b>	Probability Density Function
<b>PHY</b>	Physical Layer
<b>QPSK</b>	Quadrature Phase Shift Keying
<b>SC-FDMA</b>	Single Carrier Frequency Division Multiple Access

<b>SIC</b>	Successive Interference Cancellation
<b>SINR</b>	Signal-to-Interference plus Noise-Ratio
<b>SNR</b>	Signal-to-Noise-Ratio
<b>SUD</b>	Single User Detection
<b>TDMA</b>	Time Division Multiple Access
<b>TWTA</b>	Travelling Wave Tube Amplifier
<b>UMTS</b>	Universal Mobile Telecommunications System







# Introduction

This thesis is the outcome of the work performed within my Ph.D. course in Telecommunications Engineering. The main research efforts were on Interference Management and Link-Level Power Efficiency for Satellite Networks.

In the context of increasing demands in terms of wireless services performance, as well as support for mobility, Satellite communications are pivotal to deploy ubiquitous broadband access and will play a key role in future broadband communication networks. To satisfy the ever growing bit rate request, a significant research effort is being placed in the design of new techniques and system architectures able to improve the overall system efficiency, both by increasing spectrum exploitation and by reducing the design and operational system costs.

Traditionally, and for several decades, research efforts have been posed into the development of technologies aimed at improving link-level performance, either in terms of transfer rate, for instance with higher order constellations, or to achieve better robustness over a noisy channel, such as with advanced encoding techniques, or for dealing with the access to the radio environment, such as with Orthogonal Frequency Division Multiplexing (OFDM), Code Division Multiple Access (CDMA), Time Division Multiple Access (TDMA) and their subsequent and hybrid developments (such as Multi Frequency TDMA, or Single Carrier Frequency Division Multiple Access, SC-FDMA). This process has led to an exponential growth in link level performance, which has approached very closely the theoretical bounds imposed by Shannon's Capacity Theorem ([15]), suggesting that new research interests should be posed in optimization and fine tuning of existing techniques on one hand, and on the design of new smart system architectures and algorithms capable of better exploiting the existing available resources.

The asymptotical trend of pure link level advancements motivates a change of

perspective, according to which the design and research efforts start from the beginning by looking at the overall system of interest, instead of focussing on the pure link level, or other aspects, separately. This approach aims at improving the performance of the system by increasing the efficiency in the use of the available resources, hereby intended in a general sense, therefore including Spectrum bands, Spatial domain and Power, pursuing the goal of increased system throughput and capacity.

The work carried out in this thesis follows the described approach at different levels, considering countermeasures to the mentioned challenges in terms of: *i*) interference, which has rapidly become the limiting nuisance in many wireless networks, due to the growing need of reusing the available resources, thus generating more interference, *ii*) power efficiency, which is critical for multiple applications, ranging from mobile applications, in which power consumption is strictly related to battery life, to satellite communications, in which power availability on the payload is one of the key aspects to be taken into account when designing a system, also considering inefficiencies related to high power amplifiers (HPA) non linearity.

The first part of this thesis relates to the possibility of managing the presence of interference (i.e., interfering users allowed to use the same resources as the desired users for a certain transmission), not only by avoiding it, but also, in turn for increased computational capacity, treating interferers as part of the desired signal set, and therefore decoding them and leveraging on such knowledge to increase the capacity of the overall system. To this extent, the analysis covers different levels, following a top-down approach across different scenarios, starting by system level considerations on interference management (IM) strategies, then focussing on link-level aspects in scenarios in which those will be shown to be critical for the feasibility of the proposed approaches, and at last with reference to a specific scenario case-study, where an interference mitigation solution is designed at intra-receiver level.

The second part is related to efficiency in the power domain, since power is one of the limited resources available, and power efficiency can be included, as it will be shown, in a generalization of the traditional Shannon plane Spectral Efficiency. In this part of the thesis, the attention is posed on power efficiency, for instance in terms of required Input Back-off (IBO) at the high power amplifiers, which is critical for classical Linearly Modulated (LM) waveforms, suffering from highly varying envelopes. This motivates the analysis and the fair comparison between such waveforms and constant envelope modulation waveforms, carried out in this part of the

thesis. It is shown that, for scenarios particularly exposed to terminals characteristics (e.g., terminal amplifiers) such as the Return Link of satellite systems, or Mesh non-infrastructure networks, constant envelope modulation represents a better performing solution.

## Thesis Outline

In this thesis, the two above mentioned main areas of study, focussed on improving spectrum and power resources usage are investigated. In particular, the thesis outline is as follows:

- in Part I, Interference Management is applied to Multi-Beam satellite systems. First, in Chapter A an introduction on Beam Forming for satellite systems is given, presenting the Multi-Beam reference architecture. Chapter 1 reports the analysis of the interference environment in a real-life Multi-Beam satellite system, and the design of Interference Management strategies, based on Successive Interference Cancellation, to improve the system capacity. The approach followed in this part of the study is inspired by terrestrial cellular systems, by suggesting a similarity between terrestrial Cells and Base Stations with Clusters of Beams and Gateways of a satellite system, even though with significant differences in terms of scenarios, propagation channel and topology. A cooperation strategy between multiple gateways is proposed to parallelize the effect of interference cancellation. Chapter 2 extends the analysis to the Forward Link of a satellite system, therefore implying that the interference cancellation shall be done at the receiver terminal. It is shown that the peculiarities of this scenario are significantly different with respect to the Return Link, which might prevent successive interference cancellation completely. An alternative modified approach to interference cancellation is thus presented, based on the unbalancing of signals related to different beams (e.g. for instance in terms of Modulation and Coding format employed) to overcome the challenges of the Forward Link. Part I is concluded by Chapter 3 in which the considered scenario is a more specific one, pertaining to the Telemetry, Tracking and Control channel of a satellite system, exposed to intentional jamming. A robust receiver design is proposed to cope with intentional tone jamming in the considered Binary Frequency Shift Keying Fast Frequency Hopping (BFSK-FFH) scenario, outperforming existing architectures.

- in Part II, the focus is on the concept of generalized efficiency, which stems from the classical spectral efficiency Shannon's plane by taking into account also efficiency in the power domain. In fact, power is one of the limited resource in a satellite link, especially considering the non-linearities of high power amplifiers, that usually result in low efficiency in driving the amplifier operating point, thus wasting available power. Chapter 4 presents the reference scenario for this study, which is the case of Mesh Topology Satellite Networks, that is the case of a single-hop communications between peers, thus without leveraging on a Gateway or other ground stations, so that terminals can communicate directly and with reduced latency. Power efficiency is critical in such scenario, since both ends of the transmission are terminals, typically equipped with small, low-gain antennas, and with cheaper amplifiers with respect to what can be implemented at the gateway. The first part of the analysis, in Chapter 5, aims at assessing the performance of classical Linearly Modulated waveforms against waveforms based on continuous envelope modulations, considering waveforms from existing standards, and real-life practical conditions in terms of channel impairments and receiver non-idealities. Building on this analysis Chapter 6 reports the design of new waveforms for power-limited scenarios, in which there is the need, at the cost of lower spectral efficiency, to extend towards lower values the range of operating Signal-to-Noise Ratio (SNR). This activity is carried out while maintaining compatibility with the techniques adopted in the reference standard (DVB-RCS2) by selecting the most appropriate Continuous Phase Modulation (CPM) and Convolutional Coding (CC) parameters to face the described scenario.
- an overview on Satellite Communications Systems, definitions, architecture elements and beam-forming, are presented in Appendix A.

## **Original Contributions in this Ph.D. program**

The mentioned demand for higher system throughput and the limitation in spectrum and resources availability, resulting in the need for energy efficiency requirements and in reuse of spectrum portions, motivates the study carried out in this thesis: on one hand interference limited Satellite Communications Systems need to be considered, whereas typically SatComs have been considered only limited by noise; on the other hand power limitations, particularly in return link scenarios or in Mesh Peer-to-peer

connections, are an issue to be tackled by means of energy efficient link designs. The activities performed during the three years of this doctorate study led me to obtain original scientific contributions in several fields. With reference to the subjects of Part I, the main contributions are the following:

- detailed system-level analysis of the interference environment in a real-life multi-beam satellite system, according to parameters and antenna descriptions provided by the European Space Agency [1].
- characterization of lower and upper bounds for the overall capacity of the Return Link of a multi-beam satellite system in presence of interference [1,2].
- design of Successive Interference Cancellation strategies, inspired by terrestrial cellular communications, for multi-beam multi-gateway satellite communications systems: a first technique is proposed for cancelling the interference generated by co-channel transmissions from terminals in beams within the cluster served by the same gateway (Successive Intra-Gateway Interference Cancellation); a second architecture maintains the features of the first one but also considers a cooperation structure between multiple Gateways on ground (Successive Intra- and Inter-Gateway Interference Cancellation), which allows exchange of decoded data and thus parallelization of interference cancellation by removing also interference generated by users in beams served by other gateways, improving the capacity, which is brought closer to the upper bound at lower complexity than the optimal case. These strategies represent a design tool allowing a trade-off between computational complexity and achieved performance, based on the requirements of the system and considered scenarios. [2–4].
- analysis and physical layer performance assessment for the applicability of Successive Interference Cancellation (as presented in Chapter 1 to the Forward Link of a multi-beam satellite system, at the terminal side, as reported in [5].
- proposition of a modified novel Successive Interference Cancellation algorithm for the Forward Link of a multi-beam satellite system, based on power or Modulation and Coding format unbalance between beams, [5].
- design of a new receiver for the specific scenario of a Fast Frequency Hopping - Frequency Shift Keying system, which is being proposed as a solution for

the digitisation of the Telemetry, Tracking and Control subsystem of a satellite. The idea is based on the use of two thresholds in the demodulator, to which the received signal is compared and the output of this comparison is handled by a logic unit that takes the demodulation hard decision, improving the performance of existing receivers in presence of intentional interfering tone jamming [6].

It is worthwhile highlighting that the activities related to Part I of this thesis were performed in the context of, and represented valued contributions to, the following European Space Agency studies:

- ESA Network of Experts “Satellite Communications Network of Experts (SatNEX-III)”
- ESA Study “Next Generation Waveforms for Satellite Systems”
- ESA Study “Spread Spectrum System for TT&C and payload control links”

Regarding the study of waveform efficiency in mesh satellite networks, reported in Part II the most important contributions are:

- analysis of suitability of waveforms based on Linear and Continuous Phase Modulation formats in mesh satellite networks architectures, in reference to real-life scenarios and existing standards, and with the objective of jointly maximising spectral and power efficiency, performance evaluation and comparison, for candidate techniques selection in the considered scenario. The outcome of this activity proved that for applications with moderate required transfer rates, CPM waveforms, in real-life conditions, outperform linear waveform thanks to their constant envelope and resilience to impairments, in particular non-linearities. ([7, 8]).
- design of new proposed waveforms for the DVB-RCS2 standard, based on Continuous Phase Modulation and specifically designed to cope with applications such as terminal-to-terminal (e.g., Mesh non-infrastructured networks) in which the main requirements are imposed in terms of Power availability. In such power limited cases, lower spectral efficiency is accepted in the design, leading to choices aimed at maximising the performance at the identified spectral efficiency while using the minimum power ([9]).

Activities reported in Part II of this thesis were performed in collaboration with

- Mavigex Srl (Bologna, Italy)
- The ESA/ESTEC study “Cost Effective Satellite Terminals for MESH Overlay Networking”

Further contributions related to Part I refer to Beam Forming techniques for satellite systems, as in [10–14]



Part I

Part I: Interference  
Management in SatCom  
Systems



Space division multiple access is usually adopted by organizing the satellite coverage in separate beams, each serving a specific geographical area. Depending on the target service, the geographical area dimensions can range from large, thus requiring a small number of beams, to small, thus requiring a large number of beams up to few hundreds. Notably, Multi-Beam coverage resembles the terrestrial cellular coverage approach. However, differently from terrestrial systems that rely on multiple base stations each one with its own antenna, satellite systems are based on the use of a single antenna at the satellite with multiple feeds. In turn, this poses a significant burden on the design of the satellite antenna that must ensure enough electromagnetic separation between beams in order to realize the target Multi-Beam coverage. In this framework, single-feed per beam and multi-feed per beam architectures, possibly paired with beam forming techniques, are currently studied and adopted.

In Multi-Beam satellite networks, beams are organized in clusters, each cluster controlled by a different ground station (gateway) in order to allow for the adoption of spatial division multiplexing in the feeder link, i.e., from the satellite to the gateway. As a matter of fact, in high throughput Multi-Beam satellite communications systems, the feeder link may become the system bottleneck, since it represents the mean to carry the entire aggregated user generated traffic from the satellite towards the on ground core network. For this reason the total traffic at the satellite is split on different feeder links each one feeding a different and geographically separated gateway. For broadband satellite systems with hundreds of beams the number of gateways goes up to several tens. Multi-beam coverage is then usually combined with color reuse schemes, where a color is identified as a carrier frequency-polarization pair. Color reuse aims at reducing the interference among adjacent beams (inter-beam interference) in order to improve the user signal-to-interference-plus-noise-ratio (SINR) at the expense of a reduced total achievable throughput, as it happens with frequency reuse in terrestrial cellular systems. As a matter of fact, a trade-off can be sought between colour reuse and system throughput, as a function of the inter-beam interference that can be accepted by the system.

Conventional satellite systems try to avoid interference based on the orthogonalization principle meaning that each user is allocated a separate channel in time, frequency or code domain to mitigate such interference, or more recently in Multi-Beam systems by exploiting the spatial dimension as well, separating users spatially by means of sharp beams shape. In these cases then, Interference is therefore

avoided, rather than handled. This could therefore be categorized as Interference Avoidance (or Rejection), achieved for instance by means of orthogonal separation methods or by using Spreading techniques such as CDMA and Frequency Hopping [16–18]. Other approaches aimed at mitigating interference in satellite systems are based on precoding [19, 20]. However, it is known that in many cases interference can actually be actively exploited. Different ways of approaching Interference are in fact Interference Cancellation and Multi-User Detection (MUD) [21–24], in which the main idea is to exploit the presence of interfering signals, that can be decoded significantly improving the real operating Signal-to-Interference plus Noise (SINR). The main difference between these two approaches is that in interference cancellation, one signal is typically decoded at each time, and an iterative process is adopted to remove the interference from the original aggregate signal, progressively improving the SINR, whereas in Multi-User Detection all the detectable signals are decoded jointly, thus treating the aggregate signal as a single macro-signal, that can be decoded, at the expense of higher complexity.

An overview on Satellite Multi-Beam Systems is given in Appendix A, in which the concept of Beam Forming in satellite systems is presented. This also represents the reference Multi-Beam architecture, that will be the reference for the remainder of this Part.

This part is divided in two main distinguished study cases: Chapter 1 reports the analysis of Interference Cancellation Strategies, inspired by terrestrial cellular counterparts, in the Return Link of a Multi-Beam Satellite System, in which signals are transmitted by terminals on ground, via the Satellite and to a Gateway (Earth Station); Chapter 2 deals with the impact and challenges for Interference Cancellation strategies on the Forward link of a Multi-Beam Satellite System, in which signals are transmitted by the Gateway via the Satellite and to the terminal. It will be shown that these two scenarios present significant differences that impose specific considerations on the design and applicability of Interference Management algorithms.

Part I is then concluded by Chapter 3 in which is considered the specific scenario of a Fast Frequency Hopped - Binary Frequency Shift Keying system (FFH-BFSK), which is being considered as a solution for the next generation Tracking, Telemetry and Control channel of a Satellite System, reports the design of a novel receiver for such scenario that outperforms existing receivers architectures in terms of resilience to intentional interference (tone jamming in the considered case).

# Chapter 1

## Interference Management in SatCom Systems: Return Link

Current satellite communication systems are subject to interference between different transmissions. The typical approach to face such nuisance is the design of orthogonal transmissions, in the frequency domain, in the time domain or in the code domain. The baseline solution for all other interference sources, coming from resource reuse strategies, is to treat them as additional noise, therefore degrading the performance of the system.

In the context of ever growing demands in transfer rates and overall system capacity, and with pure physical layer techniques approaching theoretical bounds on the single link level, the trend has recently been a progressive increase in the reuse of resources, which obviously generates more interference, and forces the systems to operate in interference limited conditions. Instead of suppressing the interference then, at the expense of increased complexity, where affordable, the idea is to acknowledge the presence of interference, put in the system in a controlled way from the design, and leveraging on its description. In a way it is like expanding the set of useful signals to be decoded. This chapter analysis tackles the case of next generation FSS (Fixed Satellite Service) providing an interactive broadband type of traffic. In particular, the Return Link of such system is considered, and the purpose is to evaluate and analyse first the fundamental theoretical bound in terms of capacity of the system in presence of interference, and subsequently, the use of interference mitigation strategies, also accounting for the Multiple Gateway (GW) dimension, which is motivated in Multi-Beam system with very large number of beams, by

feeder link limitations, that is, bandwidth limitations on the link between the Satellite and the Gateway in which typically signals from different beams are multiplexed in frequency, thus requiring large bandwidths.

The optimal way to exploit the presence of interference is the one in the paradigm of [22], in which Multi-User Detection is presented (see also [23, 25–28]). In this context all signals are jointly decoded, by devising a more complex receiver. The drawback of these approaches, that would prevent practical use in the scenario considered in this chapter, is the complexity, that would be unmanageable since the number of signals to be jointly decoded would be very high, as it will be shown later when the scenario parameters will be presented. An alternative approach is the so-called Iterative Interference Cancellation, [21] (see also [29, 30]), in which instead of being jointly detected, signals are iteratively decoded one by one, and then subtracted by the aggregated signal, therefore improving the SINR at each step. In case of Minimum Mean Squared Error (MMSE) filtering, [31] it has been shown that this approach has been proven to be capacity achieving, converging to the upper bound on the capacity of the system, which is given by the multiple-input multiple-output (MIMO) joint detection [32].

The objective of the study presented in this chapter, is to devise a system architecture in which capacity is improved by means of interference management techniques. The selected techniques refer to the Interference Cancellation paradigm, and are designed to also exploit cooperation between gateways on ground.

In the following, first the reference scenario and parameters will be presented, then the lower and upper bound for the system capacity will be characterized, and then Interference Management strategies for such system architecture are discussed.

## 1.1 Scenarios and Parameters

The baseline Multi-Beam scenario of interest for this analysis is reported hereafter: it is represented by the antenna beam pattern, provided by the European Space Agency (ESA), and refers to a 245 single feed per beam pattern at 30 GHz for the Return Link providing European coverage. The number of beams will be denoted by  $K$ . The beam pattern is such that the edge at 4.3 dB below the maximum of each beam pattern allow to cover Europe without holes ("tessellate"). Fig. 1.3 shows the co-polar footprints, but the antenna pattern also includes cross-polar components, considered in this analysis. The coverage area can be defined as the union of the  $K$

footprints of the beams.

Numerically, the beam pattern provides, for each point of the grid that constitutes the coverage area, the value of the co-polar and cross-polar component of the radiation pattern for all  $K$  beams. More in detail:

- $G_{cp}(k, u, v)$  is the co-polar (cp) transmit power gain between beam  $k$  ( $k = 1, \dots, K$ ) and user terminal with coordinates  $(u, v)$  over the coverage area.
- $G_{xp}(k, u, v)$  similarly to  $G_{cp}(k, u, v)$  but referring the cross-polar (xp) component of the antenna pattern

Two main study cases have been considered, one with full European coverage and one with a supernational area coverage, the latter being selected in order to have a comparison of the impact of the considered techniques and of real-life effects such as coverage edge regions in systems of different size, and five different scenarios are considered:

- Scenario 1.a: Full coverage, 4 colours (Frequency Reuse factor  $FR = 4$ ) and chessboard colour reuse scheme, i.e., each gateway controls a number (which varies from gateway to gateway since the overall number of beam is 245 and the coverage region is irregular) of adjacent beams that uses 4 different colours, see figure 1.1. The 4 colors are generated by considering 2 frequency bands and 2 orthogonal polarizations. Consequently, the bandwidth per beam is 250 MHz.
- Scenario 1.b: Full coverage, 250 MHz bandwidth and uniform colour reuse scheme, i.e., each gateway controls a subset of adjacent beams all of which use the same colour, see figure 1.2.
- Scenario 1.c: Full coverage, full frequency reuse and constant feeder link bandwidth, i.e., the total number of gateway is increased by a factor equal to the number of frequency colours, and consequently the number of controlled beams per gateway is reduced by the same factor, with respect to scenarios 1.a and 1.b in order to keep a constant feeder link bandwidth.
- Scenario 2.a: Supernational coverage (specifically over the France-Germany-Italy-Benelux-Switzerland area) Corresponding to scenario 1.a but with reduced coverage, depicted in Figure 1.4 (4 Colours and 250 MHz of bandwidth)

- Scenario 2.b: Supernational coverage, 500 MHz of bandwidth and full frequency reuse. This is represented in Figure 1.5 (Equivalent to scenario 1.b but with reduced coverage)

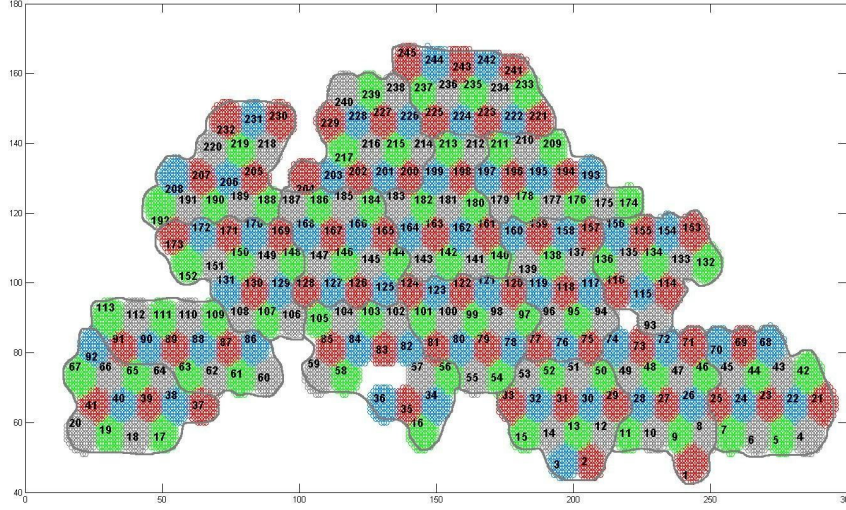


Figure 1.1: Traditional chessboard colour reuse scheme,  $FR = 4$ .

## 1.2 System model

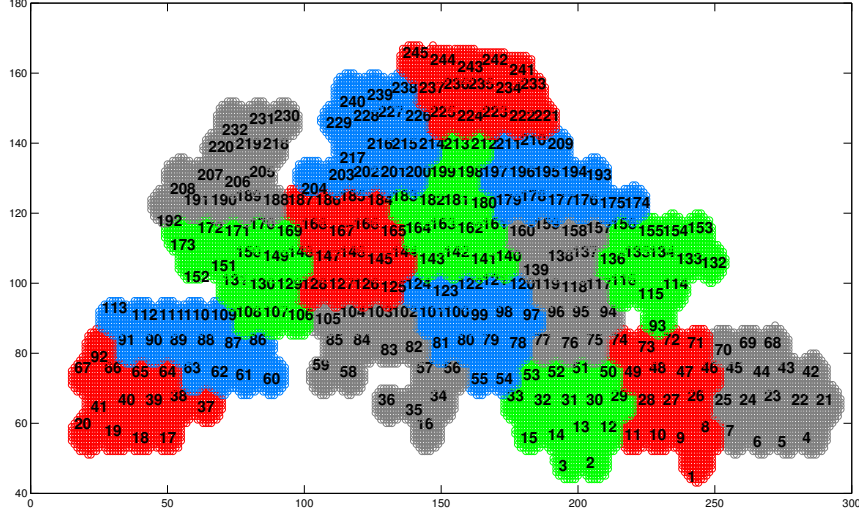
In this section the return link system model is described, considering one use of the same resources at the same time, which implies focussing on a single slot of the Multi-Frequency Time Division Multiple Access (MF-TDMA) grid of the transmitted signals. Considering a total of  $K$  beams in the system, the received signal at the satellite can be represented as

$$\mathbf{y} = \mathbf{H}\mathbf{x} + \mathbf{n} \quad (1.1)$$

where  $\mathbf{x}$  is the  $(K \times 1)$  transmitted signal vector, that includes a power allocation matrix, as

$$\mathbb{E}[\mathbf{x}\mathbf{x}^H] = \text{diag}(P_1, \dots, P_K) \quad (1.2)$$

where  $P_i$  is the the  $i$ -th user transmitted signal power. Also,  $\mathbf{n}$  is the  $(N_A \times 1)$  vector of additive white Gaussian noise (AWGN), and  $\mathbf{H}$  is the overall  $(N_A \times K)$  channel matrix.  $N_A$  is the number of satellite antenna feeds, with  $N_A \geq K$ .


 Figure 1.2: Uniform colour reuse scheme,  $FR = 4$ .

Element  $H_{jk}$  of such matrix represents the aggregate complex coefficient related to the link between the  $k$ -th user (i.e., the  $k$ -th beam) and the  $j$ -th satellite antenna feed, accounting for several effects. It can be factorized as

$$H_{jk} = \sqrt{G_k^T G_{jk}^R} / \sqrt{A_k^I} \quad (1.3)$$

in which  $G_k^T$  is the  $k$ -th user antenna gain,  $A_k^I$  is the isotropic attenuation between the  $k$ -th user and the satellite, and  $G_{jk}^R$  is the antenna gain for the the  $j$ -th satellite antenna feed in the direction of the  $k$ -th user's location.

This system model is based on two main simplifications: first, all received signals are detectable, i.e. have a strength higher than a receiver-specific threshold, which might not be the case, and secondly, all the receive feed signals are available to the ground station, which might be not true considering feeder link bandwidth limitations (it will be the assumption for the ideal case, representing the upper bound for overall system capacity). In order to extend the system model to further account for the mentioned aspects, following the approach in [33], the structure of matrix  $\mathbf{H}$  can be decomposed in more detail, distinguishing between different contributions, as follows. First, it can be written

$$\mathbf{H} = \mathbf{D} + \mathbf{P} \quad (1.4)$$

where matrix  $\mathbf{D}$  represents only detectable paths, defined as those whose detected power is above a physical threshold in the receiver's hardware, and matrix  $\mathbf{P}$  contains

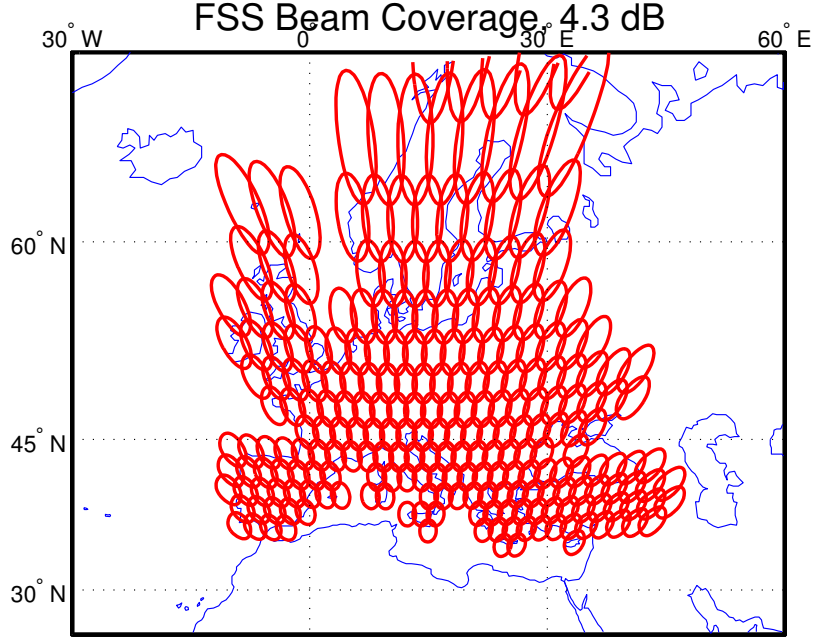


Figure 1.3: The FSS 245 beams antenna pattern. The triple point is 4.3 dB.

undetectable paths, which can be seen as a contribution to the noise floor. Hence

$$D_{jk} = \begin{cases} H_{jk} & \text{if } P_k |H_{jk}|^2 > \xi \\ 0 & \text{otherwise} \end{cases} \quad (1.5)$$

where  $\xi$  is the receiver's sensitivity. On top of this separation between detectable and undetectable paths, a further, more important extension to this model is made: matrix  $\mathbf{D}$  can be written in terms of the sum of two contributions, one related to beams served by the same GW serving, among others, the beam in which the random location of the desired user falls, and the second one accounting for all the remaining signals intended for beams served by different GWs. Focusing on a generic GW, it can then be written

$$\mathbf{D} = \mathbf{U} + \mathbf{V} \quad (1.6)$$

where an element  $U_{jk}$  of  $\mathbf{U}$  is non zero and equal to  $D_{jk}$  if and only if the  $k$ -th user is served by the GW receiving the  $j$ -th feed; on the other hand, an element  $V_{jk}$  of  $\mathbf{V}$  is non zero and equal to  $D_{jk}$  if and only if the  $k$ -th user is not served by the GW receiving the  $j$ -th feed.

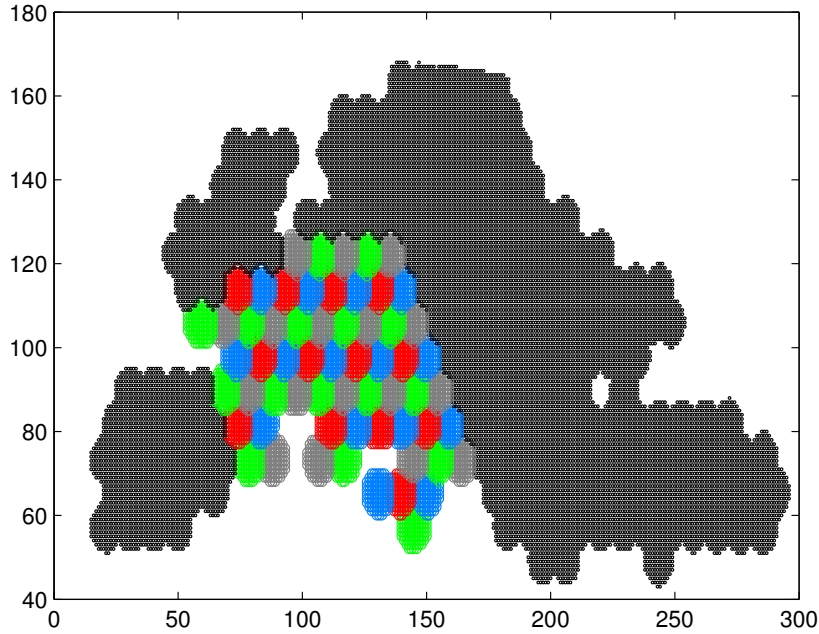


Figure 1.4: The FSS 61 beams Supernational antenna pattern.

In the next sections,  $\mathbf{d}_k$ ,  $\mathbf{u}_k$ ,  $\mathbf{v}_k$ , and  $\mathbf{p}_k$  will represent the  $k$ -th ( $N_B \times 1$ ) column vector of  $\mathbf{D}$ ,  $\mathbf{U}$ ,  $\mathbf{V}$ , and  $\mathbf{P}$ , respectively.

Table 1.1 summarizes the numerical parameters that have been used for all the computer simulations in this chapter to obtain the results being presented. In the following, only co-channel interference has been considered, being the focus of this study, since cross-polarization antenna interference is negligible with respect to the co-polar antenna pattern.

### 1.3 Return Link Interference Analysis

In this section the link budgets for the selected scenarios is reported first, and then the interference environment in such Return Link scenarios is analysed. Starting from  $C/I$ ,  $C/N$  and  $C/(N+I)$  expressions for a generic user in the system, the analysis is based on the link budget reported in Table 1.2, and the Probability Density Functions (PDFs) of  $C/I$ ,  $C/N$  and  $C/(N+I)$  are shown in figures 1.6, 1.7, 1.8, 1.9 and 1.10. These values refer to an EIRP of 45 dBW, which is representative of the typical operating range, and are calculated assuming that each gateway leverages

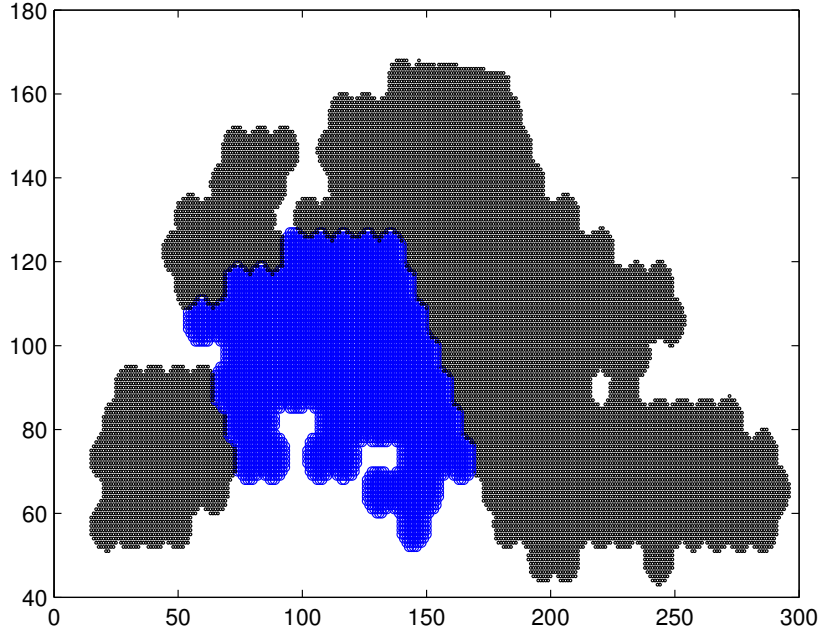


Figure 1.5: The FSS 61 beams Supernational antenna pattern.

on multi-antenna processing, which means that the gateway can leverage on the knowledge of the generic user's signal at all feeds (not only the corresponding useful one) to improve the signal to noise ratio for that user. These evaluations are considered a baseline, as there are no interference cancellation strategies involved, and the receiver is assumed to be based on matched filters, instead of optimal solutions, such as MMSE filtering. One user per beam has been considered, as it will be in the remainder of this chapter. Following the classical SINR derivation for a linear receiver as in [34], the expressions used for this evaluation are reported below, for the  $k$ -th user in the system (see also [33])

$$\left(\frac{C}{N}\right)_k = \frac{P_k \|\mathbf{u}_k\|^4}{\mathbf{u}_k^* (N_0 \mathbf{I}) \mathbf{u}_k} \quad (1.7)$$

$$\left(\frac{C}{I}\right)_k = \frac{P_k \|\mathbf{u}_k\|^4}{\mathbf{u}_k^* \left( \sum_{l=1, l \neq k}^{N_B} P_l \mathbf{u}_l \mathbf{u}_l^* + \sum_{l=1}^{N_B} P_l \mathbf{v}_l \mathbf{v}_l^* + \sum_{l=1}^{N_B} P_l \mathbf{p}_l \mathbf{p}_l^* \right) \mathbf{u}_k} \quad (1.8)$$

$$\left(\frac{C}{N+I}\right)_k = \frac{P_k \|\mathbf{u}_k\|^4}{\mathbf{u}_k^* \left( \sum_{l=1, l \neq k}^{N_B} P_l \mathbf{u}_l \mathbf{u}_l^* + \sum_{l=1}^{N_B} P_l \mathbf{v}_l \mathbf{v}_l^* + \sum_{l=1}^{N_B} P_l \mathbf{p}_l \mathbf{p}_l^* + N_0 \mathbf{I} \right) \mathbf{u}_k} \quad (1.9)$$

$$(1.10)$$

Table 1.1: User link system parameters for the Return Link

Parameter	Value
Satellite height	35786 km (geostationary)
Beam radiation pattern: $G_{cp}(l, U_k, U_k)$ , $G_{xp}(l, U_k, U_k)$ $(l, k = 1, \dots, K)$	Provided by ESA (Single feed per beam antenna)
Total number of beams	245
Number of users served at each time slot (in the frequency band of interest)	245 (one per beam)
UTs location distribution	Uniformly distributed within each beam footprint
Carrier frequency	30GHz (Ka band)
Total user link bandwidth $B_T$	500 MHz
User signal bandwidth $B_U$	5 MHz
Polarization in user link	dual
UT antenna gain $G_T^2$	46 dBi
Satellite noise temperature $T_n$	515.7 K
Feeder link bandwidth	4 GHz (2 GHz on each polarization)

It is supposed that the interference relevance is much higher in scenarios 1.b and 1.c, as in scenario 1.c there is no frequency reuse involved, while in 1.b, there is a reuse factor 4 but the beams to gateways allocation forces the interferers to be closer in space, which means that interfering beams have not vanished at the point of crossing the edge of other beams, thus their impact is more significant. It is interesting however to notice that, in the considered conditions, even scenario 1.a is limited by the interference, thus suggesting the use of IC strategies even in this case.

## 1.4 System Capacity upper and lower bounds

In this section the lower and upper bound for the system under analysis are discussed. As previously mentioned in Section 1.3, the benchmark case is based on simple Matched Filtering (MF) with no interference management processing on the signals available to a single GW.

Table 1.2: Return Link Single Beam Link Budget in Clear Sky Conditions

Parameter	Four Colours Case	Single Colour case
Transmit EIRP [dBW]	45	
Isotropic attenuation at 30 GHz [dB]	213.50	
Measured satellite antenna gain [dB]	57	
Received power [dBW]	-111.50	
Satellite noise temperature [K]	515.70	
Number of polarizations	1	2
System bandwidth [MHz]	250	500
User channel bandwidth [MHz]	5	
Number of users per beam	50	200
Noise power [dBW]	-134.49	
C/N [dB]	22.99	

The upper bound is based on the MMSE Successive Interference Cancellation (SIC) approach with centralized processing, i.e. assuming that a single equivalent GW performs all the processing. This means that it is considered that a central entity is able to process all the received signals from all beams, therefore neglecting feeder link bandwidth limitations, to represent the ideal case leading to optimal capacity. This processing has been shown to be capacity achieving, i.e. reaching the limit for a MIMO channel given by the Telatar formula [32].

For a generic user  $k$ , its spectral efficiency can be written as

$$\eta_k = \log_2 \left( 1 + \frac{1}{\Gamma} \text{SINR}_k \right) \quad (1.11)$$

where  $\Gamma$  is the back-off factor accounting for non-idealities of the forward error correction [35], in the following considered equal to 1 for simplicity.

Therefore, the average spectral efficiency among all users can be written as

$$\eta = \mathbb{E} [\log_2 (1 + \text{SINR}_k)] = \mathbb{E} [\eta_k] \quad (1.12)$$

from which the average throughput is easily obtained as

$$T = B_u \eta \quad (1.13)$$

where  $B_u$  is the user channel bandwidth.

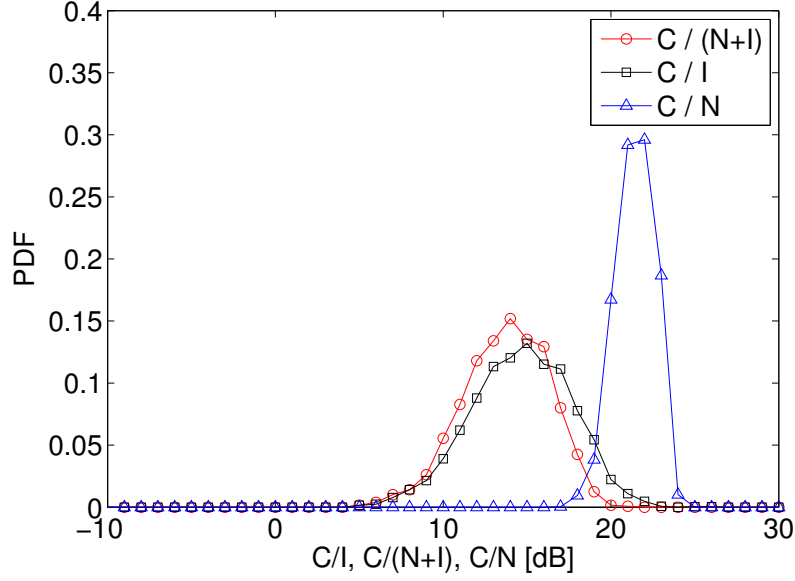


Figure 1.6:  $C/I$ ,  $C/N$  and  $C/(N + I)$  distributions for scenario 1.a at EIRP=45 dBW

MMSE-SIC is based on an iterative process composed of two stages, i.e. the MMSE filtering of the received (and buffered) signals, and then the detection of the strongest (i.e., having highest SINR) user signal and its subtraction from the received signal. Considering the  $k$ -th user, the SINR in case of Successive Interference Cancellation with Centralized Processing is

$$\text{SINR}_k = P_k \mathbf{d}_k^* (\mathbf{R}_k^C)^{-1} \mathbf{d}_k \quad (1.14)$$

where the matrix  $\mathbf{R}_k^C$  includes all nuisances contributions, i.e. users signals to be canceled, non-detectable signals, and noise, and can be written as

$$\mathbf{R}_k^C = \sum_{l=1, l \neq k}^{N_B} P_l \mathbf{d}_l \mathbf{d}_l^* - \beta \sum_{l=1}^{k-1} P_l \mathbf{d}_l \mathbf{d}_l^* + \sum_{l=1}^{N_B} P_l \mathbf{p}_l \mathbf{p}_l^* + N_0 \mathbf{I} \quad (1.15)$$

where  $N_0$  is the noise complex samples' variance,  $\beta$  is a term with value between 0 and 1 that accounts for non-ideal cancellation (when lower than 1) and  $\mathbf{I}$  is an identity matrix.

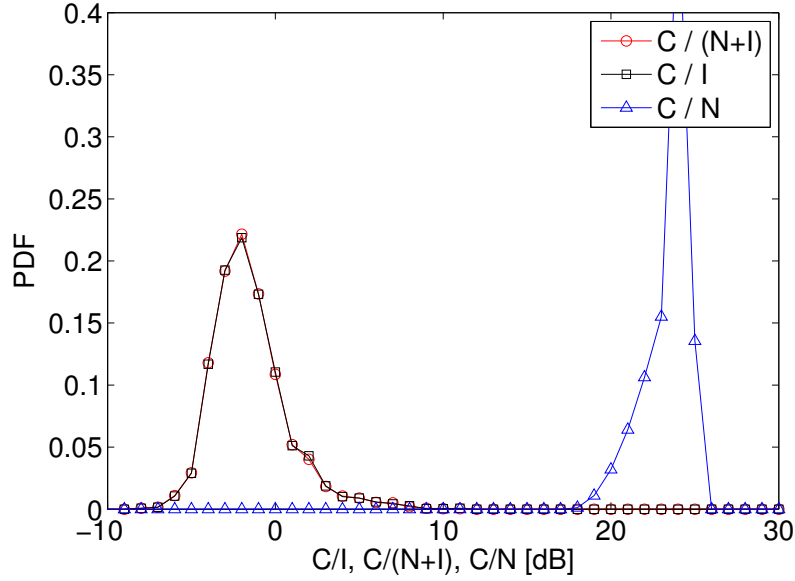


Figure 1.7:  $C/I$ ,  $C/N$  and  $C/(N + I)$  distributions for scenario 1.b at EIRP=45 dBW

#### 1.4.1 Simulation Results

Simulation results are reported for the benchmark configuration (MF processing on a single GW) and for the upper bound (Centralized Processing (CP) MMSE-SIC) in scenarios 1.a, 1.b and 1.c. More in detail, Figures 1.11 to 1.18 report the upper bounds on the per-user spectral efficiency and on system throughput. Clearly, the results for spectral efficiency and throughput confirm the fact that scenarios 1.b and 1.c are strongly interference limited. Surprisingly, also in scenario 1.a, even with much lower interference, the system is still essentially interference limited, as it can be appreciated in the PDF plots in the previous sections. For this reason, the expected impact of interference mitigation techniques is higher for scenarios 1.b and 1.c. In general, scenarios 2.a and 2.b are fairly aligned to scenarios 1.a and 1.c, respectively, on a subset of which they are indeed based, with a slight performance improvement in 2.a and 2.b. This is due to the fact that there are less interferers in the system, and therefore, each beam, when considered as the useful user's beam, is less affected by interference.

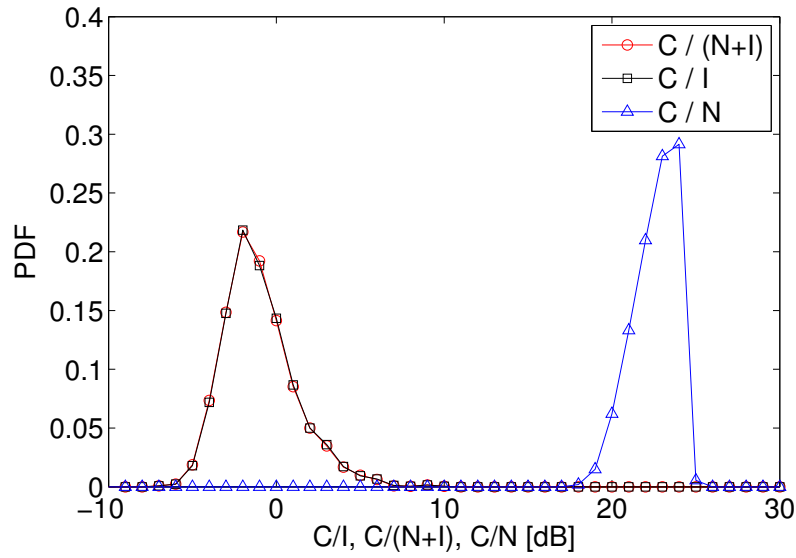


Figure 1.8:  $C/I$ ,  $C/N$  and  $C/(N + I)$  distributions for scenario 1.c at EIRP=45 dBW

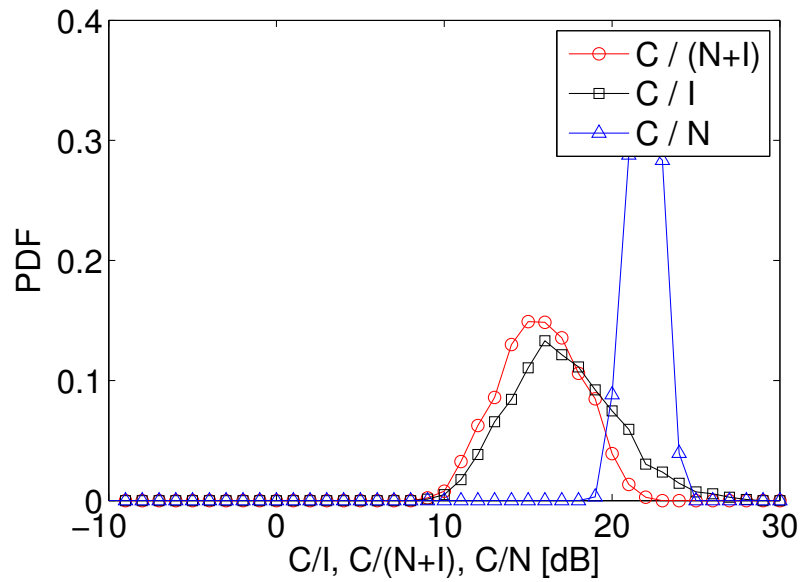


Figure 1.9:  $C/I$ ,  $C/N$  and  $C/(N + I)$  distributions for scenario 2.a at EIRP=45 dBW

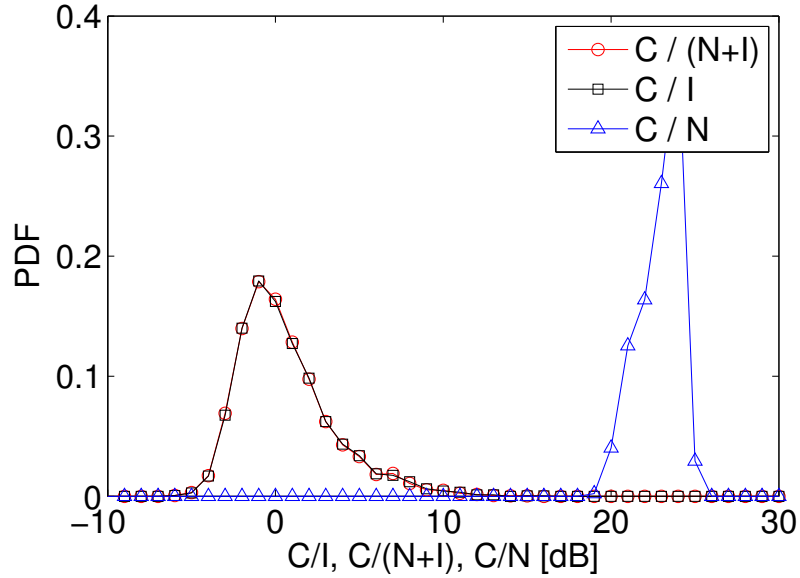


Figure 1.10:  $C/I$ ,  $C/N$  and  $C/(N + I)$  distributions for scenario 2.b at EIRP=45 dBW

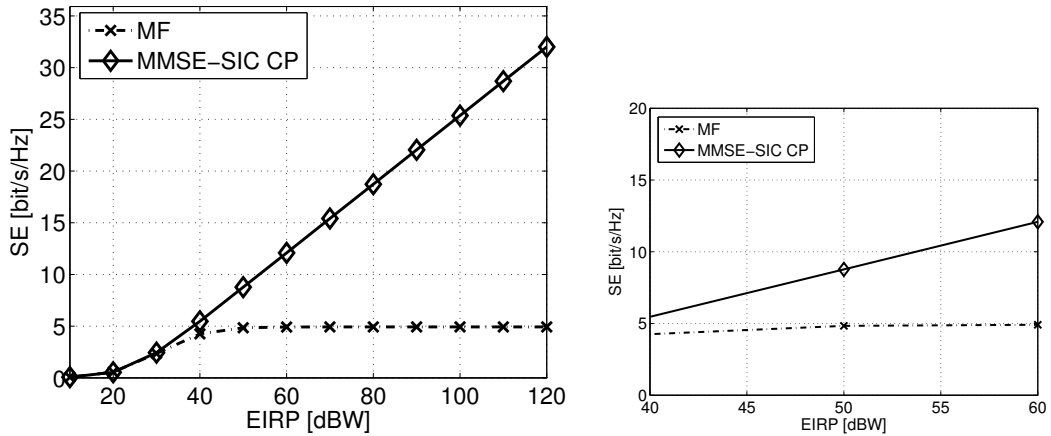


Figure 1.11: Upper bound on spectral efficiency in scenario 1.a, including zoom around EIRP=45dBW.

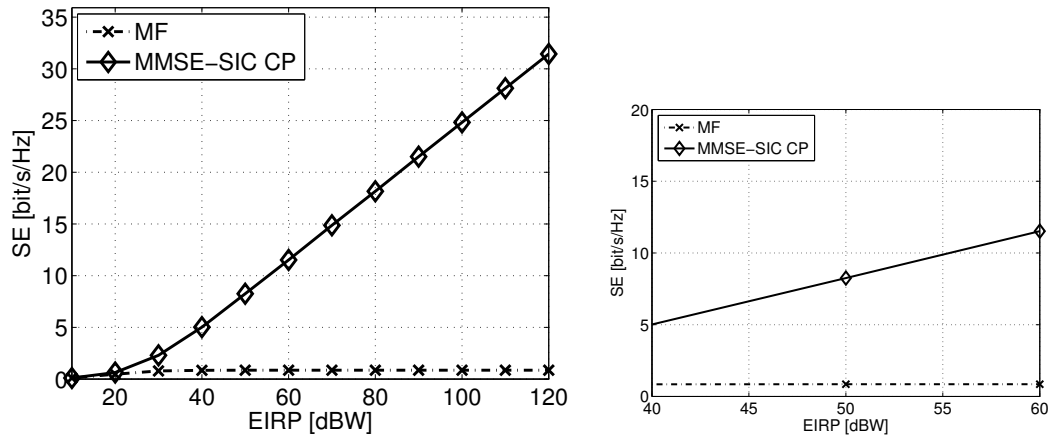


Figure 1.12: Upper bound on spectral efficiency in scenario 1.b, including zoom around EIRP=45dBW.

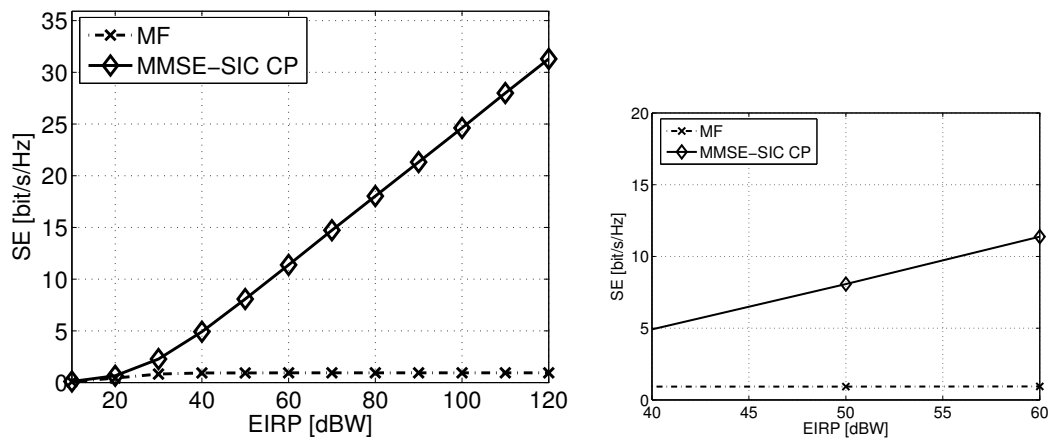


Figure 1.13: Upper bound on spectral efficiency in scenario 1.c, including zoom around EIRP=45dBW.

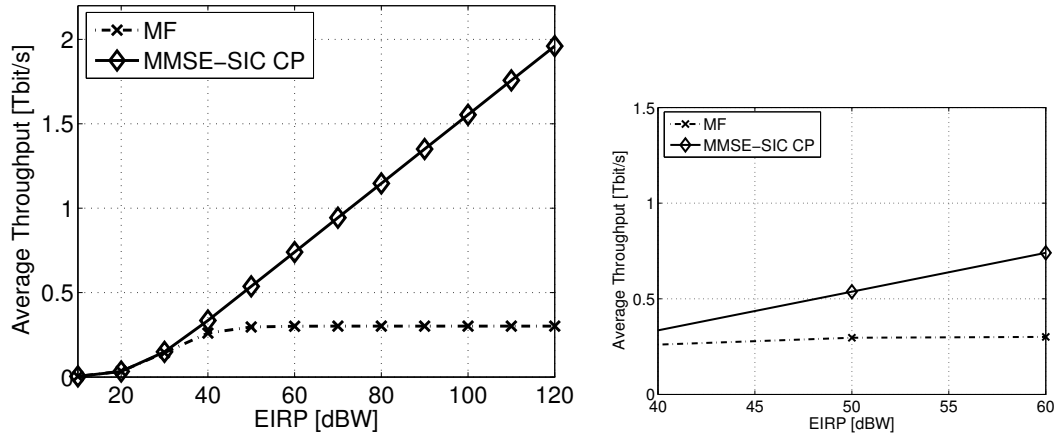


Figure 1.14: Upper bound on throughput in scenario 1.a, including zoom around EIRP=45dBW.

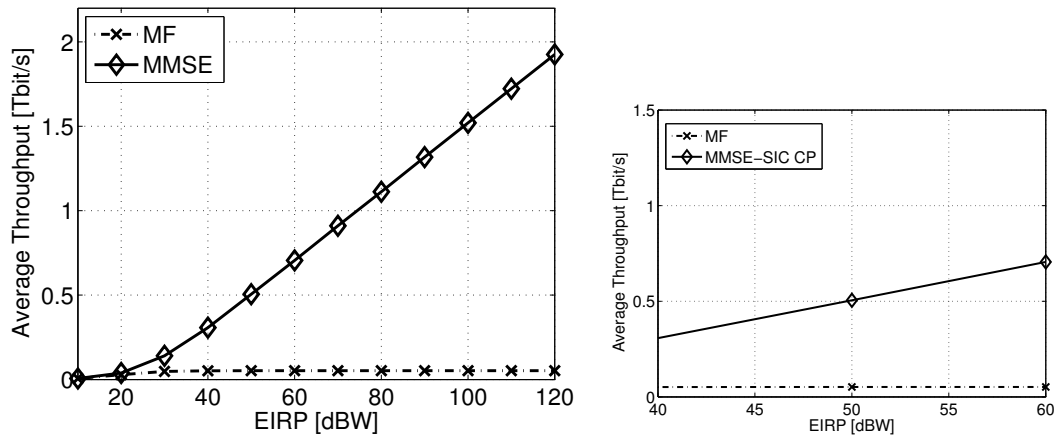


Figure 1.15: Upper bound on throughput in scenario 1.b, including zoom around EIRP=45dBW.

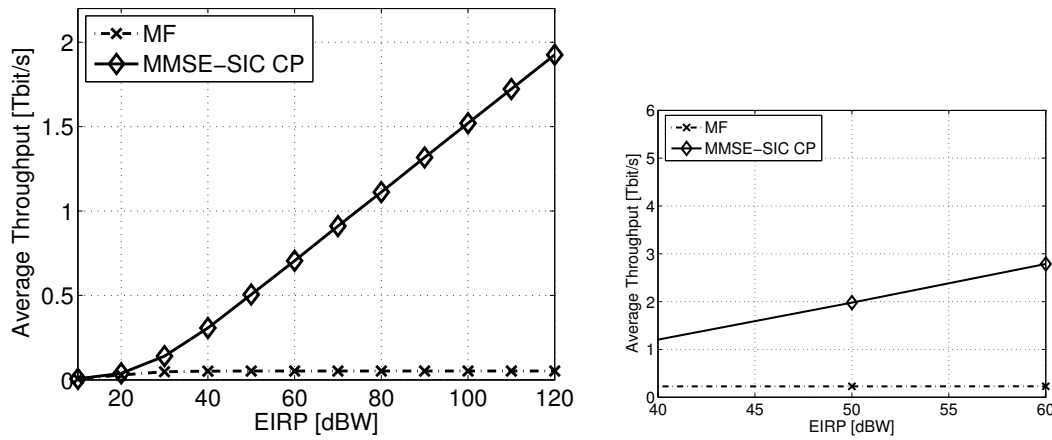


Figure 1.16: Upper bound on throughput in scenario 1.c, including zoom around EIRP=45dBW.

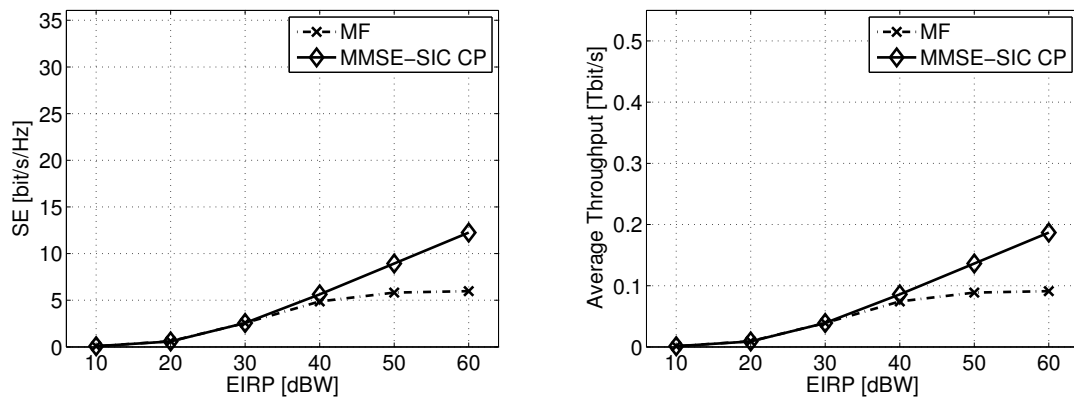


Figure 1.17: Upper bound on spectral efficiency and throughput in scenario 2.a

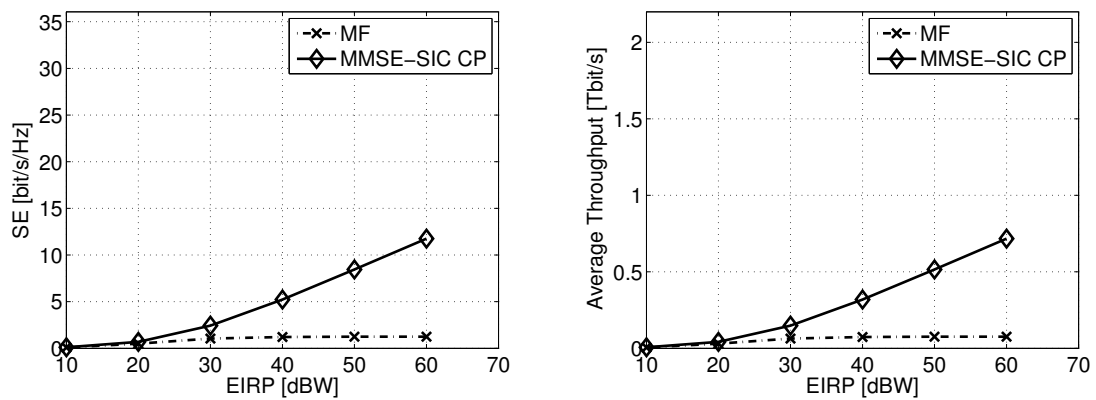


Figure 1.18: Upper bound on spectral efficiency and throughput in scenario 2.b

## 1.5 Interference cancellation strategies

In the following, the proposed interference cancellation strategies of interest are presented. The core idea is to extend and adapt the approach followed for terrestrial cellular cases, as in [33], in a Multi-Beam Satellite Scenario. It is proposed a double strategy for dealing with co-channel interference, one of which leverages also on gateway cooperation.

More in detail, intermediate solutions between lower and upper bound are represented by the Successive Intra-Gateway Interference Cancellation (SI2C) and Successive Intra- and Inter-Gateway Interference Cancellation (SI3C) which require different level of coordination and cooperation amongst GWs. Assuming a Multi-Gateway scenario, in Successive Intra-Gateway Interference Cancellation each gateway at each iteration decodes the signal showing the highest SINR, and removes it from the aggregate signal, therefore improving the SINR progressively. This is therefore a low complexity (given the reduced number of signals to be decoded with respect to SIC-CP) SIC solution. In Successive Intra- and Inter-Gateway Interference Cancellation, on the other hand it is assumed that GWs are connected through a high-speed network, and they could cooperate exchanging the decoded data, i.e. performing an inter-GW interference cancellation [1, 40]. In this second case, at each iteration, each gateway decodes the strongest signal and subtracts it from the aggregate signal composed by the signals pertaining to the beams it serves, but it also shares this decoded signals to the other gateways. Gateways receive therefore information on the interfering signals outside the cluster of beams they serve. By remodulating such signals, each gateway can subtract those from their aggregate signals, therefore obtaining a parallelization of the interference cancellation.

In the following the impact of such cancellation strategies on the SINR expression is given.

Considering a simpler matched-filter processing, we can write

$$\text{SINR}_k = \frac{P_k \|\mathbf{u}_k\|^4}{\mathbf{u}_k^* \mathbf{R}_k \mathbf{u}_k} \quad (1.16)$$

for the case of no-processing, intra GW processing and inter GW processing, these cases differing only in the structure of the matrix  $\mathbf{R}$ . In fact, for the case of no processing, already introduced in Section 1.3 we have

$$\mathbf{R}_k^0 = \sum_{l=1, l \neq k}^{N_B} P_l \mathbf{u}_l \mathbf{u}_l^* + \sum_{l=1}^{N_B} P_l \mathbf{v}_l \mathbf{v}_l^* + \sum_{l=1}^{N_B} P_l \mathbf{p}_l \mathbf{p}_l^* + N_0 \mathbf{I} \quad (1.17)$$

For the case of intra-GW processing, it can be written

$$\mathbf{R}_k^I = \mathbf{R}_k^0 - \beta \sum_{l=1}^{k-1} P_l \mathbf{u}_l \mathbf{u}_l^* \quad (1.18)$$

where  $\beta$  includes the effect of non-ideal interference cancellation. For the case of inter-GW processing

$$\mathbf{R}_k^{II} = \mathbf{R}_k^I - \beta \sum_{l=1}^{k-1} P_l \mathbf{v}_l \mathbf{v}_l^* \quad (1.19)$$

Similarly

$$\text{SINR}_k = \frac{P_k \|\mathbf{d}_k\|^4}{\mathbf{d}_k^* \mathbf{R}_k^C \mathbf{d}_k} \quad (1.20)$$

holds for the case of a single equivalent GW, which can be achieved through coordinated processing. Note that in this case column vectors in the expression of the SINR take from matrix  $\mathbf{D}$  instead of matrix  $\mathbf{U}$ , since in the case of centralized processing, all the antenna elements are used, therefore there is no distinction between matrices  $\mathbf{U}$  and  $\mathbf{V}$ . Considering MMSE signal processing, the receiver SINR can be written as

$$\text{SINR}_k = P_k \mathbf{u}_k^* \mathbf{R}_k^{-1} \mathbf{u}_k \quad (1.21)$$

where  $\mathbf{R}_k$  has the same meaning as above (i.e. it may be equal to  $\mathbf{R}_k^0$ ,  $\mathbf{R}_k^I$ , or  $\mathbf{R}_k^{II}$ )

### 1.5.1 Interference Cancellation: Performance Analysis

#### 1.5.1.1 System Throughput

In this section the performance of the IC techniques previously described is shown, in terms of average system throughput, in order to study how beneficial those could be with respect to the baseline case, and how close to the upper bound the system can get. Performance is evaluated in the AWGN channel as a reference, and considering the effect of rain fading (accounted for as per the ITU p1853 Model, [36], parameters being set for northern Italy) and the case of non-ideal cancellation. This latter case translates into having  $\beta < 1$  in the cancellation stage, for instance due to non-ideal detection of the signals to be cancelled and non-perfect estimation of the corresponding channel coefficients.

The behaviour of each IC technique varies depending on the considered scenario as it can then be observed in Figures 1.19 to 1.23. As expected, in all cases, SIC with Centralized Processing (which in case of MMSE filtering matches the optimal Joint Detection performance) is the best performing technique. Depending on the

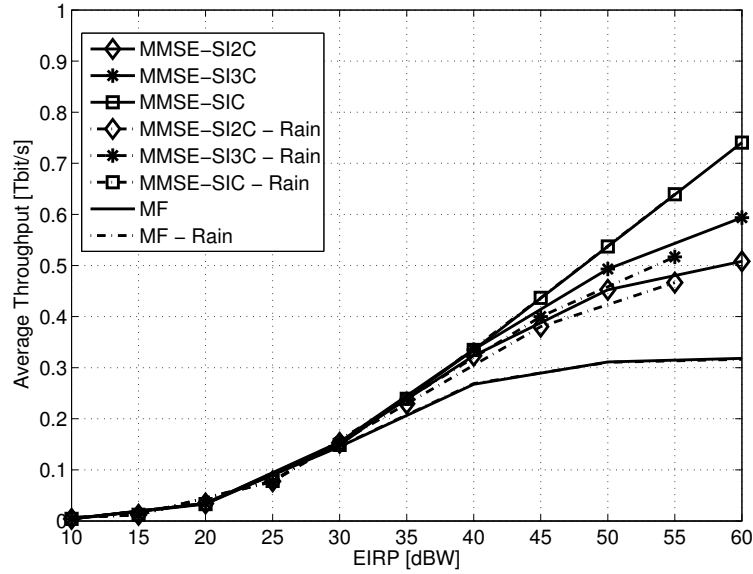


Figure 1.19: IC Techniques Performance Average System Throughput vs. EIRP [dBW] - Scenario 1.a AWGN and AWGN with Rain Fading

Frequency Reuse pattern and on the scenario, SI3C can yield marginal benefits in scenario 1.b, where the interference is mainly coming from inside the same cluster (i.e., beams served by the same gateway) thus cancelling interference from other gateways does not bring much improvement to system throughput, but also significant benefits to all other scenarios, in which gateways cooperation improves the performance by about 15% to 50%, the highest referring, as expected, to the cases of reuse factor 1, where there is more interference to be cancelled.

Similar conclusions are drawn from Figures 1.24 to 1.28, in which non-ideal cancellation is taken into account. More in detail, it is assumed that each cancellation, being non-ideal, leaves a 1% residual, which means that the residual is 20 dB lower than the original signal to be deleted. This represents a more harmful impact than rain fading on the overall performance.

When both nuisances are considered, counter-intuitively, it can be seen that, with non-ideal cancellation, the Rain Fading has a slight beneficial effect, being a further attenuation for all signals, i.e., also for all the interferers. This is reported in Figures 1.29 to 1.33.

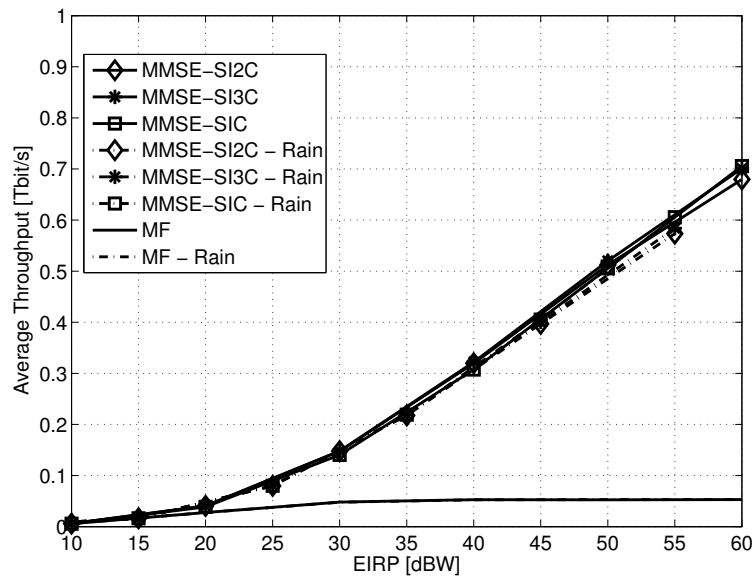


Figure 1.20: IC Techniques Performance Average System Throughput vs. EIRP [dBW] - Scenario 1.b AWGN and AWGN with Rain Fading

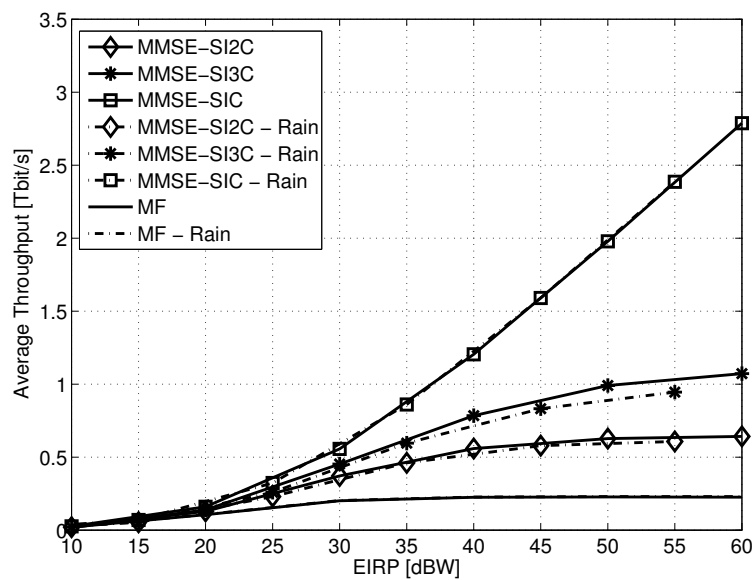


Figure 1.21: IC Techniques Performance Average System Throughput vs. EIRP [dBW] - Scenario 1.c AWGN and AWGN with Rain Fading

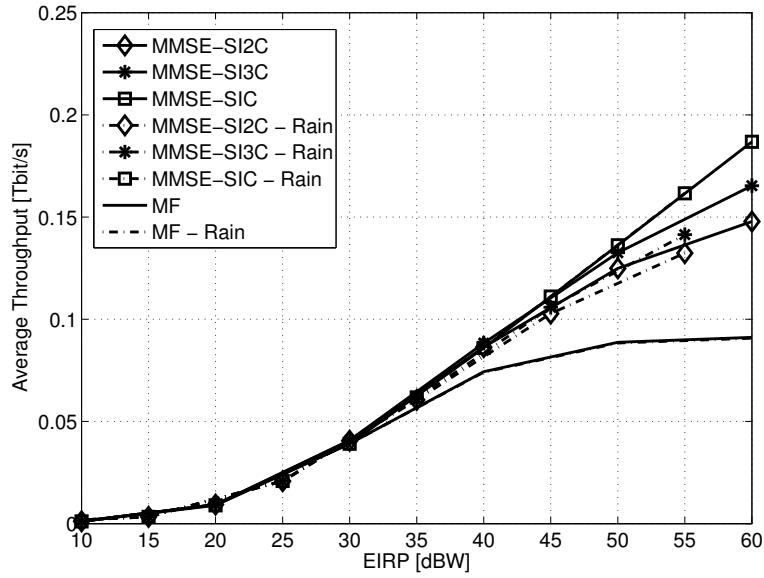


Figure 1.22: IC Techniques Performance Average System Throughput vs. EIRP [dBW] - Scenario 2.a AWGN and AWGN with Rain Fading

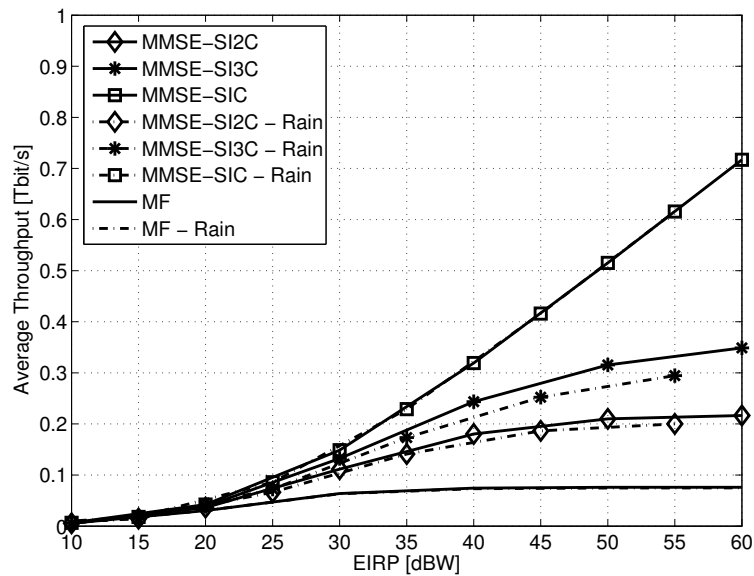


Figure 1.23: IC Techniques Performance Average System Throughput vs. EIRP [dBW] - Scenario 2.b AWGN and AWGN with Rain Fading

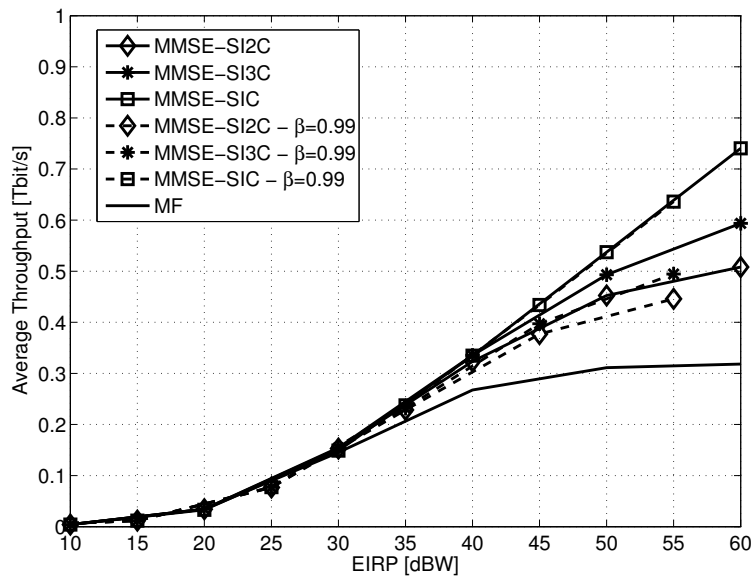


Figure 1.24: IC Techniques Performance Average System Throughput vs. EIRP [dBW] - Scenario 1.a AWGN and AWGN with Non-Ideal Cancellation ( $\beta = 0.99$ )

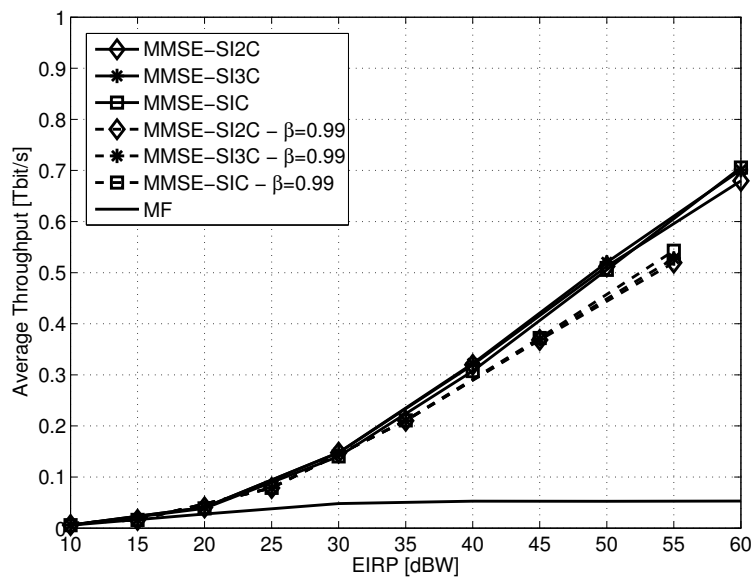


Figure 1.25: IC Techniques Performance Average System Throughput vs. EIRP [dBW] - Scenario 1.b AWGN and AWGN with Non-Ideal Cancellation ( $\beta = 0.99$ )

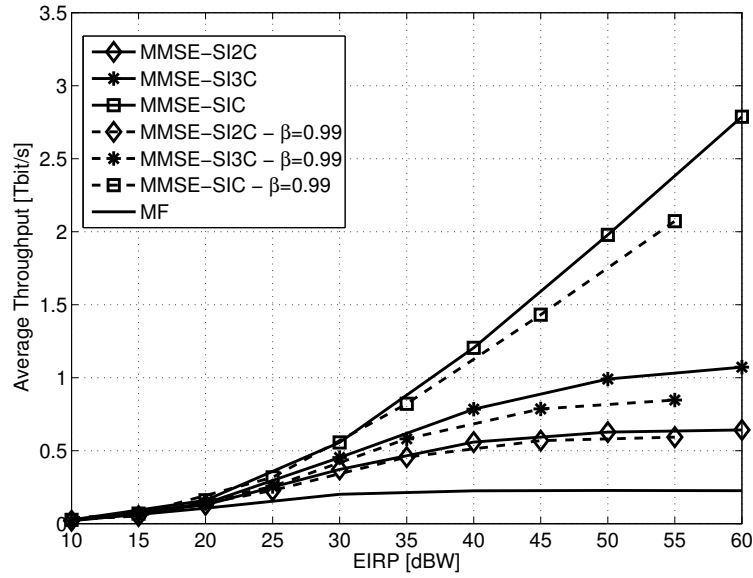


Figure 1.26: IC Techniques Performance Average System Throughput vs. EIRP [dBW] - Scenario 1.c AWGN and AWGN with Non-Ideal Cancellation ( $\beta = 0.99$ )

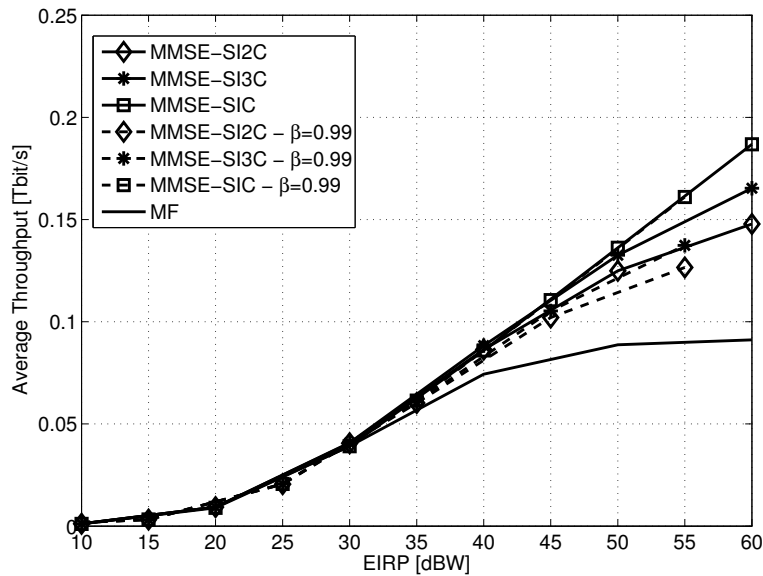


Figure 1.27: IC Techniques Performance Average System Throughput vs. EIRP [dBW] - Scenario 2.a AWGN and AWGN with Non-Ideal Cancellation ( $\beta = 0.99$ )

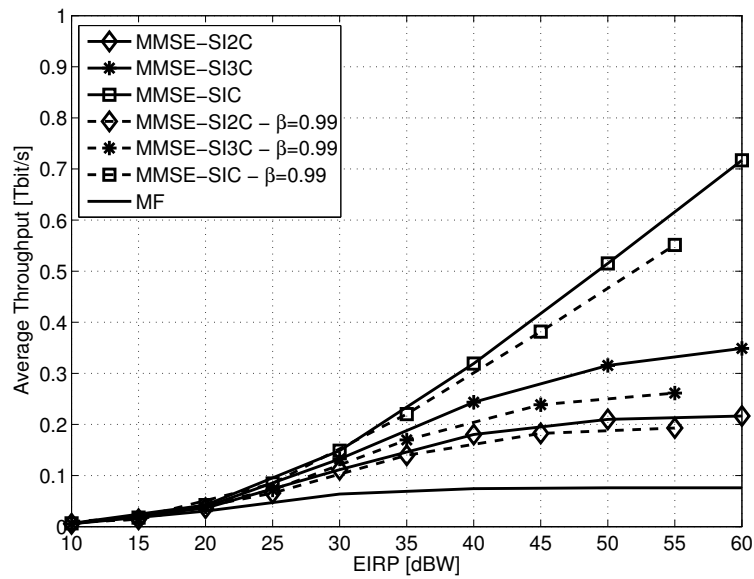


Figure 1.28: IC Techniques Performance Average System Throughput vs. EIRP [dBW] - Scenario 2.b AWGN and AWGN with Non-Ideal Cancellation ( $\beta = 0.99$ )

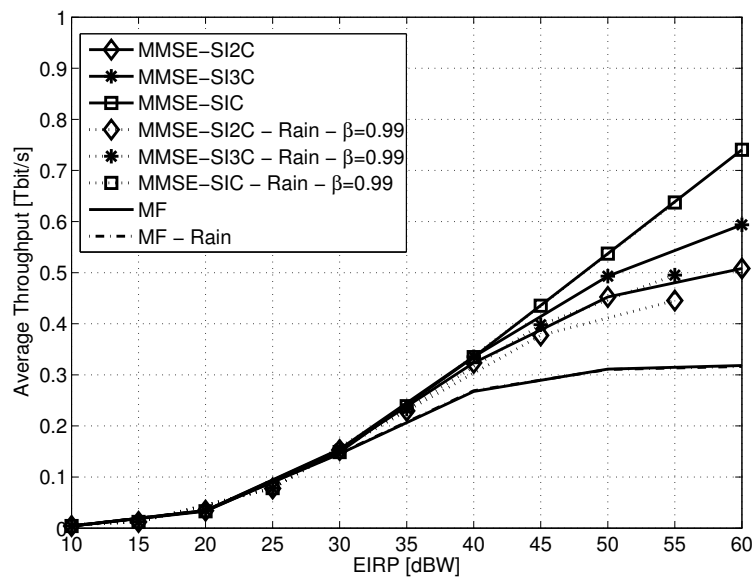


Figure 1.29: IC Techniques Performance Average System Throughput vs. EIRP [dBW] - Scenario 1.a AWGN, Rain Fading, and Non-Ideal Cancellation ( $\beta = 0.99$ )

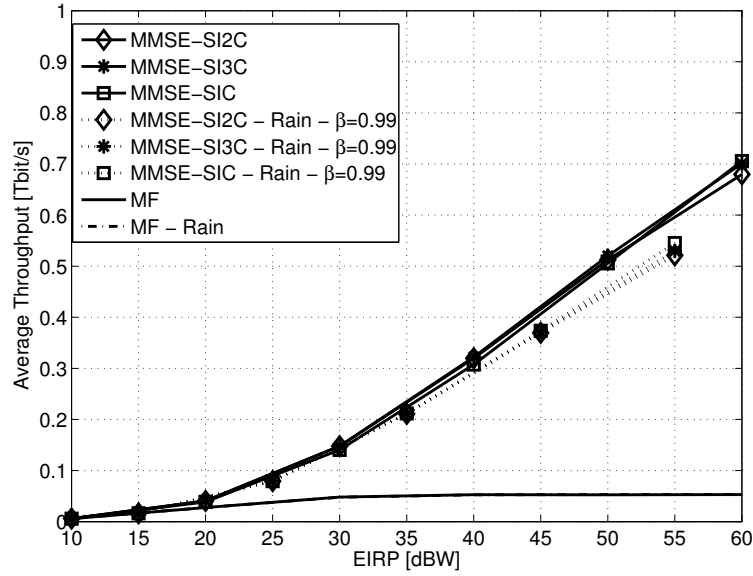


Figure 1.30: IC Techniques Performance Average System Throughput vs. EIRP [dBW] - Scenario 1.b AWGN, Rain Fading, and Non-Ideal Cancellation ( $\beta = 0.99$ )

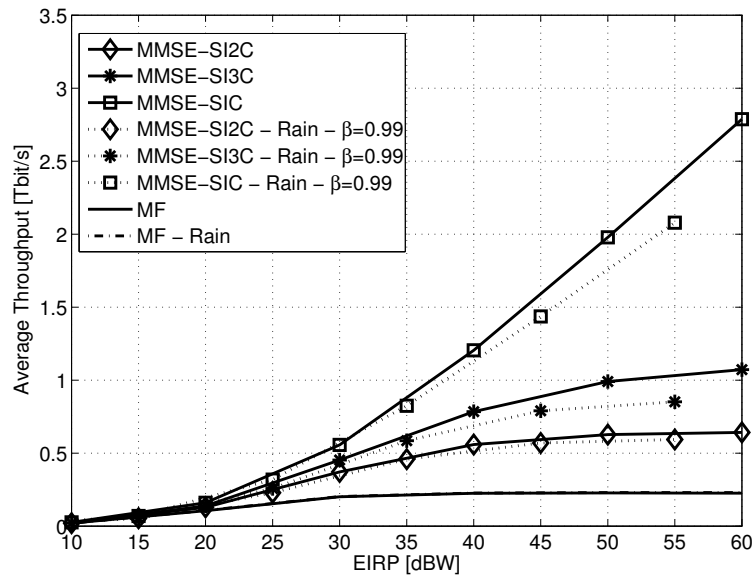


Figure 1.31: IC Techniques Performance Average System Throughput vs. EIRP [dBW] - Scenario 1.c AWGN, Rain Fading, and Non-Ideal Cancellation ( $\beta = 0.99$ )

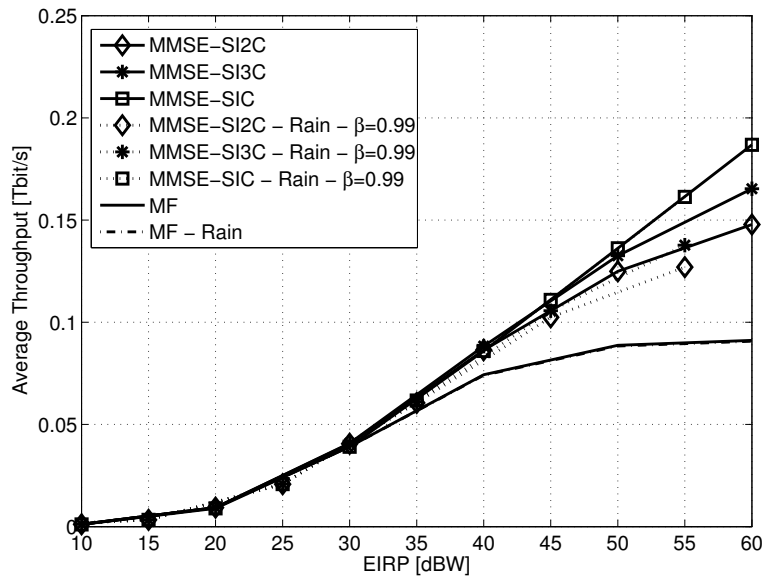


Figure 1.32: IC Techniques Performance Average System Throughput vs. EIRP [dBW] - Scenario 2.a AWGN, Rain Fading, and Non-Ideal Cancellation ( $\beta = 0.99$ )

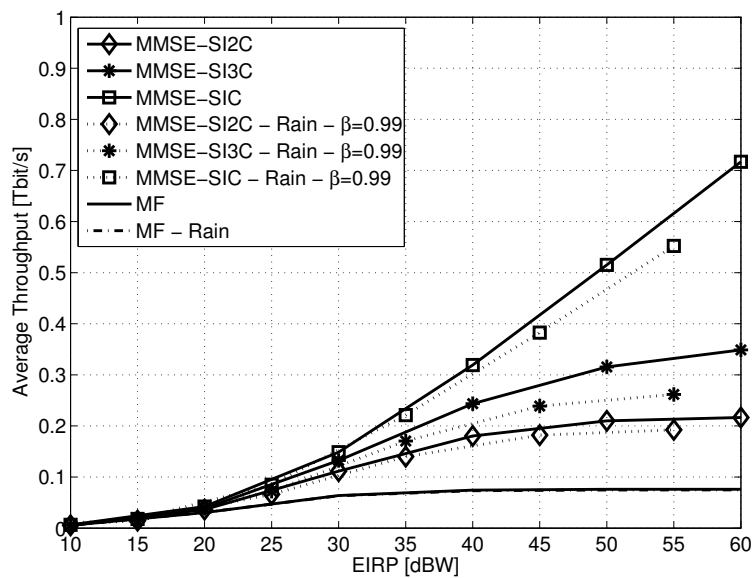


Figure 1.33: IC Techniques Performance Average System Throughput vs. EIRP [dBW] - Scenario 2.b AWGN, Rain Fading, and Non-Ideal Cancellation ( $\beta = 0.99$ )

### 1.5.1.2 System Availability

The analysis carried out so far has been focussing on the throughput (or spectral efficiency, equivalently) as the only measured figure of merit of the system. On top of this, an evaluation of the system availability is presented in this section, intended as the probability that the operating SINR (for instance, throughout the iterative process) is greater than a certain design (or required) value. This analysis leverages on the evaluation of the SINR probability distributions and can further assert the soundness of the proposed solutions. To this extent, the Cumulative Distribution Function (CDF) of the SINR for the IC techniques were computed. The results are plotted in figures 1.34 and 1.35 for scenario 2.a and 2.b, respectively, while the number of beams in scenario 1 does not allow to perform this analysis in an acceptable computer time. Starting from the CDF of the SINR, which represent the probability that the SINR is less or equal to a certain value, the availability is simply given by  $1 - CDF$ , to be evaluated at a relevant SINR. In figures 1.34 and 1.35 there are two vertical lines, representing the SINR threshold required for reliable transmission with two DVB-RCS2 modcod, i.e. the ones having the lowest and the highest spectral efficiency. As it can be seen, in Scenario 2.a, in which four frequency colours are used, interference does not completely prevent the system availability: the black vertical line represents in fact the minimum SINR required for the L1 waveform in the DVB-RCS2 standard, which corresponds to the lowest spectral efficiency, i.e., the highest waveform protection, and the availability is 100% even for the case of MF with no IC. On the other hand, if the highest spectral efficiency waveform is considered, i.e. S10 in DVB-RCS 2, which is the least protected, with simple MF, the availability would reach roughly 81% which is barely acceptable in practice. This means that IC techniques allow for the adoption of the highest MOD/COD, or, in future, include the presence of such techniques in the design of even higher order MOD/CODs, thus increasing the overall throughput.

A different case is represented by scenario 2.b, in which only one colour is used, thus much more interference is allowed into the system. In this case, even for the lowest MOD/COD, without IC, successful transmission would be prevented, since availability for MF would be around 55%, whereas the adoption of IC techniques yields great benefits: already SI2C shows an availability of around 99%, while SI3C, and the ideal case of CP-SIC tend to 100%. Moreover, in this case, is shown that even with IC techniques, the availability for the highest MOD/COD (S10) is not acceptable, except for CP-SIC, but intermediate MOD/CODs, higher than L1, could

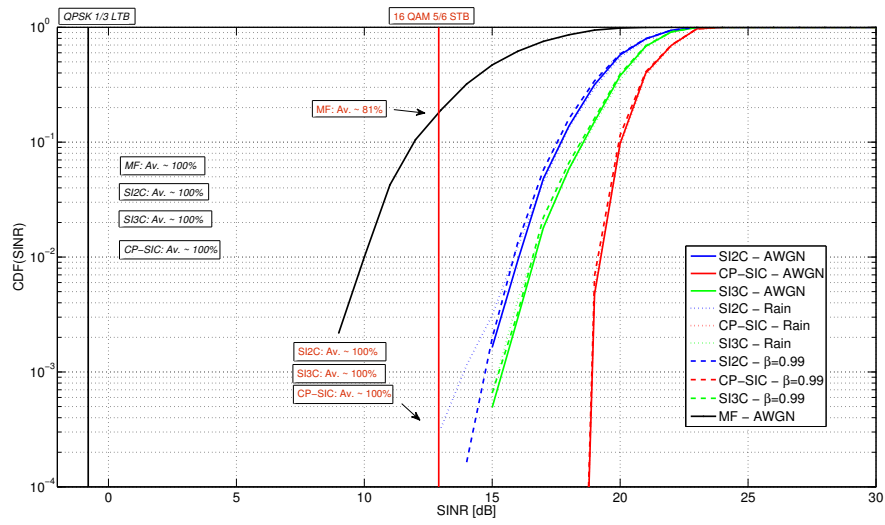


Figure 1.34: Availability for L1 and S10 Waveforms from the DVB-RCS2 standard - Scenario 2.a

be safely used for successful transmission.

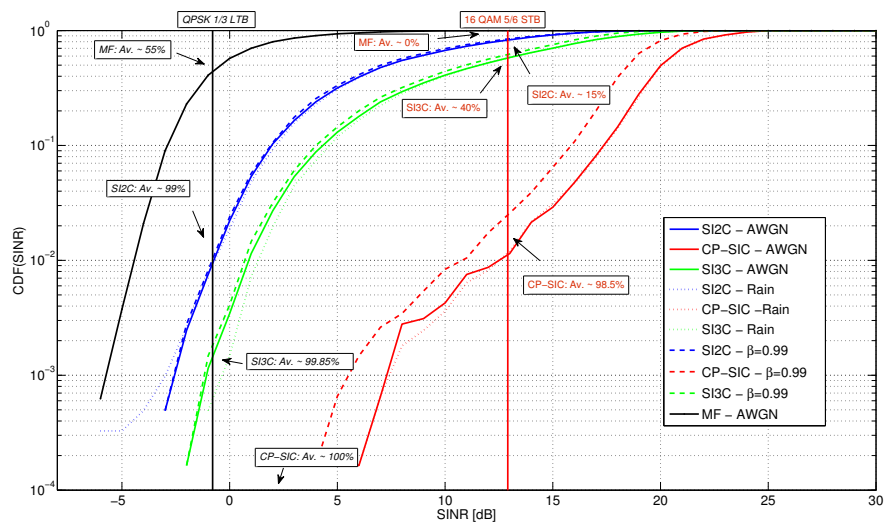


Figure 1.35: Availability for L1 and S10 Waveforms from the DVB-RCS2 standard - Scenario 2.b

### 1.5.1.3 Decoding and Cancellation Order Analysis

In this section an additional investigation is reported, related to the decoding and cancelling order and its impact on the overall system performance. The decoding and cancellation ordering has been verified not to affect the system throughput (i.e. the sum rate), as expected, in case of MMSE-SIC, since the SINR of all iterations is employed in the calculations of the sum rate in any case, regardless of the order of cancellation. This can be easily extended to the case of SI2C, which can be thought as several small-scale CP-SIC systems affected by co-channel interference. This is more interesting in case of SI3C, for which the optimal ordering is based on both intra-gateway and inter-gateway interference reduction: in this case canceling with a maximum SINR criterion of each gateway is not necessarily optimal for the other gateways perceived interference, thus for the overall system.

However it can be seen that the maximum SINR cancellation ordering criterion improves the SINR average distribution (over all the signals in the different iterations), as it is shown in Figures 1.36 - 1.40, in which the PDFs are shifted to the right (i.e., more contributions at higher values of SINR in dB) and the CDFs' slope is increased as a consequence, which is in line with what expected. The interpretation of this is an increased fairness among the users: when random order (e.g. no ordering) is adopted, although the end sum rate remains the same for the system, there might be larger unbalance between users SINR. On the other hand, it is shown that with ordering based on the highest SINR at each stage, the SINR PDFs are shifted to the right (and correspondingly, the CDFs show increased slope) with higher average value peak (i.e., larger number of occurrences around the average), which indicates that the SINRs of all users are distributed more fairly towards an higher average value.

The evaluations shown in the previous section already include this ordering strategy.

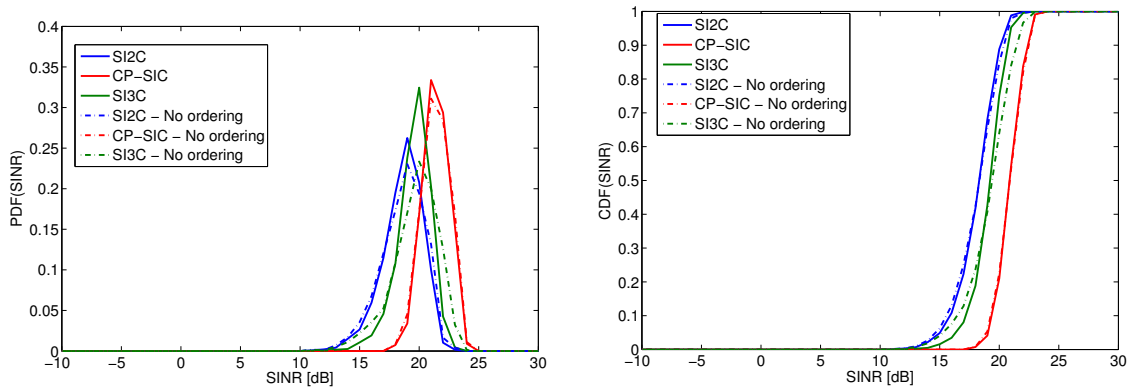


Figure 1.36: SINR PDF and CDF: fixed vs. maximum SINR based cancellation ordering at EIRP=45dBW - Scenario 1.a

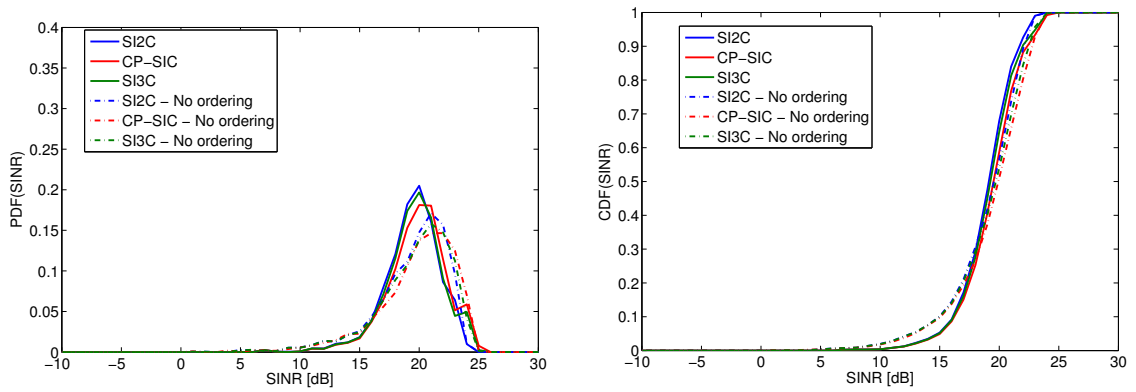


Figure 1.37: SINR PDF and CDF: fixed vs. maximum SINR based cancellation ordering at EIRP=45dBW - Scenario 1.b

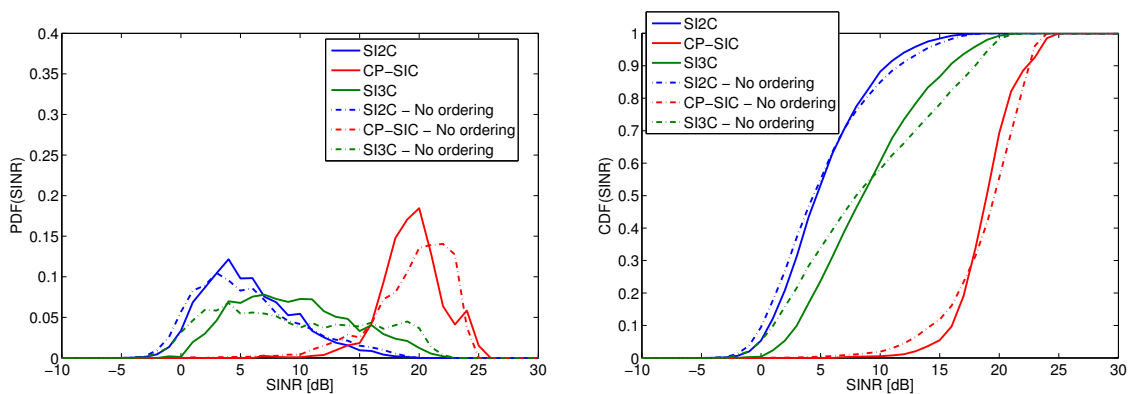


Figure 1.38: SINR PDF and CDF: fixed vs. maximum SINR based cancellation ordering at EIRP=45dBW - Scenario 1.c

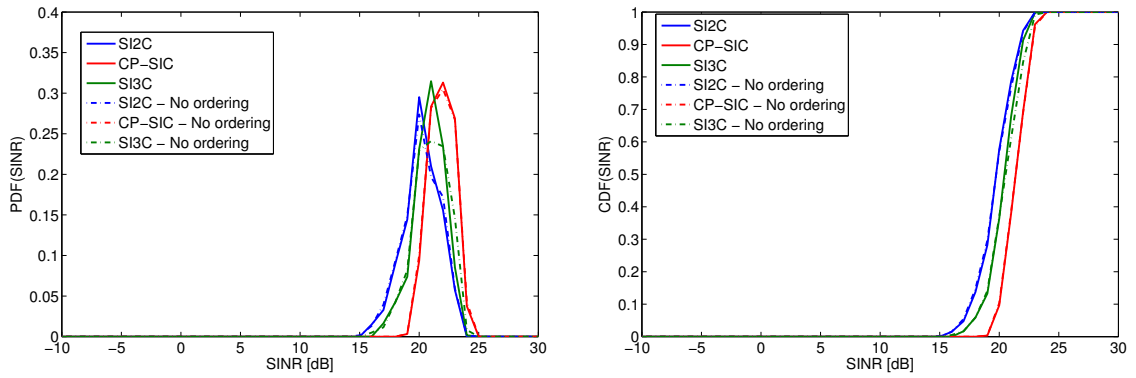


Figure 1.39: SINR PDF and CDF: fixed vs. maximum SINR based cancellation ordering at EIRP=45dBW - Scenario 2.a

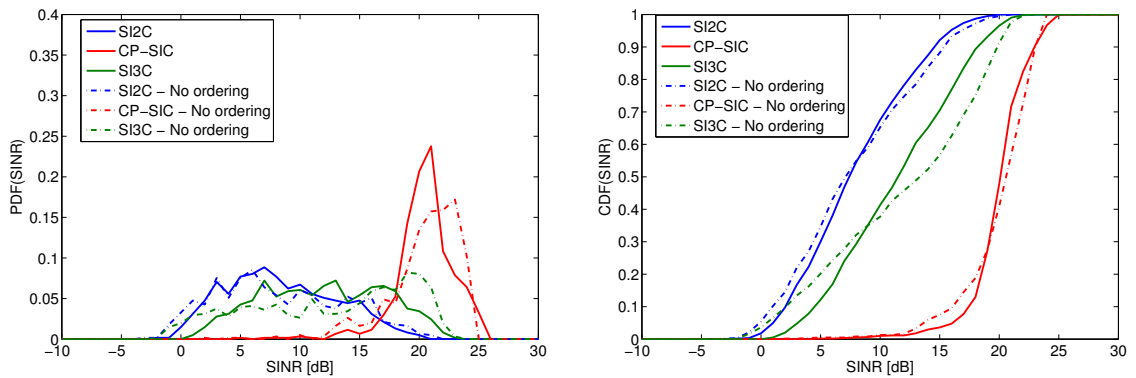


Figure 1.40: SINR PDF and CDF: fixed vs. maximum SINR based cancellation ordering at EIRP=45dBW - Scenario 2.b

## 1.6 Results Summary

The target of this chapter analysis was to devise a Multi-Beam satellite system architecture capable of managing co-channel interference. Starting by the characterization of lower and upper bound in system capacity, the design was based on Successive Interference Cancellation within the cluster of beams served by one gateway and also allowing a degree of cooperation between gateways. This analysis has shown that, although a reuse factor of 4 reduces the relevance of interference, thus the gaps to be filled by IC techniques with respect to the ideal joint detection bound are smaller, still, significant benefits are brought to the system performance by removing interference, and it was shown that, unlike classical satellite systems, Multi-Beam architecture, based on real-life parameters and antenna descriptions, operate in interference limited mode, rather than in noise limited mode. Therefore IC techniques and gateway cooperation are of interest to both cases of full frequency reuse, and reuse factor 4. In the first case, a large amount of interference is allowed into the system, therefore the benefits coming from the use of IC techniques is macroscopic, both in terms of throughput and availability, whereas in the latter case, overall system benefits are achieved, as the adoption of less TWTA amplifiers due to frequency reuse, which might be a requirement for the satellite platform, while still bringing throughput and availability improvements, although less dramatically in this case.

Tables 1.3 and 1.4 summarize the results achieved in terms of throughput and availability, at a practical EIRP value of 45 dBW, for each scenario and each IC techniques, highlighting the relative gain in percentage with respect to the reference case of no IC and MF filtering. Availability is reported for the lowest and highest DVB-RCS2 ModCods.

This activity suggests, as an inspiration for future works already ongoing at the moment of submitting this thesis, that the design of IC techniques shall be performed jointly with the design of the antenna system. In fact existing antennas are designed without taking into account the possibility of cancelling interference, thus aiming at great directivity. If the antenna is redesigned starting from acknowledging the presence of IC capabilities in the system, relaxed constraint, allowing more overlaps between beams (i.e., more interference) might be envisaged thus resulting in reduced antenna system costs at the same level or even at higher level of performance.

Table 1.3: Supernational System (61 beams): results summary - Scenario 2.a (with DVB-RCS2 ModCods)

Scenario	RF	IC scheme	Sum Throughput [Gb/s]	% gain	Availability (L1 DVB-RCS2 Mod-Cod)	Availability (S10 DVB-RCS2 Mod-Cod)
2.a Reference	4	NoIC-MF	81	/	$\geq 99.99\%$	$\geq 81\%$
2.a	4	SI2C-MMSE	102	26%	$\geq 99.99\%$	$\geq 99.99\%$
2.a	4	SI3C-MMSE	106	31%	$\geq 99.99\%$	$\geq 99.99\%$

## Acknowledgement

This work has been in part supported by the European Space Agency (ESA) Project n. 23089/10/NL/CLP “ESA Support to the SatNEx III Network of Experts”.

Table 1.4: Supernational System (61 beams): results summary - Scenario 2.b (with DVB-RCS2 ModCods)

Scenario	RF	IC scheme	Sum Throughput [Gb/s]	% gain	Availability (L1 DVB-RCS2 Mod-Cod)	Availability (S10 DVB-RCS2 Mod-Cod)
2.b Reference	1	No IC - MF	74	/	$\geq 55\%$	0
2.b	1	SI2C - MMSE	182	146%	$\geq 99\%$	$\geq 15\%$
2.b	1	SI3C - MMSE	240	223%	$\geq 99.85\%$	$\geq 40\%$

# Chapter 2

## Interference Management in SatCom Systems: Forward Link

Different considerations hold for the Forward Link (or Downlink, using a more terrestrial-like names set). The first, and perhaps most important difference in this case, is in the fact that the receiving end of the transmission is the terminal, not the gateway, which implies several considerations. On one hand, hardware complexity and capabilities are significantly reduced with respect to the return link, since a terminal typically has to cope with reduced size, computational capabilities and available power resources, and on the other hand, the interference generation process happens in a significantly different way than on the Return Link; in fact, whereas in the Return Link the overall SINR at the receiving end depends on the positions of all users on the coverage region (i.e.: antenna gains and channel state of each transmitting terminal location), in the Forward Link signals are transmitted by the gateway to the terminals through the satellite. This means that the interference contributions and the SINR level only depend on the reference (desired) user position (i.e., reference and interferers antenna gains and channel state in its location).

Typical approaches to Interference Management in the Forward Link are based on Precoding, and several instances of it ([19, 20] and references therein), and it has been shown to potentially have a significant impact on the system performance. There are, however, several technological aspects that suggest that interest should be posed also into other solutions for managing interference. First, practical aspects such market penetration or time to market of a system being designed, suggest that

the system could benefit from being based on existing, widely diffused standards, for instance a broadband system based on the DVB-S2 specifications. In such case, although supported, non-broadcast transmission is based on the creation of a frame which comprises information bits directed to different users, which are then coded, interleaved and modulated, therefore, in this scenario, the transmitting end might have to change precoding matrix at a rate down to symbol time order of magnitude. On a second level, precoding relies on feedbacks from the terminals, used for channel estimation, so on the presence of a Return Channel in the system, which is true in an interactive system, but might not be the case for Direct-to-Home (DTH) services, therefore Precoding might not be an option. Also, one side effect of precoding is typically an increased signal dynamic due to linear combinations of signals by means of the precoding matrix, and this too might be a relevant nuisance for the satellite on board amplifier.

Building on these consideration, in this chapter, the applicability on the Forward Link of a Satellite System, of Interference Management strategies based on Successive Interference Cancellation, as presented in Chapter 1 is discussed. In particular this part of this thesis focusses on IM approaches at the user terminal side, i.e. at the receiver side of the forward link of satellite communication systems, with the objective of reducing the impact of co-channel interference on the desired signal.

## 2.1 Forward Link Scenario and System Model

The considered scenario refers to a single Satellite Forward Link with Co-Channel Interference generated by beams at the same frequency reuse color. More in detail, this scenario models the CCI generated on the user terminal by a Multi-Beam transmission from the satellite also with challenging frequency reuse which, due to the interference level, would prevent correct decoding of the reference signal by means of a conventional DVB-S2 receiver without any interference mitigation technique. In compliance with ESA Channel Model for DVB-SX [37], a Multi-Beam system is considered, with a Color Reuse equal to 2, in which two interferers are considered to affect the reference signal, i.e., only the neighbouring beams on the same frequency actually interfere with the reference signal, meaning that farther interfering beams are negligible.

Mainly, two cases are considered for the C/I analysis using two interferers, both referring to practical conditions of real-life applications:

- Case 1: Interferer 1 :  $C/I_1 = 0dB$  ; Interferer 2 :  $C/I_2 = 10dB$  ;
- Case 2: Interferer 1 :  $C/I_1 = 4dB$  ; Interferer 2 :  $C/I_2 = 6dB$  .

The reference scheme for this scenario is shown in Figure 2.1.

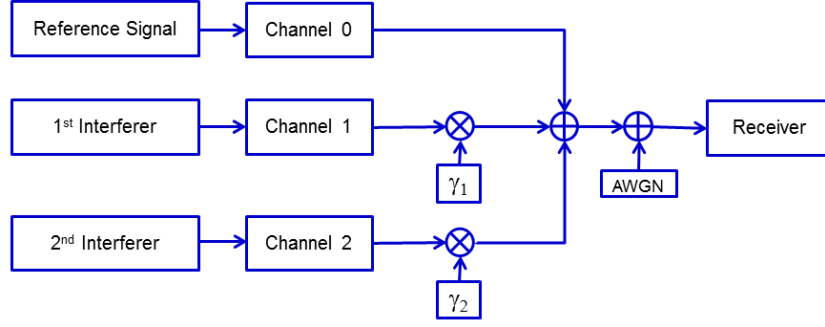


Figure 2.1: General Block Diagram for the considered Scenario

The forward link system model is based on a K-user, time-invariant, downlink DVB-S2 system [38]. The transmitted signal to the k-th user can be modelled as

$$X_k(t) = A_k \sum_{n=0}^{L_F-1} b_k(n)g(t - nT_s) \quad (2.1)$$

where  $A_k$  represents the  $k$ -th user signal amplitude,  $L_F$  is the frame length in number of symbols of the DVB-S2 standard,  $b_k(n)$  is the  $k$ -th transmitted symbol drawn from a complex-valued PSK or APSK signal constellation [18] with cardinality  $M$ ,  $g(t)$  denotes the normalized squared root raised cosine filter and  $R_s = 1/T_s$  is the symbol rate.

The baseband equivalent received signal can be written as:

$$r(t) = \sum_{k=1}^K A_k \sum_{n=0}^{L_F-1} b_k(n)g_r(t - nT_s) + w(t) \quad (2.2)$$

where  $g_r(t) = g(t) * h(t)$ ,  $h(t)$  represents the baseband impulsive response of the communication channel and  $w(t)$  is the complex additive white Gaussian noise with zero mean and variance  $\sigma_n^2$ .

The received signal has unknown delay, frequency and phase at the output of the matched filter, taken into account by the parameters  $\tau_k$ ,  $\nu_k$  and  $\theta_k$ , which express

the uncertainty about the beginning of the symbol interval and the carrier frequency and phase, respectively, all for the  $k$ -th user. Therefore, the received signal can be written as:

$$r(t, \tau_k, \nu_k, \theta_k) = \sum_{k=1}^K A_k \sum_{n=0}^{L_F-1} b_k(n) e^{j(2\pi\nu_k t + \theta_k)} g_r(t - nT_s - \tau_k) + n(t) \quad (2.3)$$

where  $n(t)$  is the complex additive white Gaussian noise at the output of the matched filter with zero mean and variance  $\sigma_n^2 = N_0/2$ .

## 2.2 Decodability Analysis: $E_s/(N_0 + I_0)$ vs. $E_s/N_0$

The peculiarities of this forward link scenario motivate considerations on the decodability of the received signals at the terminal. In fact, the interference cancellation techniques, based for example on an instance of the ones presented in Chapter 1, work differently in the forward link. In the return link, cancellation is performed by the gateway, that decodes all the received signals, all of which are of interest for the gateway, since all carry relevant information. In the return link, thus, the order in which signals are decoded and cancelled is not relevant as far as the decoding of the signals itself is concerned, although (as shown in Chapter 1) it affects the fairness between users in terms of average SINR.

On the other hand, in the forward link considered scenario, the receiving end of the transmission is the user terminal, which, unlike the gateway in the return link, is only interested in decoding the single signal being transmitted to it. This motivates an analysis of physical layer decodability of the reference and interfering signals in the considered scenario, which, as it will be shown in the following, depends on the relative values of the interferers with respect to the reference signal.

In order to speculate on the possible behavior of the system in the considered scenario, in Figure 2.2 and Figure 2.3, for the two cases 1 and 2, the achievable Energy per Symbol over Noise plus Interference spectral density ratio  $E_s/(N_0 + I_0)$  is studied as a function of the single signal Energy per symbol over Noise spectral density ratio  $E_s/N_0$ , with the decoding thresholds of three DVB-S2 mod-cods, i.e. QPSK-1/4, QPSK-1/2, and QPSK-2/3.

Figure 2.2 reports the achievable  $E_s/(N_0 + I_0)$  vs.  $E_s/N_0$ , for scenario A Case

1, i.e. interferer 1 at  $C/I_1 = 0dB$  and interferer 2 at  $C/I_2 = 10dB$ . The results of this analysis are based on the following receiver definitions:

- *Ref. Signal - no IC*:  $E_s/(N_0+I_0)$  for the reference receiver with no interference management;
- *Interf. 1 - no IC*:  $E_s/(N_0 + I_0)$  for the first (strongest) interferer with no interference management;
- *Interf. 2 - no IC*:  $E_s/(N_0 + I_0)$  for the second (weakest) interferer with no interference management;
- *Ref. Sign - IC on Interf. 1*:  $E_s/(N_0 + I_0)$  for the reference receiver after ideal cancellation of the first (strongest) interferer; this is to be considered as a theoretical behaviour obtained in presence of two interferers when the strongest one is ideally cancelled, hence when only interferer 2 is present;
- *Interf. 2- IC on Interf. 1*:  $E_s/(N_0 + I_0)$  for the second (weakest) interferer receiver after ideal cancellation of the first (strongest) interferer;
- *No Int*: it represents the ideal case of no interference and hence it represents the upper bound the achievable  $E_s/(N_0 + I_0)$ ;
- *QPSK 1/4*: decoding threshold at BER= $10^{-4}$ ;
- *QPSK 1/2*: decoding threshold at BER= $10^{-4}$ ;
- *QPSK 2/3*: decoding threshold at BER= $10^{-4}$ .

The decoding thresholds (above which the receiver can decode the signal in waterfall region) reported in Figure 2.2 and Figure 2.3 are taken from the DVB-S2 standard, [38].

The interpretation of these results is as follows: whenever a particular curve, therefore a particular receiver case, exceeds one of the modcods decoding thresholds then the receiver is also able to decode. On the contrary, if a curve remains under the threshold, the corresponding receiver cannot decode the corresponding signal. In particular, by inspection of Figure 2.2 it can be observed that the Receiver performance for the reference signal and the strongest interference, i.e., "Ref Signal no IC" and "Interf 1 - no IC" respectively, can successfully decode only QPSK-1/4 when  $E_s/N_0$  is above 1 dB, while they are not able to decode for any other modcod at any  $E_s/N_0$  and also the two receivers have the same performance since the  $C/I$  for the

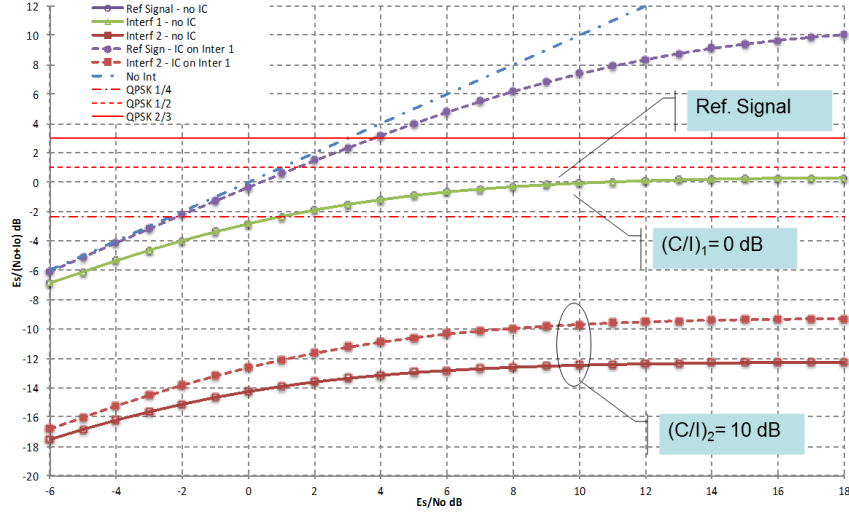


Figure 2.2:  $E_s/(N_0 + I_0)$  analysis for Case 1

first interferer is equal to 0 dB. Moreover, when the first interferer is ideally removed from the input signal then the reference receiver performance, i.e., "Ref Sign – IC on Inter 1", converges to the "No Int" reference behaviour since the remaining nuisance attains only the second interferer which is at  $C/I=10$ dB, thus, almost negligible for moderate to low SNR, whereas it becomes relevant for very high SNR, thus when the interference contribution becomes greater than the noise, which motivates the compression of the "Ref Sign – IC on Inter 1" curve with respect to the case of no interference. Also, the SINR curve of the weakest interferer receiver, i.e. "Interf 2 – no IC" and "Interf 2 – IC on Inter 1" always remains below threshold because of the reference signal interference, which means that the second interferer can never be decoded.

The same analysis is reported for Case 2 in Figure 2.3, i.e. Interferer 1 at  $C/I_1 = 4$  dB and Interferer 2 at  $C/I_2 = 6$  dB, for the same receiver configurations of Figure 2.2 along with the additional configuration "Ref Signal -1 Interf ( $C/I=4$ dB) – no IC":  $E_s/(N_0 + I_0)$  for the case of the reference receiver with no interference management in presence of a single interferer at  $C/I=4$ dB.

Considering Figure 2.3 it can be observed that the two interferer receivers do not decode at any  $E_s/N_0$  when the reference signal is present, which means that decoding shall start from the reference signal. Also, the reference signal receiver decodes at different values of  $E_s/N_0$  with an impact of the interferers that clearly increases when reducing waveform protection and that is almost negligible for QPSK-1/4.

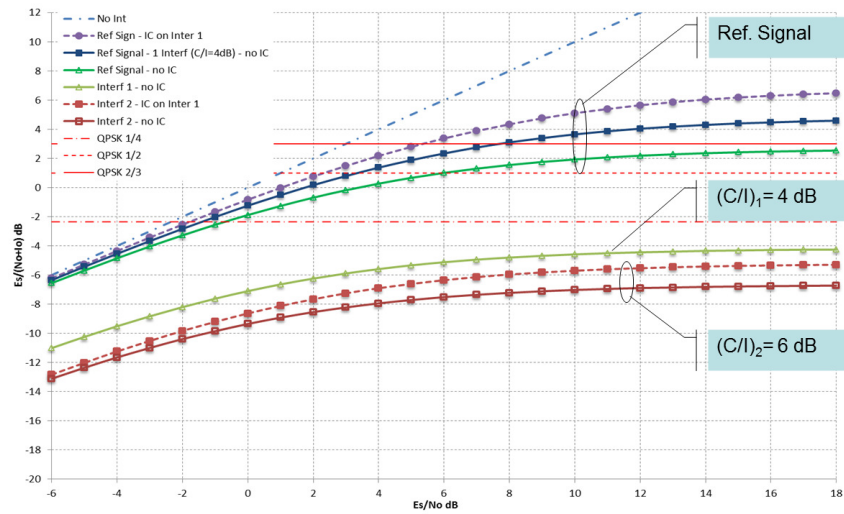


Figure 2.3:  $E_s/(N_0 + I_0)$  analysis for Case 2

From the above analysis it can be observed that in Case 1 the receiver is not able to decode if no interference mitigation techniques is used. On the other hand, conventional IC techniques are not suitable due to the impossibility of decoding either the reference signal or the interferer. The same consideration apply to Case 2 in terms of feasibility of the conventional IC techniques.

It is worthwhile noting that the above analysis of decodability is based on the assumption that noise plus interferer can be approximated as a Gaussian process, which is usually verified for a relatively large number of interferers. In order to validate this assumption, Figure 2.4, reports histograms of the interferer, the noise, and the interferer plus noise amplitude for  $C/I = 0\text{dB}$  and  $E_s/N_0 = 4\text{dB}$  showing that the histogram of noise plus interferer maintains a Gaussian behaviour for the considered case.

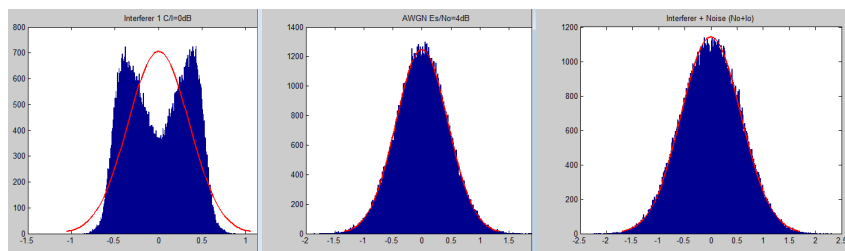


Figure 2.4: Histograms plot for interferer, noise, and interferer plus noise

On the basis of the previous analysis the several interesting considerations can be

drawn on the applicability of MUD techniques at the terminal side. First, IC/MUD at the user terminal (forward link) differs from classical IC/MUD at the gateway (return link), because the interest is just on a single signal (i.e. the Reference Signal), which in general, in the considered scenarios, according to realistic conditions, is also the strongest one, and not necessarily to the entire set of received signals. The case can happen often of the reference signal being stronger than the interferers, in which case no advantage is brought by interference cancellation, since the reference signal has already been decoded. This means that in the forward link, it is likely that some interferers might never be decoded, because the reference signal is always decoded first, e.g., the second interferer in the considered scenario. Hence, these interfering signals are to be considered additional background noise, which cannot be exploited for processing.

As a consequence, the number of interferers to be considered is limited to a few. For example, in the VSAT scenario devised by ESA [37], the number of interferers to be processed equals 1 (interferer 1), since the second interferer would always decode after the reference signal. In this case, it is very likely that the reference signal and the interferer to-be-cancelled have about the same SINR or the interference has lower SINR than the useful signal. Hence, either the reference signal can be decoded, and thus there is no need to perform IC, or the reference signal can't be decoded, in which case, obviously, the interferer can't be decoded as well. In this sense therefore, it appears that in the considered scenario, interference cancellation, at least if adopted exactly as described in chapter 1, is either unfeasible, or not beneficial.

These considerations coming from the analysis of decodability are proved by means of computer simulation in next section.

The main outcome of this analysis is that in order for the interference cancellation strategy to bring a benefit to the reference signal decoding, interferers should be higher in power than the reference signal itself, since, in that case, the iterative process would start from the decoding of the interfering signal, therefore improving the conditions for the reference signal. Based on these considerations, in next sections, the focus will be posed on Case 1 of the considered scenario, since all the limiting aspects for interference cancellation of the above scenario are further highlighted in Case 2, whereas in Case 2 conventional single user detection, i.e., no interference management would bring better performance due to a lower interference.

## 2.3 Performance evaluation

### 2.3.1 Baseline Performance without Interference Cancellation

In this section, numerical simulation results are reported in order to assess the achievable performance of IC/MUD techniques in the considered scenario.

In order to validate through simulation the analytical approach used in the previous section, it is important to verify the decoding performance at the receiver side without any interference mitigation techniques in terms of error rate, both for case 1 of the considered Scenario.

The general simulation chain used for this purpose is shown in figure 2.5.

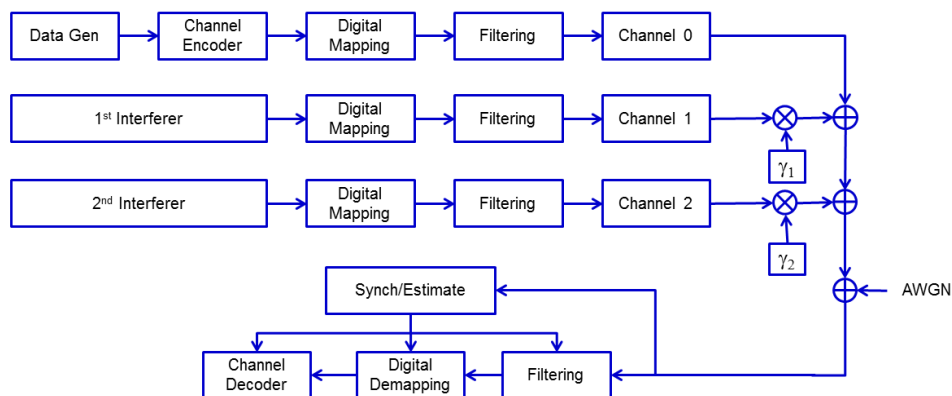


Figure 2.5: Block diagram of the simulation chain for the considered scenario without IC

The first branch is the canonical DVB-S2 transmission chain where the Channel Encoder block is composed of a BCH (Bose, Chaudhuri, Hocquenghem) encoder, and Low Density Parity Check (LDPC) encoder and an interleaver. Since, there is no need to perform the Forward Error Correction (FEC) operations for the two interferers in this test, the corresponding FEC blocks are not here reported.

The multiplicative constants,  $\gamma_1$  and  $\gamma_2$ , are due to the  $C/I$  value of the two interferer and so, for example, considering Case 1 they are equal respectively to 1 and 0.316 (normalized to the reference signal). At the receiver side, since the aim of this simulation is to validate the  $E_s/(N_0 + I_0)$  vs.  $E_s/N_0$  analytical model, all channel offsets introduced by the block Channel 0 are considered as known and so it is assumed an ideal parameters estimation processing. It is also important to let the de-mapping stage be aware of the actual the noise power which is not only given

by  $N_0$  but by  $(N_0 + I_0)$ . Case 1 BER performance are shown in 2.6 where:

- *No Interferer LOGMAP* refers to known BER performance behaviour for QPSK 1/2 mod-cod in DVB-S2 when LOG-MAP algorithm for LLRs is adopted [40, 41].
- *No Interferer LOGMAX* refers to known BER performance behaviour for QPSK 1/2 mod-cod in DVB-S2 when LOG-MAX algorithm for LLRs is adopted [40, 41].
- *1 Interferer C/I=0dB LOGMAP*: BER performance in presence of a single interferer with  $C/I=0\text{dB}$  with no interference management when LOG-MAP algorithm for LLRs is adopted.
- *1 Interferer C/I=10dB LOGMAP*: BER performance in presence of a single interferer with  $C/I=10\text{dB}$  with no interference management (LOG-MAP).

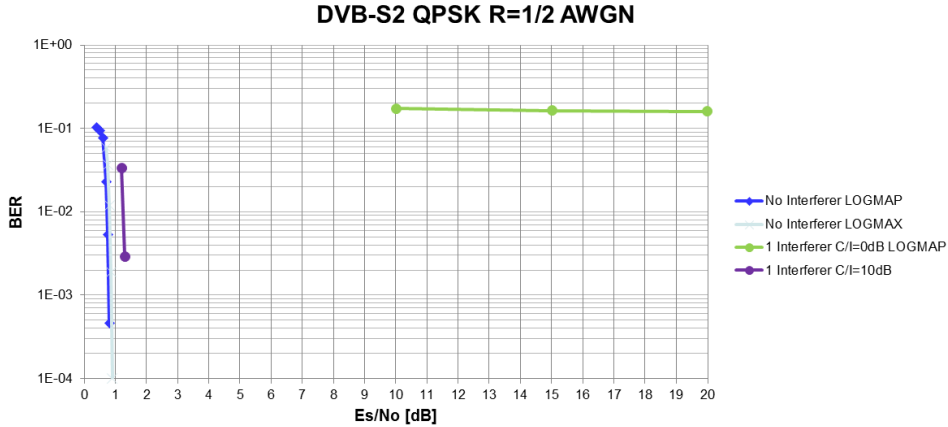


Figure 2.6: BER performance Case 1 without IC/MUD: QPSK 1/2 MODCOD

The “*No Interferer LOGMAP*” and “*No Interferer LOGMAX*” curves are reported in order to validate the simulation chain. The green curve is obtained by setting  $\gamma_1 = 1$  and  $\gamma_2 = 0$  (without Interferer 2). Considering QPSK 1/2 MODCOD, it is quite evident that the receiver is not able to decode in presence of an interferer at the same power because it never starts to decode. As a consequence, there is no need to perform simulation with also interferer 2. These results confirm the decodability analysis reported in the previous section. It must be underlined that this result is obtained using QPSK1/2 MODCOD because, as it could be seen in Figure 2.7, the receiver is able to decode using QPSK 1/4, QPSK 1/3 and QPSK 2/5

MODCODs. To further confirm the validity of the approach, the BER performance is shown in the presence of Interferer 2 but without Interferer 1, which corresponds to the assumption of ideal cancellation of the interferer 1. The 0.5dB loss shown in Figure 2.2 is also apparent in the numerical simulation results, represented by the purple line.

The analysis done for the QPSK 1/2 MODCOD utilization, can be easily extended to other low order MODCODs in the DVB-S2 standard. In order to anticipate simulation results it is possible to extend the  $E_s/(N_0 + I_0)$  vs.  $E_s/N_0$  analytical model as shown in Figure 2.7 where additional thresholds with respect to the previous decodability analysis are reported, corresponding to other MODCODs.

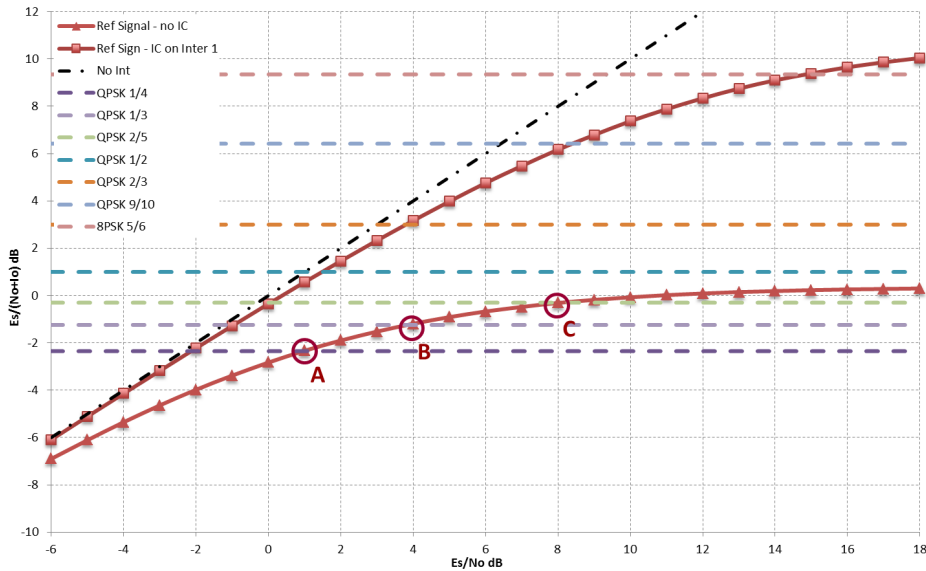


Figure 2.7:  $E_s/(N_0 + I_0)$  analysis for Case 1 for extended set of MODCODs

Considering the curve pertaining to the case of no interference cancellation at the receiver, named "Ref Signal - no IC", it is easy to see that there are only three MODCODs able to decode in this scenario which are QPSK 1/4, QPSK 1/3 and QPSK 2/5, respectively pointed out by A, B and C circle. The analysis shows in addition that the required  $E_s/N_0$  at the receiver for Single-User Detection (SUD) (i.e., no Interference Cancellation) are respectively 1 dB, 4 dB and 8 dB. Without any interference management techniques all the other modcod cannot be decoded.

Simulations performed using QPSK 1/4, QPSK 1/3 and QPSK 2/3 MODCODs for SUD, in addition to QPSK 1/2 which was already shown in Figure 2.6, are reported in Figure 2.8. All curves plotted confirm respectively, that the first two

MODCOD are able to decode in this Scenario at about  $E_s/N_0$  equal to 1 dB and 4 dB while the other two are not able to decode.

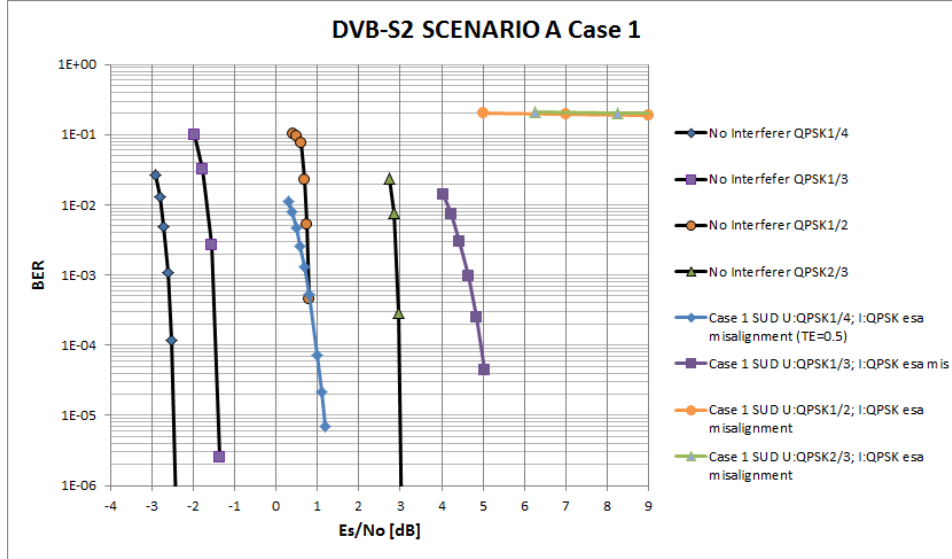


Figure 2.8: BER performance for Case 1 without IC/MUD

## 2.3.2 Interference Cancellation at the Terminal

### 2.3.2.1 Conventional Interference Cancellation

As clearly shown in Figure 2.2, and following the considerations made in section 2.2, and after having underlined that for the purpose of the interference cancellation paradigm, Case 1 is the most relevant to this analysis, it is very easy to understand that if the reference signal and the main interferer are at the same level, as a C/I of 0 dB indicates, then conventional interference cancellation strategies are unable to improve the system performance, since, unlike the return link scenario, in this case, the receiver is either able to decode directly the reference signal, for which the same SNR is needed as for the main interfere, or it is not able to decode neither of the two signals. Therefore in this scenario, conventional interference cancellation is not helpful.

This result is also apparent if looking again at figure 2.8: indeed, for the lowest modcods, the system is able to operate in single user detection, and since the interferer is at the same level, no benefit is brought by interference cancellation; for higher modcods, decoding is not possible, therefore, single user detection is not possible on one hand, but on the other hand, interference cancellation does not kick

in since the receiver can't decode the interfering signal either.

These results motivated the seek for an alternative solution, with respect to traditional interference cancellation, which is presented in the next section.

### **2.3.2.2 Interference Cancellation Based on ModCod Unbalance**

Since traditional interference cancellation in practical forward link scenario such as case 1 and 2 of the considered scenario does not work, or works at most with the same performance of single user detection, due to the fact that the interference is too low to being successfully decoded before the reference signal and bring benefit after cancellation, the main idea, represented in this section, is to devise a modified version of the cancellation algorithm, operating at the system level (or at the scheduling layer of the system) to generate an element of distinction between the signals, so that the cancellation process can work.

All the results and considerations made so far in this analysis have been based on the assumption that, besides the C/I definitions for the scenario under analysis, all the signals use the same modcod.

The above mentioned distinction can be achieved by forcing neighbouring beams not to use the same modcod: in particular, it is considered the case in which the interfering signal uses a more protected modcod. In the considered algorithm, the reference signal uses a QPSK 1/2 modcod, and the main interferer uses a QPSK 1/4 modcod (more protected). Considering figure 2.2, when the aggregation of reference signal, interferer 1 and noise, arrives at the receiver, both the reference signal and the interferer decodability is represented by the green curve: this means that the reference signal could never be decoded, since it never gets over the decoding threshold, even for very large SNR, whereas the interfering signal can be decoded after around 1 dB of SNR.

The algorithm is therefore as follows: first the interfering signal is decoded, provided a sufficient SNR (which is more likely, since the interferer uses a very protected modcod) to fall above the decoding threshold. The interferer is therefore removed from the aggregated signal. At this point then, the aggregate signal is made of the reference signal plus the noise, assuming error-free cancellation of the interfering signal, and the second interferer.

This means that the reference signal decodability, after the first decoding and cancellation iteration, is represented by the purple curve, referring to the case in which interference cancellation is successfully performed on the first interferer. At

this stage therefore, the reference signal can be decoded, as indicated by figure 2.2, therefore allowing the system to operate in a condition where it would not otherwise.

The performance of interference cancellation based on ModCod Unbalance is reported in figure 2.9, in which the black curves represent different modcods behaviour in the case of no interference, the rightmost curves, green line with triangle marker and blue solid line, represent the case of no interference cancellation in presence of interferers as per Case 1 of the considered scenario.

Notably, the blue and green lines with square markers, represent the performance of QPSK 1/2 and QPSK 2/3 at the reference user, after a cancellation phase in which the first interferer has been remove successfully. In this case the reference signal can be decoded thanks to interference cancellation, whereas without any interference management this would not be possible. The degradation with respect to the case of no interference is acceptable being 0.5 dB for QPSK 1/2 and around 1 dB for QPSK 2/3 (both cases referring to the interfering signal using QPSK 1/4), and being mainly due to the residual presence of the second interferer that cannot be decoded and therefore does not enter the interference cancellation process.

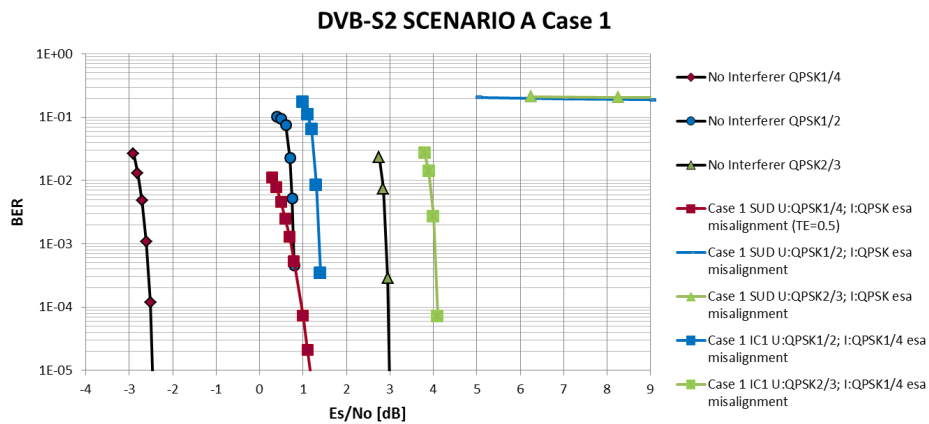


Figure 2.9: BER performance for Case 1 using different MODCOD for Reference Signal and Interferers

It is interesting also to note that similar results can be achieved by forcing an unbalance in power, meaning that different beams transmit different power levels. This is a different way of implementing the same strategy, that aims at allowing reference signal and interferers to have different operating decoding thresholds: in the case of ModCod Unbalance, the thresholds are adapted since different modcods are chosen, whereas in the case of Power Unbalance, the same modcod can still be

used since the unbalance is in power, therefore one of the two signals (the interferer to be compliant to the modcod unbalance example) can be above the threshold allowing decoding and cancellation.

Other research interests on this subject are being posed on pure Multi-User Detection, mainly considering that the typical drawback of optimal joint detection approaches is the complexity at the receiver, and that in this case this might not be an issue, since the number of signals to be decoded is very limited (up to 3 signals if considering both interferers in this scenario). Examples of this approaches are based on specific instances of the Sum-Product algorithm and on Factor Graphs, implementing a Soft Input Soft Output (SISO) receiver and are found in [42] and references therein.

## 2.4 Results Summary

In this chapter, the analysis of interference cancellation strategies reported in chapter 1 has been extended to the case of the forward link of a satellite system. Due to the peculiarity of this scenario, it was shown that interference is generated in a different way than in the return link, and that interference cancellation cannot be applied in the same fashion since in the forward link the end of the transmission is the terminal (as opposed to the gateway, in the return link), that is only interested in decoding the reference signal. A detailed analysis of the scenario and a physical layer analysis of the decodability of reference and interfering signals has been presented, the main outcome of which was acknowledging the fact that interference cancellation cannot be implemented as in the return link.

This issue was overcome by the proposition of a modified version of the interference cancellation algorithm, based on ModCod (or Power) unbalance: in this case it is shown that interference cancellation is still beneficial to the system, at physical layer. The impact of such interference management on the overall system throughput is strictly related on the design of the ModCod allocation (if fixed) or scheduling (if it is designed to change dynamically).

The results presented in this chapter clearly show that thanks to the proposed technique it is possible to decode a ModCod that would otherwise be undecodable due to severe interference in the practical scenario, and this technique is particularly beneficial in limited transfer rate applications.

## Acknowledgements

The activity reported in this chapter has been performed in the context of ESA Study "Next Generation Waveforms for Satellite Systems".

# Chapter 3

## Interference Management for the TT&C component of a SatCom System: Receiver Design for a BFSK-FFH Control Channel

In this chapter, Interference Management is considered, according to the mentioned top-down approach, at intra-receiver level. In fact in this chapter a specific application case is considered, related to the Telemetry, Tracking and Control subsystem and the corresponding communication link. This is therefore a specific case which does not refer necessarily to a multi-beam scenario, but rather to a satellite system more in general, but in which the main focus is still dealing with interference, only from a different perspective, which motivates it being reported in Part I of this thesis.

The Telemetry, Tracking, and Control (TT&C) subsystem of a satellite is designed to establish a connection between the satellite itself and the ground stations. The purpose of this subsystem is to monitor the satellite and make sure that it behaves as expected. Among the main tasks carried out by the TT&C subsystem there is the constant monitoring of data coming from other elements of the platform, such as to track the health of the satellite, as well as precise positioning and other features. Recent research interests have been posed into the design of the next generation communication channels for the TT&C subsystem.

In this context, a particularly suitable waveform for operating in presence of

interference is the FSK-FFH (Frequency Shift Keying - Fast Frequency Hopping) [43]. The advantage of Frequency Hopping lies essentially in providing frequency diversity, i.e. different replicas of the same signal, since some of them are likely to be unaffected by the interference. Similarly, the advantage of FSK is given by its non-coherent detector, which does not require the estimation of channel parameters, since this task is particularly difficult in presence of strong interference.

Several improvements were studied with respect to the classical FSK-FFH demodulator [44], [45]. These improvements provide an increased robustness with respect to the interference while requiring a very slight complexity increase. The authors of [46], on the other hand, follow a different approach, i.e. reducing the complexity of the ML (maximum likelihood) demodulator for jammed FSK-FFH signals [47], in the same way the authors of [48] have done with respect to the ML demodulator for AWGN only.

In the proposed approach, which holds some of the advantages of [44], performance is enhanced by examining the energy values on both the BFSK demodulator branches before the accumulation stages. The following sections describe the proposed demodulator. Assuming BFSK as the reference modulation, Section 3.1 presents the system model, Section 3.2 briefly introduces the reference existing technique [44], then presenting the details of the novel approach proposed, Section 3.3 provides numerical results showing the performance of the proposed demodulator, and results are summarized in Section 3.4.

### 3.1 System Model

The reference system model for this work is based on Binary FSK (BFSK) modulation, in combination with Frequency Hopping as baseline countermeasure against the effects of the intentional jamming. Information bits are mapped on binary symbols denoted by  $d_j \in \{-1, +1\}$ , each corresponding to a tone on either frequency  $f_0$  or frequency  $f_1$ , and it will be assumed, in the following, that binary data are mapped to FSK tones as

$$d_j = -1 \rightarrow f_0 \quad d_j = 1 \rightarrow f_1$$

The frequency separation  $\Delta f$  between the two BFSK frequencies has to be chosen such as to ensure orthogonality between the two tones: for FFH it can be written

$$\Delta f = \frac{1}{T_H}$$

in which  $T_H$  represents the time interval between two hops (i.e. the duration of a single hop). Using FH implies that the frequency bin corresponding to the BFSK tones is free to move in the frequency domain, according to some pseudo-random pattern defined in a sequence. Fast Frequency Hopping (FFH) has been considered in this work, which means considering a number of hops per symbol  $N_{HS} \geq 2$ , since this allows the exploitation of diversity receptions.

The complex envelope of the BFSK-FFH modulated signal can be expressed as

$$s(t) = \sum_{i=-\infty}^{\infty} \exp \left[ j2\pi \left( \frac{\Delta f}{2} d_{\lfloor \frac{i}{N_{HS}} \rfloor} + \Delta f_H c_i \right) t + j\phi_i \right] \text{rect} \left( \frac{t}{T_H} - i \right) \quad (3.1)$$

where

$$\text{rect}(x) = \begin{cases} 1 & x \in \left[-\frac{1}{2}, \frac{1}{2}\right] \\ 0 & \text{elsewhere} \end{cases}$$

and the summation in Eq 3.1 is over the hop intervals<sup>1</sup>  $i$ . The frequency hopping is taken into account by the bin spacing  $\Delta f_H$ , while  $c_i$ , the bin number, is randomly drawn for each hop from the set

$$\mathcal{C} = \left\{ \frac{-N_B + 1}{2}, \frac{-N_B + 3}{2}, \dots, \frac{N_B - 3}{2}, \frac{N_B - 1}{2} \right\}$$

where  $N_B$  is the total number of FFH bins. Finally,  $\phi_i$  represents a phase term which can vary hop-by-hop.

Note that there are no constraints in terms of FH bin separation ( $\Delta f_H$ ), and two strategies are presented in the literature [16]: overlapped and non-overlapped tone allocation. The former strategy adopts  $\Delta f_H = \Delta f$ , such that one tone can be  $f_1$  for a bin, and  $f_0$  for the successive bin; on the contrary, the latter strategy presents a clear distinction between  $f_0$  and  $f_1$  tones, requiring  $\Delta f_H = 2\Delta f$ . In this study the second strategy has been adopted.

For what concerns the Jammer, it is assumed to have perfect knowledge of the system, except for the hopping sequence, which is the key element of the envisaged interference mitigation strategy.

The reference Jamming signal model used in this work is that of Continuous Wave (CW) multi-tone Jammer, which can be seen as a sum of  $N_{int}$  sinusoidal tones which can periodically change frequency, according to a hopping pattern, as it happens for the useful signal, therefore the CW Jammer can be assumed as an

<sup>1</sup>assuming that hopping intervals and symbol intervals are synchronous, for the symbol time  $j$ , then  $j = \lfloor i/N_{HS} \rfloor$

hopping Jammer with hopping rate having the same order of magnitude of the useful signal. Moreover, for simplicity, the assumption was made that the Jammer hopping instants are perfectly synchronized (in time) with the useful signal ones and that it can use, as interference tones, only the frequency range used as FSK-FH tone set. This assumption assures perfect orthogonality between FSK-FH tones and Jamming tones, leading to an error probability depending only on the distribution of hopping sequence.

As a reference, the analytical expression of the probability of error for the CW Jammer is provided for the case of negligible noise contribution (i.e., the system is interference limited), and with CW jamming tones, each having power just higher than the useful signal tones, as derived in [16]. This means that in a jammed chip, a slightly higher energy is fed into the accumulator on the wrong FSK tone branch. This probability equals to

$$P_e = \left( \frac{N_{int}}{2N_B} \right)^{N_{HS}} \quad (3.2)$$

which takes into account that an error occurs when a Jammer tone falls onto the complementary FSK frequency of a FSK bin, with respect to the useful tone, in all the diversity receptions (i.e., in all the hops). This latter aspect motivates the exponent term, whereas the base term takes into account the probability of the jammer falling on the bin where there is no signal, which is 1/2 in a regular FSK system, and on top of which the number of FFH bins must be taken into account. Finally the fact that there is more than one interferer is taken into account. Indeed, in the case of having  $N_{HS}$  ties between useful signal and jammer, even a  $N_{HS}$ -fold diversity cannot protect the desired signal, causing the useful information to be lost. However, this event's probability is now reduced with respect to the same probability for a non-hopped reception, exponentially depending on  $N_{HS}$ .

## 3.2 Double-Threshold Demodulator

The classical FSK-FFH demodulator takes as input the energy values measured on each FSK branch, and then feeds it to an accumulator. After the accumulation, carried out over all the diversity receptions (i.e., all the hops), the decision is made in favor of the frequency, thus the symbol, corresponding to the branch with the highest accumulated energy.

In this study an enhanced demodulator is proposed, which can achieve better protection against the jammer, even in severe jamming condition, with respect to

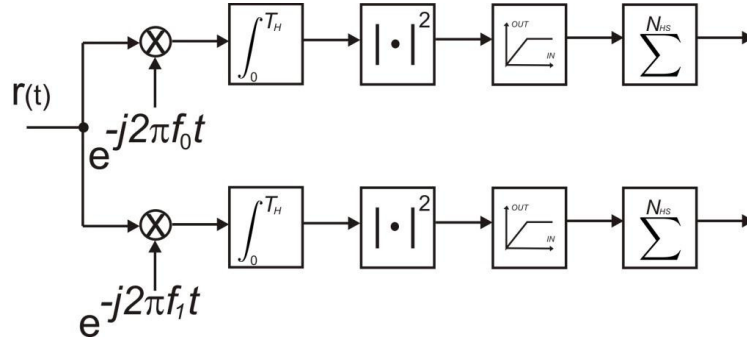


Figure 3.1: Clipper Demodulator

existing receivers. Prior to introducing the proposed technique, a classical improvement to the baseline FSK-FFH receiver is presented.

### 3.2.1 Clipped-Linear Combining

In [44], the classical BFSK-FFH demodulator resilience to intentional interferers is improved by means of a clipping stage, operating on both the BFSK branches. The aim of the clipping operation is to cut the maximum energy per chip which is fed into the accumulation block, to avoid those cases in which jammed chips accumulate enough energy on the wrong FSK frequency that the useful symbol is lost. In fact the useful energy per symbol ( $E_s$ ) is  $N_{HS}$  times the energy per chip ( $E_c$ ), whereas the jamming energy over a single chip can be much higher than  $E_s$ , depending on the jamming power. By clipping the energy of all the FSK branches to some optimized value (i.e., a threshold) less than or equal to the useful signal chip energy, a jammed chip is only affected by a so-called *tie* situation, in which the same energy is accumulated on both branches of a BFSK modulation. In this way, a jammed chip will not affect the decision process, and the demodulator will leverage on the other diversity receptions (i.e. the other chips). Errors occur when there is a tie (i.e. when same energy is detected on both demodulator branches) in every chip, this event being the more unlikely the larger the number of hops per symbol ( $N_{HS}$ ).

A pictorial representation of the BFSK-FFH clipper demodulator is given in Fig. 3.1. The received signal  $r(t)$  is sent to two branches, each corresponding to a BFSK tone, and the correlation of the received signal with both the possible FSK tones is calculated. This could result in high energy values, measured at the output of each correlator, due to either presence of useful signal tone, presence of jamming, or superimposition of both. These energy values are then clipped to a threshold, and

then sent to the accumulator stage. The demodulator makes a decision in favor of the branch, i.e. the FSK tone, which shows the higher energy.

Note that, in this way, the expression of the probability of error in Eq.3.2 is scaled by a factor 2 as

$$P_e = \frac{1}{2} \left( \frac{N_{int}}{2N_B} \right)^{N_{HS}} \quad (3.3)$$

This is due to the fact that in presence of a tie in all the hops, having the same value at the output of the accumulator on both branches, the Clipper receiver chooses randomly the detected symbol with equal probability.

### 3.2.2 Double-Threshold approach

The proposed demodulator represents an improvement of the existing one presented above since it exploits more of the available information, i.e. it considers the energy values of both branches for each chip at the same time.

If the useful signal is present on a tone and a high power jammer is present on the other tone of the same BFSK bin, a clipper demodulator would face a tie because the same value, due to thresholding, would be accumulated on both branches, while a second threshold (which gives the *Double-Threshold* receiver its name) can instead improve the performance, since the presence of the jamming can be detected with more accuracy by the second threshold comparison for both BFSK branches. Once the jammer has been detected, the signal on a BFSK branch can be either blanked out or threshold-limited, based on the value of the energy on the other BFSK branch.

The Double-Threshold Demodulator block diagram can be shaped as in Figure 3.2, in which a logic unit is in charge of feeding the accumulators of both branches with the most suitable value, operating accordingly to Table 3.1, and based on the energy measured on the FSK tones.

If a tone energy is above the higher threshold and the other one is below the lower threshold, then the accumulation is performed as in the clipper demodulator. On the other hand, the difference with respect to the clipper is twofold: first, if both tones show energy levels between the two thresholds, one of them is likely to have been jammed, and then both are nulled out, to avoid jammed tones to affect the combining statistics; secondly, if a tone energy is above the higher threshold and the other tone energy is between the two thresholds, only the second one is accumulated, since the first one is believed to be affected by the jammer.

In this case the optimization of the threshold values is an important issue, since it can affect the performance. The lower threshold can be optimized according to

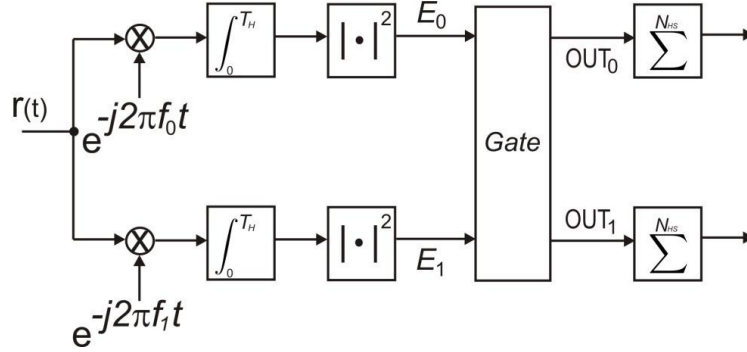


Figure 3.2: Double-Threshold Demodulator

the same criterion used for the Clipper, while the upper threshold requires different considerations: first of all, it has to be larger than the useful signal chip expected energy  $E_c$  and lower than jammer energy per tone. However if the threshold does not respect this last constraint, the demodulator performance does not worsen with respect to the clipper, therefore the sensitivity to the upper threshold value is not high. Nevertheless, for a good performance, this threshold must be adapted to the Jammer power. In this study the following expression has been considered

$$\xi_U = E_c + \frac{1}{\alpha} \frac{J/S}{N_{int}} \quad (3.4)$$

which shows that the threshold is set to an higher value when the jammer is more relevant, i.e. when the jammer-to-signal  $J/S$  ratio is higher. The rationale behind this strategy is that if the jammer has higher energy, it is more easily distinguishable from the useful signal energy, thus the higher threshold can be set significantly far from the lower one, while still ensuring that the jammer presence is detected. Note that hereby  $J/S$  is intended as overall, i.e.  $J$  is the overall jamming tones power, this being the reason for introducing the parameter  $N_{int}$  in Eq 3.4. The additive constant value  $E_c$  is used to set a lower bound for the threshold, to prevent it from falling under the value of the lower threshold in the case of high jammer-to-signal ratios (or jammer absence), and  $\alpha$  is an optimization parameter. Tuning runs of the simulator have suggested the use of  $\alpha = 3$  for this implementation, since this is the value that has lead to the overall best performance in terms of BER. This is due to the fact that, as it has been observed by simulation, tuning both thresholds affects different ranges of  $J/S$  in different ways, in some cases bringing benefits, in others worsening the performance.

Table 3.1: Description of the Logic Unit of the Double-Threshold Demodulator

$E_0$	$E_1$	$OUT_0$	$OUT_1$
$E_0 < \xi_L$	$E_1 < \xi_L$	$E_0$	$E_1$
$E_0 < \xi_L$	$\xi_L \leq E_1 < \xi_U$	$E_0$	$E_1$
$E_0 < \xi_L$	$E_1 \geq \xi_U$	$E_0$	$\xi_L$
$\xi_L \leq E_0 < \xi_U$	$E_1 < \xi_L$	$E_0$	$E_1$
$\xi_L \leq E_0 < \xi_U$	$\xi_L \leq E_1 < \xi_U$	0	0
$\xi_L \leq E_0 < \xi_U$	$E_1 \geq \xi_U$	$E_0$	0
$E_0 \geq \xi_U$	$E_1 < \xi_L$	$\xi_L$	$E_1$
$E_0 \geq \xi_U$	$\xi_L \leq E_1 < \xi_U$	0	$E_1$
$E_0 \geq \xi_U$	$E_1 \geq \xi_U$	0	0

Table 3.2: Simulation scenario

Parameter	Value
Total Bandwidth	1 MHz
Bit-Rate	5 kbit/s
Hop-rate	25 khop/s
FFH bins type	non-overlapping
FFH bins number	20
Number of interfering tones	5
J/S	20 dB

### 3.3 Performance Analysis

The proposed demodulation scheme shows its effectiveness when operating with high jammer to signal ratio ( $J/S$ ), since in such cases jammed chips present a high energy and can be easily discarded by the double-threshold demodulator, while the values accumulated by a clipper demodulator would affect the decision statistics, leading to errors.

In order to evaluate the improvement of the Double Threshold demodulator, an uncoded BER performance comparison is presented in Figure 3.3, considering as a reference scenario the simulation parameters reported in Table 3.2

The solid line represents the performance in case of no jammer and standard FSK-FFH receiver. The squares marked line shows the improvements the proposed demodulator yields with respect to the linear clipped combining receiver (triangles

marked line) in the considered scenario. More precisely, a gain of around 2 dB is achieved at a BER of  $10^{-3}$ , but the gain is significantly larger in higher SNR ranges. In fact Figure 3.3 also shows that the Clipper receiver's performance converges, as  $E_s/N_0$  grows, to the theoretical expression given in Eq. 3.3, represented by the dashed line, and which represent the performance floor given by the presence of interferers. This is not the case for the proposed demodulator, which instead, does not show a lower bounded performance curve, since the interferers effects are, at least partially, nulled out. This translates into a gain of around 4 dB at a BER of  $10^{-4}$  and an even larger gain for higher SNR, considering that there is no longer a performance floor. For instance, it can be noticed that the performance curve of the Clipper receiver does not even reach a BER of  $10^{-5}$ .

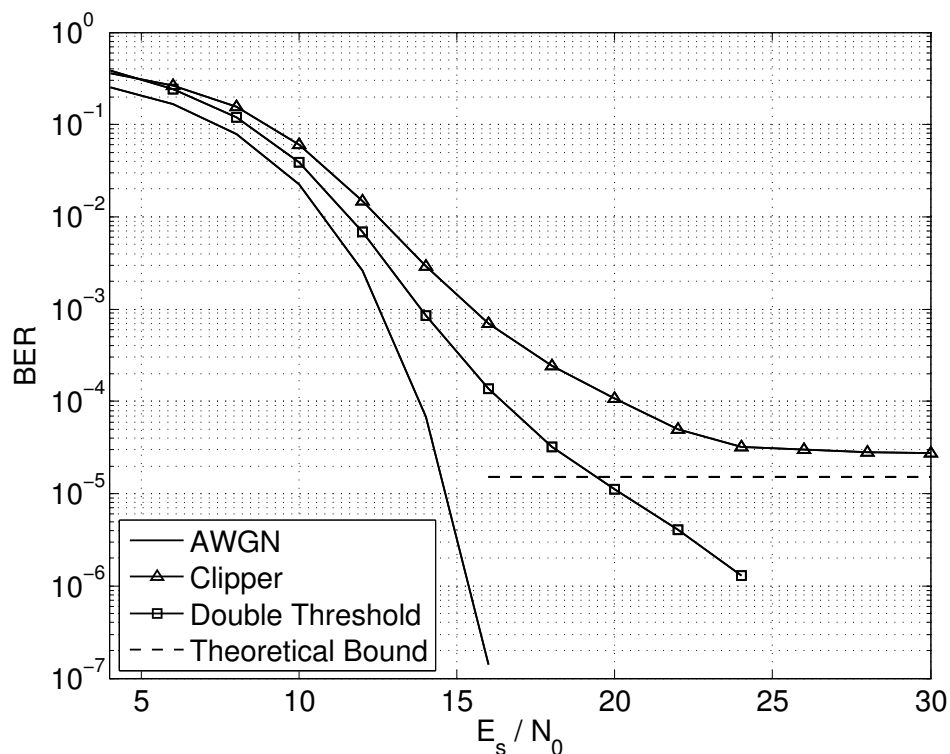


Figure 3.3: BER performance with 5 interference tones, 5 hops per symbol, 20 frequency bins, and  $J/S = 20$  dB

The Double Threshold receiver, then, outperforms the Clipper Demodulator with a significant BER improvement in the range of high Jammer which is the intended scenario for such receiver. On the other hand, this receiver's advantages become progressively lower or null, when the level of the single interferer is close to the

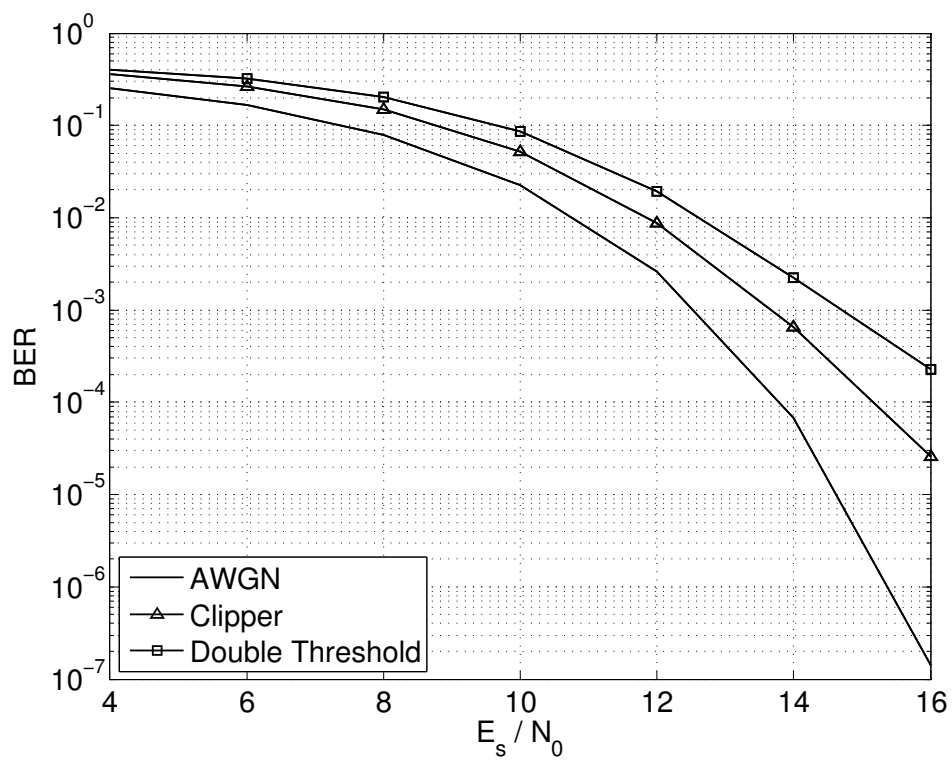


Figure 3.4: BER performance with 5 interference tones, 5 hops per symbol, 20 frequency bins, and  $J/S = 3$  dB

level of the useful tone. In fact, it is easy to understand that the worst case for the presented Double Threshold demodulator is the case of the useful tone and the jammer being at exactly the same level, hence the performance degradation towards that critical point, which is however outside of the target scenario of application for this receiver.

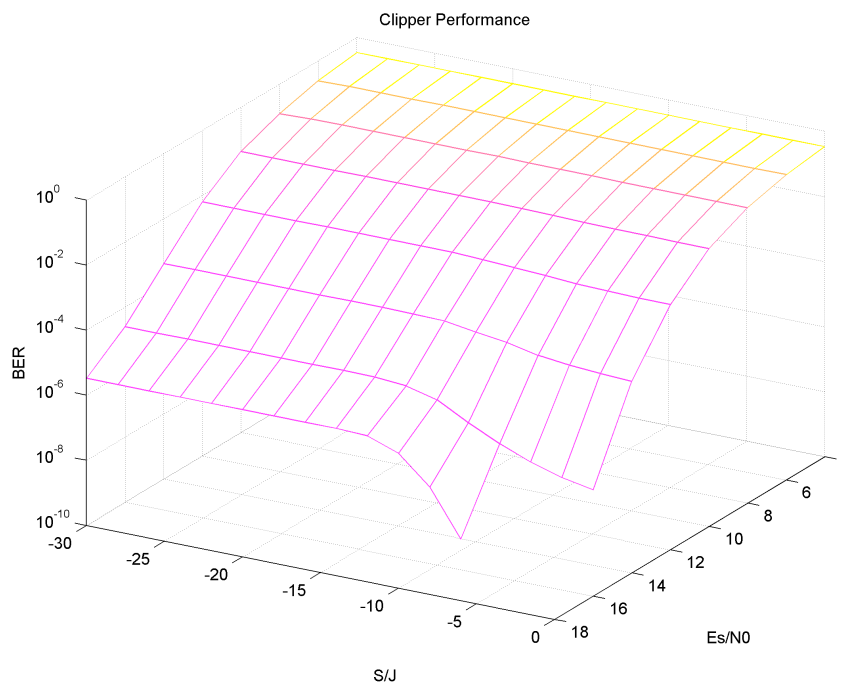


Figure 3.5: Clipper Demodulator Behaviour: Full Range Analysis

However, even in this case, when the jammer is not particularly strong, i.e., it is not appreciably higher in level than the useful signal, the presented technique still performs very closely to the clipped linear combining receiver. This means that this anti-jammer strategy does not particularly suffer cases outside its design scenario. This is shown in Figure 3.4, in which the case of low  $J/S$  is considered, since it represents a potential issue for such receiver because the interferer level might be very close to the useful signal, making it difficult for the demodulator to distinguish and take a hard decision based on the thresholds. In this case in fact a low  $J/S$  has been considered, while all the other parameters have been kept to the values already listed above. As it can be observed, the gap between the Clipper receiver and the proposed demodulator in this condition is less than 1 dB in this case, whereas for high  $J/S$  values there is a significantly larger gain. This can be better appreciated by

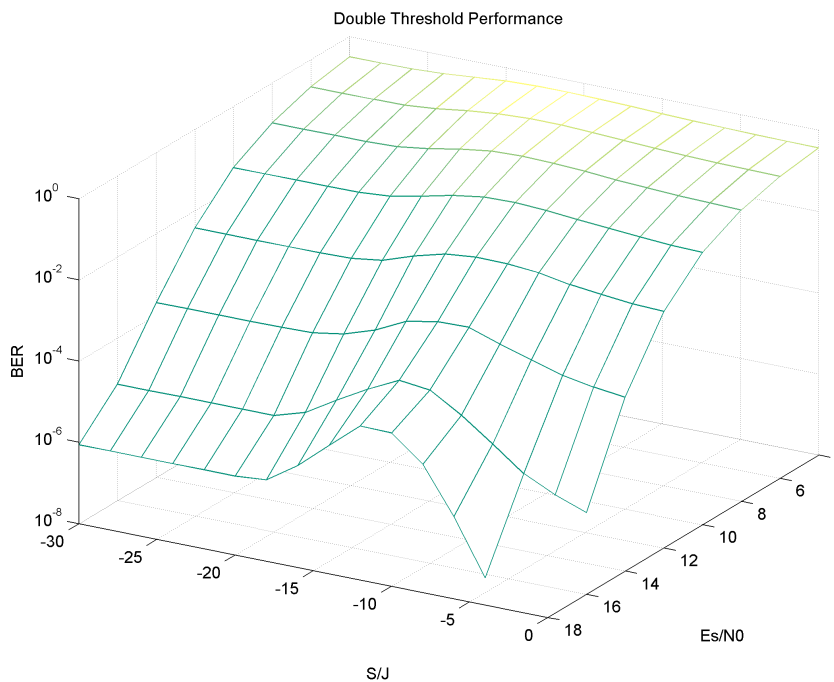


Figure 3.6: Double Threshold Demodulator Behaviour: Full Range Analysis

comparing the full range behaviour of both the Clipper and the Double Threshold Demodulators, in Figure 3.5 and 3.6, where the Bit Error Rate is shown in a 3D plot, with respect to both the SNR and the J/S. It can be seen that the double threshold demodulator begins to suffer a performance degradation towards the -10 dB region in S/J (inverted J/S, here used for sake of plot readability). In fact, a -10 S/J ratio (corresponding to a 10dB J/S) means that the aggregate interference power is 10 dB higher than the useful signal, which, spreading across 5 interfering tones (assuming equal power for interferers) becomes 3dB of J/S per-tone, as considered in Figure 3.4.

Therefore the double threshold receiver, appears to be the best performing technique for high J/S since it discards the chips above the second threshold (which must be set to a high value, to discard the chips which are most likely to have been hit by the jammer). This is due to the underlying principle on which it is based, which is to examine both branches before accumulating the energy. The mentioned non-monotonous behavior of double-threshold demodulator performance with respect to the J/S can be justified considering that the circuit has been devised for an high J/S scenario, while for lower J/S, the threshold values may require a different op-

timization to avoid the intermediate range of values in which the double threshold approach shows a penalty with respect to the clipper demodulator.

### **3.4 Results Summary**

A novel FSK-FFH demodulator is presented, that outperforms the clipped-linear combining receiver in high J/S scenarios, i.e., in severe jamming conditions, by jointly observing the energy per branch and discarding the chips which are most likely to have been jammed. Performance results indeed show that, by properly setting the thresholds, this circuit is able to achieve better performance in terms of error probability with a negligible complexity increase. Moreover it has been shown that even being designed to work in the above described scenario, this receiver still performs close to the existing technique previously used as countermeasure for jamming (i.e., the Clipper receiver).

This demodulator could be further improved, in future research activities, by providing an optimal expression for both the thresholds. These optimal threshold values will be dependent on the signal-to-noise ratio and the jamming-to-signal ratio, thus the double-threshold demodulator will operate in an adaptive fashion. Furthermore, the behaviour of the double-threshold itself can be modified dynamically, in order to provide the optimal performance with different J/S ranges. For example, the behaviour of the circuit for low J/S could be made more similar to the linear clipper, while for higher J/S the chips affected by the jammer are easily detected and their contribution can be blanked out.

### **Acknowledgements**

This work has been supported in part by ESA Project AO/1-5836/08/NL/JK “Spread Spectrum System for TT&C and Payload Control Links”.



## **Part II**

# **Part II: Waveform Energy Efficiency for SatCom Systems**



As described in Part I of this thesis, one of the key challenges of wireless communications is Efficiency. Although efficiency is typically mainly related to the best exploitation of Spectral Resources, limited by nature, another major aspect in which Efficiency is the ultimate goal for the design stage, is the best use of the available transmission power. This is for different sorts of reasons, starting from the need of extended battery life in mobile scenarios, moving to requirements that may be imposed by regulation or devices capabilities, and also down to the waste of power that might result from non-linearities involved in the system (e.g., Power Amplifiers). Of course this applies to the case of Satellite Communications, in which some aspects are even magnified with respect to terrestrial wireless communications. In fact, sensitivity to such aspects is particularly magnified in specific cases, such as the return link of a satcom system, in which the transmitting end of the communication is the terminal, which is typically equipped with small antennas, which translates in gain loss (with respect to ground stations) in the link budget, and with smaller and cheaper internal components, such as filters and power amplifiers, that make the transmission suffer for more severe nuisances. This rationale extends also to emerging scenarios, such as Mesh Networks, in which the idea is to lose the infrastructure of the network, which means operating in absence of a gateway and other central control entities, in order to allow direct (one-hop) connectivity between peer terminals via the satellite. This is very important in a number of applications related to emergency scenarios and disaster recovery situations, in which terrestrial links might be unavailable, including terrestrial components of satellite systems, therefore making Mesh systems a very appealing solution for directly connecting emergency (fixed, mobile or nomadic) facilities with each other and potentially allowing a temporary partial services in the involved area. Obviously, such network topologies can also be of interest for regular use, since, as it will be shown in this part of this thesis, mesh connectivity significantly helps real-time applications, by reducing latency to half. This is achieved thanks to a single hop connection, since it is no longer required an intermediate hop towards the gateway.

This part is organized as follows: first an introduction on Mesh Network Scenarios is given in Chapter 4, providing highlights on the use cases and on the major challenges involved; a detailed link level analysis of waveform trade-offs for mesh satellite networks is reported in Chapter 5, where it is shown that for scenarios in which the transfer rate required is limited, such as Machine to Machine (M2M) applications for instance, waveforms based on constant envelope modulations out-

perform linearly modulated waveforms; building on the previous analysis, the design of new better performing waveforms is proposed in Chapter 6, for application cases in which the main constraints are imposed on the operating SNR, which must be very low, even accepting lower spectral efficiency. To this extent a design of new waveform is carried out for this specific case, which is shown to outperform existing solutions. Results are summarized at the end of the chapter.

# Chapter 4

## Mesh SatCom Networks

An interesting evolution of the future satellite communication systems is the possibility to allow mesh connectivity among user terminals as opposed to star connectivity, which is currently dominant in the market. This will lead to a growth of the satellite market deriving from the enabling of peer-to-peer applications which are currently not well served by satellite networks based on a star topology. A double hop is in fact required for peer-to-peer connections in star networks which doubles the latency and the satellite resources consumption. Such large latency is unacceptable in applications like VoIP, collaborative conferencing (including video, audio and data), cellular systems backhauling, teleconsultation, etc. Mesh approach appears very promising for several market segments including enterprise, government, emergency, e-health, etc.

Notably, mesh connectivity with single beam coverage or fixed/semi-static routing has been already considered and implemented, [49–51]. In the latter case, beam routing is pre-defined or is controlled by the on-ground hub; however this is much slower than that achievable with On Board Processing (OBP), thus limiting the mesh system performance and applicability scenarios. A different approach is pursued by the authors of [52–54], in which on-board switching based on header-only demodulation has been considered and compared in terms of switching flexibility, complexity, spectral efficiency and cost.

This chapter is organized as follows. Section 4.1 describes alternative mesh network solutions, considered as the reference in this chapter, detailing the main on-board features and the related link budgets for each topology, respectively. Section 4.2 presents the trade-off analysis carried out in order to assess the different solutions

in terms of key performance parameters.

This scenarios represent the reference for the analysis carried out in the next chapters.

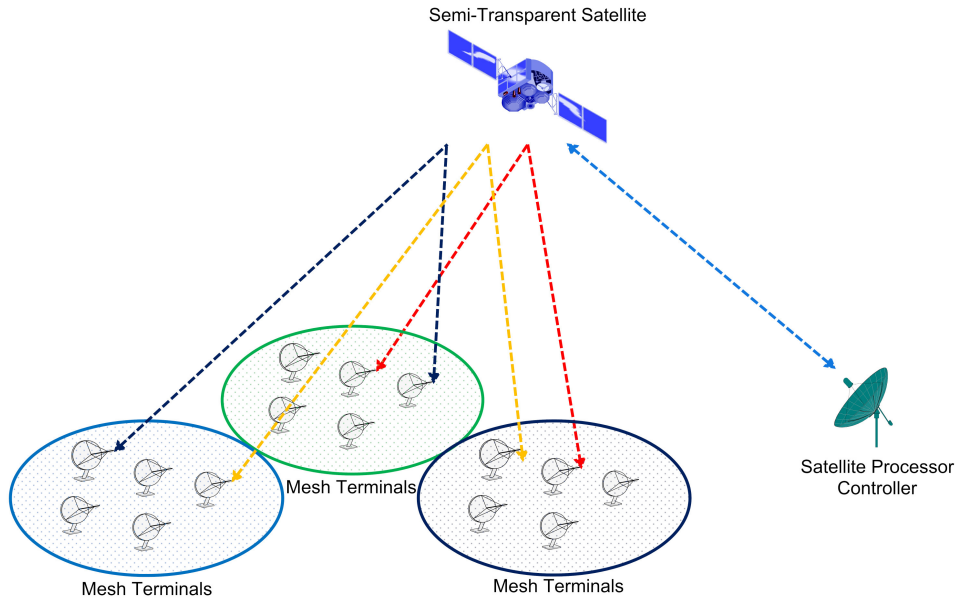


Figure 4.1: Mesh System Scenario

## 4.1 Satellite Mesh Solutions

The reference scenario set for this study is based on both semi-transparent and regenerative satellites with on-board packet processing. This allows full-mesh connectivity between two or more terminals without an on-ground Hub station for routing and controlling traffic, thus implementing a real-time collaborative network, as depicted in Figure 4.1. In order to establish a single-hop connection between two peers without using a gateway, on-board switching capabilities are required. In addition, this halves the transmission delay, which becomes around 300 ms, thus offering quality improvements with respect to a double hop connection. In order to clearly show the advantages coming from each of the analysed strategies, the reference model has been subdivided into several architectures, differing from each other for the resource assignment strategy, but all sharing the goal to optimize the complexity-flexibility trade-off. In this way, the most significant differences between the considered approaches can be shown incrementally.

Alternative Mesh network solutions are presented hereafter:

- **Semi-Static inter-beam interconnection Matrix (SSM)**

In this case, spectral resources are allocated on a semi-static basis, by using a frequency plan that is set up by the Satellite Processor Controller (SPC), thus imposing a fixed routing rule between uplink and downlink beams until a new configuration is provided by the SPC. This translates into reducing the required signalling resources. Unfortunately, in this case a limited number of beams can be effectively managed.
- **Dynamic Selection of inter-beam interconnection Matrix (DSM)**

In this second network solution, a dynamically established slot-by-slot relationship for time-frequency uplink resources and downlink beams is considered, represented by the interconnection matrices. The interconnection matrix is selected by the SPC slot-by-slot. This solution can be implemented in the payload with limited complexity by storing a pool of interconnection matrices. In this case a higher number of beams can be supported.
- **On-board Header Demodulation for packet routing (HD)**

This case represents a trade-off between the fully regenerative and the transparent solutions, since, in this architecture, the satellite is able to demodulate only the signalling which is contained in the headers of the packets, [52]- [53]- [54]. Thus, the satellite can route uplink packets to the corresponding downlink beams, on the base of the received signalling information. This represents a more dynamic solution, pursuing a fully mesh network. In this case, a further increase on the number of beams, yielding an enhancement of the network flexibility.
- **Complete on-board Packet Demodulation (PD)**

In opposition with the first solution, in which the complexity is reduced at the minimum, but the performance is limited by the low degree of the dynamic, in this last case it is assumed a fully regenerative payload. This means that the on-board processing is not only related to the switching, but also to the complete demodulation of the incoming packets. This brings further complexity but allows a regeneration of the signal. Here the satellite is supposed to operate with 64 beams, and the dimensioning is carried out under the hypothesis that the whole system is limited by the link having the worse transmission conditions. This means that the mutual information for the cascade of uplink and downlink is equal to the lower one, and equivalently, the total C/N is lim-

ited by the minimum one. However, this results in higher  $C/N$  with respect to the HD solution, because of the signal regeneration.

Detailed Link-Budgets and parameters for all the above scenarios can be found in [7].

## 4.2 Trade-offs in Mesh SatCom Networks topologies

The four network topologies described in the previous section can be assessed in terms of flexibility, complexity, cost and capacity in order to highlight the strengths and weaknesses of each proposed solution.

One of the most interesting features offered by the proposed architecture schemes is the switching level flexibility. This feature is mandatory to enable a fully meshed satellite network. On the other hand, another crucial aspect that must be carefully addressed in the design of a satellite system is the on-board hardware complexity. Indeed, a high-complex payload may be considered economically unacceptable, and it will be more exposed to hardware failures.

For each of the four network solutions illustrated in Section 4.1, a different trade-off between the offered switching level flexibility and the on-board hardware complexity is reached. As detailed in the following, the different solutions provide an increasing degrees of flexibility at the expense of on-board implementation complexity.

SSM is characterised by the lowest on-board complexity enabling both low complex payload implementations and minimum signalling requirements. On the other hand, the switching flexibility offered by this scheme is limited to the semi-static nature of the resources allocation.

DSM solution deals with this problem by allowing dynamic beam routing. In this case the switching matrix is selected slot-by-slot from a preset alphabet of matrices.

HD and PD solutions enable the highest degree of switching level flexibility, since the header of each packet, containing the routing signalling data is decoded and processed on-board. These solutions enable a fully mesh network connectivity. On the other hand, the full demodulation of the signal will significantly increase the on-board hardware complexity. In order to overcome this problem, HD proposes a semi-transparent payload design where only the headers are decoded so that the amount of digital operation in charge of the payload can be significantly reduced without any loss in term of switching level flexibility.

# Chapter 5

## Waveform trade-offs in Mesh SatCom Systems

In this chapter the focus is moved from the system point of view to the link level, focusing on waveform-level aspects and on the effect of channel impairments and transceivers non-idealities in the selection of the most suitable waveform parameters for Mesh Satellite Systems in the considered scenarios.

This chapter presents a performance assessment carried out in presence of real-life channel imperfections, i.e., adjacent channel interference, phase noise, and frequency offset, or transmitter non-linearities. Particularly this latter aspect is greatly magnified in mesh systems, since both ends of the communication link will be terminals, which implies that a small antenna will be used. This is different to a conventional 2-hop satellite link in which one end is a terminal and the other is typically a Gateway, i.e., an earth station, equipped with significantly larger antennas. Indeed, in a double hop link the antenna gateway, that acts as receiving antenna in the first hop and as transmitting antenna in the second hop, is typically characterized by an extremely large gain, that makes the link budget challenges be easier to cope with. In a single hop, like a mesh link, the communication link terminates at both ends at the user terminal that is equipped with a small and low cost antenna. In addition, the need of keeping the terminal cost at a market competitive level imposes also the use of low cost amplifiers at the user side that further make the non-linear distortion effects critical for such applications.

The analysis carried out in this chapter is largely based on seeking a the trade-off between error rate performance, resilience to receiver instabilities, robustness against

non-linearities and achievable spectral efficiency. This is motivated by the fact that, on one hand, linear modulations are able to provide high spectral efficiencies, but suffer from highly varying envelope, which imposes stringent requirements in terms of amplifiers back-off; on the other hand, Continuous Phase Modulations' main feature is having constant envelope, which allows signals not to suffer distortion when fed through a power amplifier, without any need of back-off. This directly translates in power savings, but at the expense of a limited spectral efficiency.

## 5.1 Reference Scenario

The reference system on which this analysis is based, is the mesh scenario presented depicted in Figure 4.1, as described in chapter 4 [7]. More in detail, semi-regenerative capabilities are taken as a reference for the satellite segment [52–54], in order to achieve full-mesh connectivity of multiple terminals in complete absence of ground stations like Hub or Gateways.

The satellite HPA is set to operate in linear region, in order to prevent non-linear distortion on the multiplex of signal presented to its input, that would affect the frequency orthogonality, i.e., users separation. On the other hand, user terminals implement low cost HPAs, set at a working point as close as possible to compression. Therefore, both in-band distortion and out-of-band spectral regrowth can be easily generated at the user side of the transmission chain.

As mentioned, this study compares the behaviour in the above Mesh scenario of Linear Modulation and Continuous Phase Modulation based waveforms, by taking actual real-life waveform parameter sets, as defined in the new DVB-RCS2 standard [55]. The choice of this particular standard is based on the simple consideration that these waveforms have been designed for a mass-market terminal-to-satellite return link, which is very similar in its characteristics to each link of a single hop mesh network. On top of this, to keep the analysis as realistic as possible, channel impairments considered in this study have been taken from the ones adopted throughout the DVB-RCS2 standardization process, i.e., the frequency error is uniformly distributed over  $[-4kHz, 4kHz]$ , the phase noise model is reported according to what is described in [55]. For what concerns adjacent channel interference (ACI), 6 interferers are considered, all having equal power among them and with respect to the useful signal.

## 5.2 Waveform Solutions

In the following, the alternative link level solutions for the considered link, in terms of waveform are presented, primarily subdivided into Linear and Continuous Phase Modulations.

### 5.2.1 Linear Modulation Waveforms

Waveforms based on Linear modulation schemes as included in the DVB-RCS2 standard are based on QPSK, 8PSK and 16QAM constellations and a 16 circular states turbocode (known also as Turbo- $\Phi$ ) operated in a circular manner with nominal code rate equal to  $1/3$ , whereas, as typical, it is possible to obtain intermediate code rates by means of puncturing. The interleaver is embedded in the turbo encoder and there is a bit ordering specific for each modulation and code-rate combination (ModCod). Overall, by spanning across all tunable variables mentioned, there are 30 possible DVB-RCS2 Linear Modulation (LM) waveforms.

For this analysis two waveforms have been selected as a reference benchmark: QPSK with code rate  $1/3$ , and 8PSK with code rate  $2/3$ , as they are in a range in which it is possible to have a meaningful comparison with CPM counterparts. The complete parameters set is reported in Table 5.1 together with other specific values and simulation parameters used for performance evaluation.

Table 5.1: Linear Modulation Waveform Parameters

DVB-RCS2 Waveform ID	3	8
Modulation	QPSK	8PSK
Code-rate	$1/3$	$2/3$
Packet length (bit)	304	920
Roll-off	0.2	
Spectral efficiency	0.606	1.818
HPA type	Ka-band SSPA	
HPA IBO [dB]	0	4
HPA OBO [dB]	0.422	1.134
Normalized Carrier Spacing	1.1	
Number of Adjacent channels	6	

The spectral efficiency computation is based on the carrier spacing, i.e., the spacing between adjacent channels, therefore the spectral efficiency can be defined

as

$$\frac{r \cdot \log_2(M)}{B_{cs}}$$

where  $M$  is the modulation cardinality,  $r$  is the code-rate and  $B_{cs}$  is the carrier spacing normalized to the symbol-rate.

A first stage of this study is related to finding the most suitable operating point for the user SSPA (Solid State Power Amplifier). To this extent, two criteria have been considered: first, the aim is being compliant with the RCS2 spectral mask [55], second, the minimization of the degradation of the useful signal is sought. The first criterion relates to out of band emissions, which are highlighted by non linear effects but must be kept under control, while the second one aims at minimizing the effect of in-band distortion without excessively reducing the transmit power. For the latter task, the total degradation ( $TD$ ) has been computed, defined as:

$$TD = \Delta SNR + OBO \quad [dB]$$

where  $\Delta SNR$  is the difference (in dB) between the required  $SNR$  (signal-to-noise ratio) for a given quality of service in the scenario under investigation and in a linear channel, and  $OBO$  is the output back-off of the amplifier, defined as the ratio between output saturation power and output average power.

The outcome of this first step in the analysis shows that QPSK has good resilience to non-linearity issues, at least in terms of fulfilling the DVB-RCS2 spectral mask, meaning that no additional back-off is necessary, while still achieving a very low degradation. The most suitable working point in this case is, therefore, the one reported in Table 5.1. Different conclusions are drawn in case of 8PSK: in this case the emission in the nearest adjacent channels has to be limited artificially. This is achieved, in practice, by backing off the working point of the amplifier in order to comply with the spectral mask. Figure 5.1 reports an example of TD plot vs. OBO in the absence and in presence of adjacent channel interference (ACI): as it can be seen, in such a case, the most appropriate working point is shifted to higher OBO values because the total degradation is affected also by the ACI spectral regrowth as well as by the useful signal distortion. Obviously, the TD does not tend to the OBO straight line (as it does in absence of ACI) because the considered OBO range is too low for this asymptotic convergence.

The LM receiver structure, depicted in Figure 5.2, is based on Rife and Boorstyn [56] coarse frequency estimation, modified as in [57] to let the estimator operate on different data fields, and on a Gardner timing estimator [58]. The phase noise

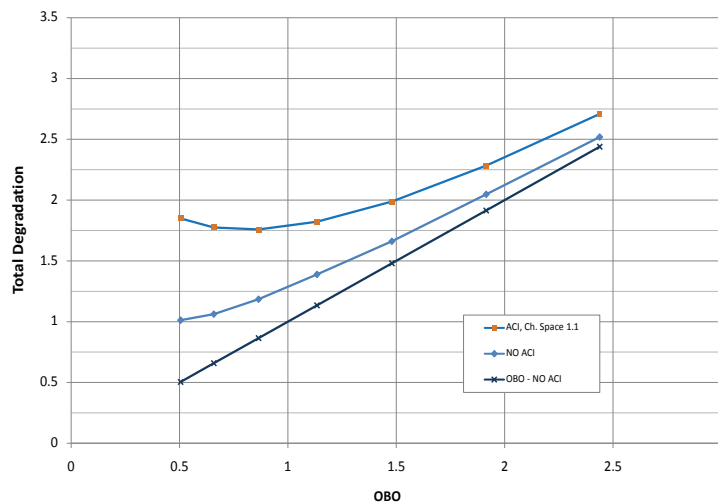


Figure 5.1: Total Degradation analysis for LM waveform 8: 8PSK 2/3

compensation can be performed by a digital phase locked loop (PLL) [59] operating on both known symbols and hard decisions as in [60], or, when necessary, by the CBC demodulation algorithm [61], which yields finer estimation, being thus advisable for high order modulations, at expense of additional complexity.

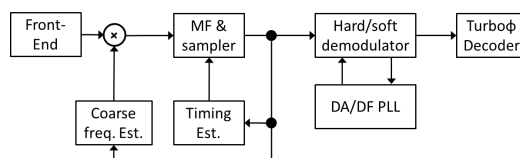


Figure 5.2: Block Diagram of the LM receiver

### 5.2.2 Continuous Phase Modulation Waveforms

The considered partial response CPM schemes, as per DVB-RCS2 [55], are serially concatenated with a convolutional code. This study has started with the analysis of two waveforms which provide spectral efficiencies equal to 0.5 and 1.8 bit/s/Hz. A second step in the analysis has led to investigate also waveforms with intermediate spectral efficiencies, as explained in the following of this chapter. The waveform parameters for all the considered CPM schemes are reported in Table 5.2, in which the pulse type refers to the CPM pulse shape, which is the weighted average (AV) of the raised-cosine (RC) and rectangular (REC) pulse shapes [55], such that

$$g(t) = \alpha_{RC}g_{RC}(t) + (1 - \alpha_{RC})g_{REC}(t) \tag{5.1}$$

Table 5.2: CPM Modulation Waveform Parameters

DVB-RCS2 CPM Waveform ID	3	5	7	8
Pulse Type	Q2AV			
AV Pulse $\alpha_{RC}$	0.98	0.75	0.75	0.625
Modulation index $h$	2/5	2/7	1/4	1/5
Code-rate	1/2	2/3	4/5	6/7
Packet length (bit)	400			
Spectral efficiency	0.5	1.1	1.5	1.8
HPA type	Ka-band SSPA			
HPA IBO [dB]	0			
HPA OBO [dB]	0			
Normalized Carrier Spacing	2	1.21	1.0667	0.974

where both  $g_{RC}(t)$  and  $g_{REC}(t)$  have time support  $0 \leq t \leq 2T$ , and are defined, respectively, as  $g_{RC}(t) = \frac{1}{4T} (1 - \cos \frac{\pi t}{T})$  and  $g_{REC}(t) = \frac{1}{4T}$ .

The CPM signal can, therefore, be written as:

$$s(t) = \cos \left[ 2\pi f_c t + 2\pi h \sum_{k=-\infty}^{\infty} a_k \int_{-\infty}^t g(\tau - kT) d\tau \right] \quad (5.2)$$

where  $f_c$  is the carrier frequency,  $h$  is the CPM modulation index, and  $a_k$  is the data symbol at time interval  $k$ .

Also, due to the CPM waveform constant envelope, the user terminal HPA does not need any input back-off (IBO), hence resulting in no output back-off (OBO).

On the receiver side, in ideal channel conditions, coherent detection based on the Rimoldi decomposition of the CPM signal [62], is performed. When channel impairments are considered, non-coherent detection is performed instead.

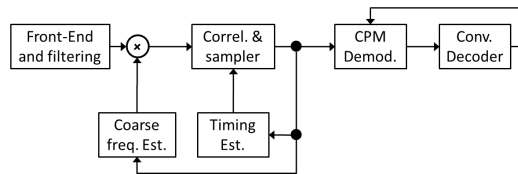


Figure 5.3: Block Diagram of the CPM receiver

The CPM receiver for non-coherent detection is reported in Figure 5.3. It is based on a phase synchronization technique embedded in the BCJR algorithm of the CPM detector leveraging on the Bayesian approach [57], in which a statistical model is

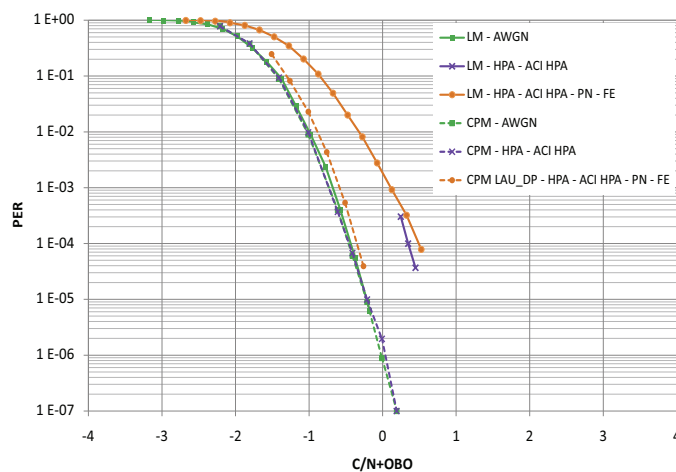


Figure 5.4: PER comparison: LM vs. CPM, RCS2 waveform ID = 3, considering phase noise (PN), frequency errors (FE), and ACI

assumed for the phase noise process. A Laurent decomposition is used [63,64] which is truncated to the first  $M - 1$  components, for complexity reduction, and the phase is discretized into  $R$  values, where  $R$  depends on the CPM modulation index  $h$ . It is worth mentioning that the demodulation process is performed in an iterative fashion together with decoding, yielding a better performance. In addition, the considered CPM non-coherent receiver employs a Rife and Boorstyn coarse frequency estimator [56] and the timing estimator proposed in [65].

### 5.3 Performance Analysis

In the following, numerical simulations of LM and CPM performance are presented and compared in order to draw conclusions for the analysis. In particular, Figure 5.4 and Figure 5.5 show performance in terms of PER (Packet Error Rate) as a function of the overall C/N (carrier to noise ratio) plus OBO for both CPM and LM, and refer to two spectral efficiencies, 0.5 and 1.8 bit/s/Hz, respectively.

In Figure 5.4, considering the square and cross marked lines (both solid and dashed) it can be seen that CPM performs close to QPSK 1/3 in AWGN. When the effect of the user HPA and of the ACI is considered, CPM outperforms LM by around 1 dB (at  $\text{PER} = 10^{-4}$ ). This is due to the fact that CPM waveforms pass undistorted through the user HPAs. This can be appreciated observing the good match between CPM performance with and without HPA and ACI.

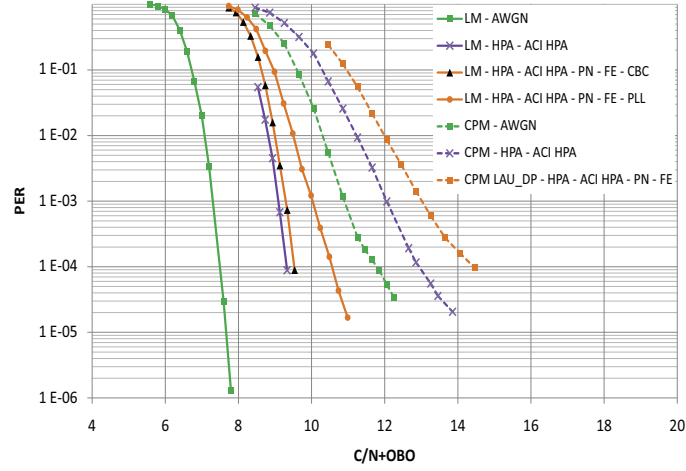


Figure 5.5: PER comparison: LM vs. CPM, RCS2 waveform ID = 8, considering phase noise (PN), frequency errors (FE), and ACI

The analysis is further extended by taking into account receiver instabilities in the performance assessment. Considering the solid and dashed circle marked lines in Figure 5.4, it can be seen that the degradation due to channel impairments is almost negligible, in the order of 0.1 dB for CPM, bringing the CPM advantage on LM to 1.1 dB.

In the same channel conditions, CPM and LM are compared for spectral efficiency of 1.8 bit/s/Hz in Figure 5.5. In this case, CPM shows a significant degradation when ACI is considered because of the tighter spacing between carrier that is needed to reach such high spectral efficiency. On the other hand, the gap between the ideal AWGN case and the case with ACI and HPA is significantly lower for CPM than for LM, implying that CPM waveform can better cope with user HPA non idealities in the characteristics and in the control of the operating point. Regarding LM, on the other hand, the performance improvement obtained by using a CBC demodulator rather than a PLL is about 1 dB at  $\text{PER} = 10^{-4}$ , thus confirming the interest in more robust (although more complex) demodulation schemes for high order constellations.

When channel impairments are also considered, the same considerations hold true: the overall gap from the AWGN performance is larger for LM than for CPM. This observation suggests to investigate the CPM waveform behavior also for intermediate spectral efficiencies in order to assess performance trends of such promising scheme in the considered channel conditions. Figure 5.6 shows a comparison between

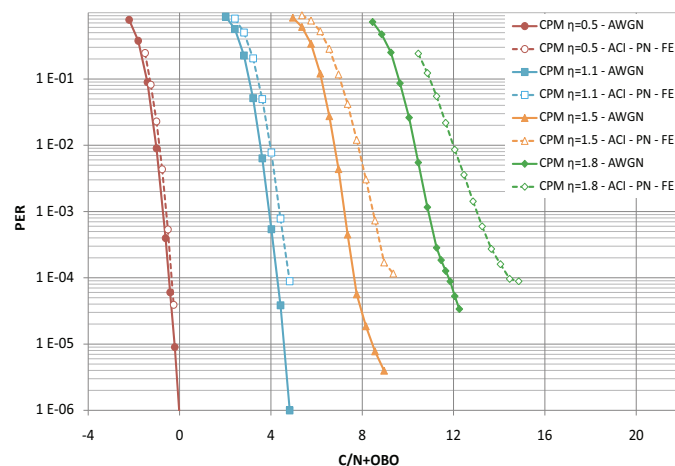


Figure 5.6: CPM waveforms comparison

CPM waveforms for spectral efficiencies  $\eta$  equal to 0.5, 1.1, 1.5, and 1.8 bit/sec/Hz.

As it can be seen, for  $\eta = 1.1$  the degradation coming from ACI and non idealities with respect to AWGN is of the order of 0.4 dB, while for  $\eta = 1.5$  is of around 1 dB. Therefore, both are more resilient to ACI and non idealities than the highest spectral efficiency waveform ( $\eta = 1.8$ ) while still providing significantly better performance in terms of PER. This behaviour can be justified considering that for high SNR the system is ACI-limited rather than AWGN-limited, and that a similar behaviour has been observed in several other studies on CPM modulation, e.g. in [66].

Finally, Figure 5.7 reports all the considered waveforms on the Shannon plane, and it is worthwhile recalling the following ideal conditions assumed for comparison purposes:

- the ACI power is perfectly balanced with the power of the useful signal;
- the ACI HPAs working point is ideally controlled;
- the useful signal HPA working point is the optimal one (i.e., non-ideal SSPA control is neglected).

The above assumptions have a significant impact on the analysis, as they represent an optimistic baseline for the LM performance, hence suggesting that CPM waveforms can be suitable for mesh applications, since such applications are supposed to operate in a low SNR range, and for this case properly designed CPM waveforms do not suffer for any additional degradation due to channel imperfections.

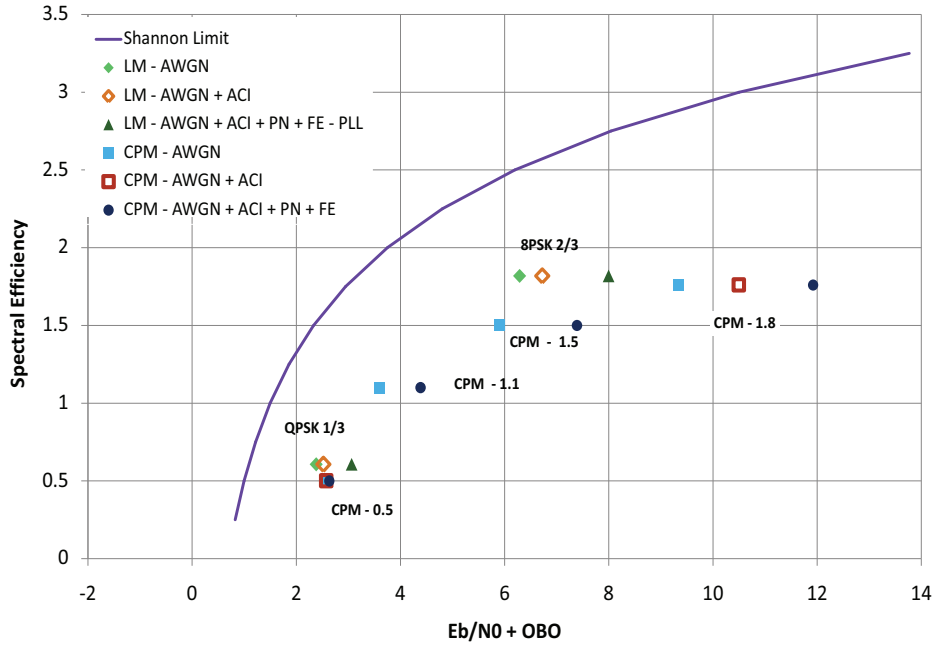


Figure 5.7: Spectral Efficiency: CPM vs. LM comparison

## 5.4 Results Summary

In this chapter an analysis of air interfaces performance into a Mesh satellite scenario was presented. Non-linearities, receivers instabilities, channel imperfections (i.e. user terminal characteristics, phase noise and carrier recovery errors) were taken into account in this analysis, along with the effect of adjacent channel interference (ACI) caused by signals directed to other users but in the same multiplex of signals forwarded to the satellite.

It is shown that CPM is potentially suitable for the Mesh scenario under consideration, since it is more resilient to real-life impairments that affect transmissions for low to medium spectral efficiencies. For high efficiency cases, LM waveforms performs better, thanks to higher cardinality and lower coderate (i.e., better protection of data bits). CPM is however more appealing because, thanks to its constant envelope, is prone to mesh mass-market system characterized by low cost devices that will increase the need of robust and resilient waveforms.

## **Acknowledgment**

This work has been in part supported by the ESA Project n. 4000102296/11 “Cost Effective Satellite Terminals for MESH Overlay Networking”.



# Energy Efficient CPM Waveform Design for SatCom Mesh Systems

The analysis carried out in the previous chapter show that CPM is a good candidate solution for satellite mesh networks with single or multi beams coverage for low to medium spectral efficiencies, due to its constant envelope and its resilience to impairments that affect transmissions, such as Adjacent Channel Interference (ACI), phase noise, uncompensated frequency offset, and transmitter non-linearities. Satellite mesh networks in hub-less configurations are in fact characterized by terminals with a small and low-cost antenna as well as a transmit amplifier with moderate to low output saturated power, which impose several constraints on the link budget.

This chapter considers such power-limited scenarios, in which the main requirement is to fulfill power constraint mainly due to the characteristics of the terminals, translating in imposing a range of useful operating SNR values, in which, thus, the decoding of the signal must be successful. In this context, the attention is drawn to the design of new waveforms to meet the above power constraints, based on CPM since it has been shown that CPM waveforms have advantages in terms of power efficiency with respect to LM alternatives. Note that the ultimate goal is, considering a constraint on the terminal power, to achieve the best performance in terms of Packet Error Rate vs. SNR, at a given spectral efficiency, extending the SNR operating range towards lower SNR with respect to existing DVB-RCS2 waveforms in the most efficient way. This analysis, thus, can have an impact on the definition of applications and services that are feasible, since power constraint are related via the link budget also to antenna size and other characteristics.

The easiest way to obtain a lower spectral efficiency waveform, for instance in order to comply with tight power requirements, is the so-called Burst Repetition (BR) technique, based on transmitting each burst twice over the channel, at least to increase the capabilities of the receiver to successfully detect the signal. This is beneficial, for example, for fading channels, due to the exploitation of time diversity. Since each burst is transmitted two times, a 3dB gain in  $C/N$  is achieved with respect to the conventional single transmission, where  $C$  is the received power of each received replica. Burst repetition therefore produces a 3dB power gain in turn for a 3dB spectral efficiency loss. It must be noted, however, that such gain is not achieved in  $E_b/N_0$ , since  $E_b$  is the average energy per information bit, and although each burst is transmitted twice, the transmitted information content is not increase in the double transmission. Also, the mentioned gain in  $C/N$  is only achievable under the assumption of perfect combining, which involves an ideal channel and timing estimation. Therefore, although attractive, due primarily to the straightforward implementation in an existing standard, is not the optimal one as it does not fully exploit the introduced redundancy.

These considerations have motivated the design of a completely new CPM waveform, which, can be more suitable to cope with challenging requirements imposed by power-limited scenarios, thanks to increased robustness, even if at the expense of lower efficiency.

### 6.1 CPM Scheme Selection

This study's objective is the selection of the most suitable modulation and coding parameters for CPM waveforms to be employed in power-limited scenarios, which typically translates into lower spectral efficiency values with respect to usual operating conditions. In particular, the spectral efficiency value  $\eta = 0.25$  b/s/Hz has been selected. The investigation starts with the selection of the most effective CPM modulation parameters to cope with the mentioned scenario, which are mainly the modulation index  $h$ , the cardinality of the modulation  $M$ , the modulation memory length in symbols  $L$ , the phase pulse type, and the bandwidth normalized to the symbol rate ( $FT$ , where  $F$  is the frequency spacing between two adjacent users and  $T$  is the symbol time). The most effective modulation formats have been first selected by using the information-theoretic analysis described in [66]. A set of binary modulation formats with rectangular (REC) and raised-cosine (RC) frequency pulse

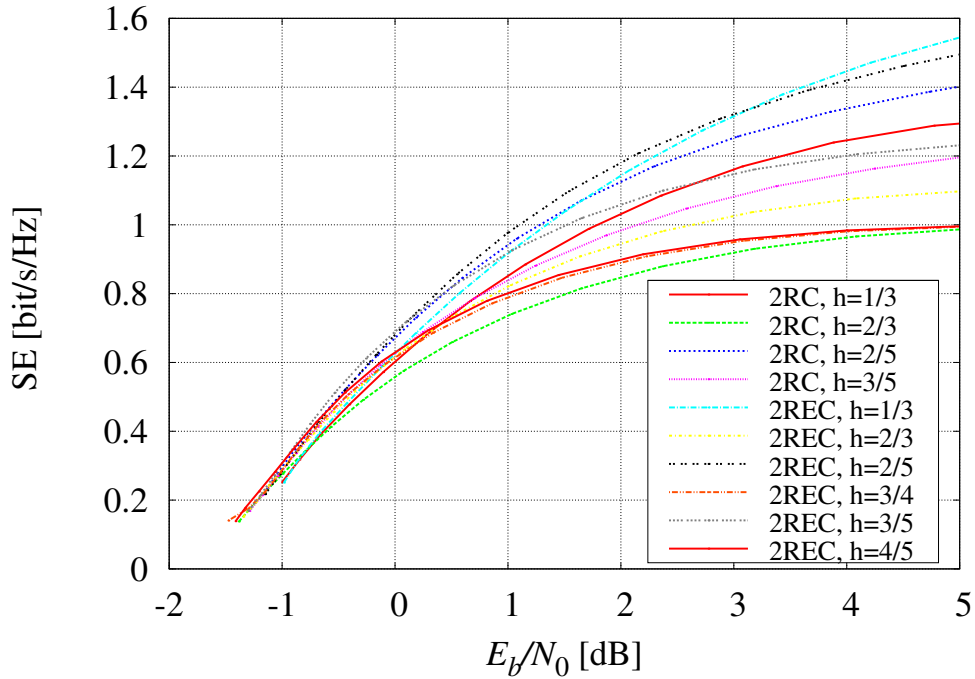


Figure 6.1: Maximum achievable spectral efficiency as a function of  $E_b/N_0$  for different CPM formats.

has been considered, with at most  $L = 2$ , to guarantee that the receiver can be designed by considering the principal component of the Laurent decomposition [63] only, as proved in [67]. For the considered CPM formats, the spectral efficiency versus  $E_b/N_0$  is reported. It is worthwhile pointing out that, when computing the spectral efficiency for a given value  $E_b/N_0$ , it is assumed that adjacent users were present with the same power and the same modulation formats of the useful signal. Also, as in [66], the spacing between two adjacent signals is taken as a measure of the bandwidth, optimized for each CPM modulation format and each  $E_b/N_0$  value. In Fig. 6.1, the maximum achievable Spectral Efficiency (SE) as a function of  $E_b/N_0$  is represented for the selected CPM schemes with REC and RC pulses. From these curves, it can be observed that for low  $E_b/N_0$  values, where the systems are thermal-noise limited, the selected modulation formats have a similar performance in terms of maximum achievable spectral efficiency.

The selected CPM schemes perform similarly for low achievable spectral efficiency values, therefore the selection has been made according to an EXIT chart analysis, following the paradigm provided in [68–70]. This has been done by plotting

Pulse	$h$	Spacing	Code rate
2REC	4/5	1	1/4
2RC	2/3	1	1/4

Table 6.1: Selected CPM modulation formats

the complete EXIT chart for the CPM modulation formats and for several potential convolutional codes. The selection of the most suitable CPM formats has been carried out by neglecting all the formats that would lead to a so-called closed tunnel in the EXIT chart, which means that the iterative decoding process can never reach convergence, and those which, even before selecting the most appropriate Convolutional Code, would show a very narrow tunnel or other characteristics that would imply worse performance of the iterative decoding process, such as higher number of required iterations. The end result of this EXIT chart based selection is represented in Figure 6.2, in which is also the selected CPM formats are reported together with the characteristic of a 16-state and a 4-state convolutional codes. After these two steps, the modulation formats in Table 6.1 have been selected. Notice that the code rate is uniquely determined by the spectral efficiency and the (optimal) channel spacing.

Once the CPM modulation parameters have been determined, the second step has been to seek for the convolutional codes to be concatenated with the selected modulation formats. The investigation based on EXIT charts has been taken as the first step in the code selection. In Fig. 6.2, the two schemes in Table 6.1 are considered and the two rate-1/4 convolutional codes with 16 (generators [21, 23, 27, 31]) and 4 (generators [5, 5, 7, 7]) states, respectively. The EXIT curves for the CPM detector have been computed at  $E_b/N_0 = 1$  dB, which corresponds to a point in the waterfall region of the decoder for the better performing waveforms, as it will be shown, thus is a proper observation point for comparison.

This analysis suggested that 4-state convolutional codes with rate 1/4 shall be considered, since 16-state code would end up, as shown, in a closed tunnel in the EXIT chart (see Fig. 6.2), which as anticipated, results in a crossing between the inner and outer code mutual information characteristics. When this is the case, it is always prevented the possibility of reaching the top-right corner of the EXIT chart throughout the iterative process, which means that some information will always be lost, regardless of the number of iterations allowed. On the contrary, the 4-state code is more powerful in the start of the iterative process, thanks to a wider open

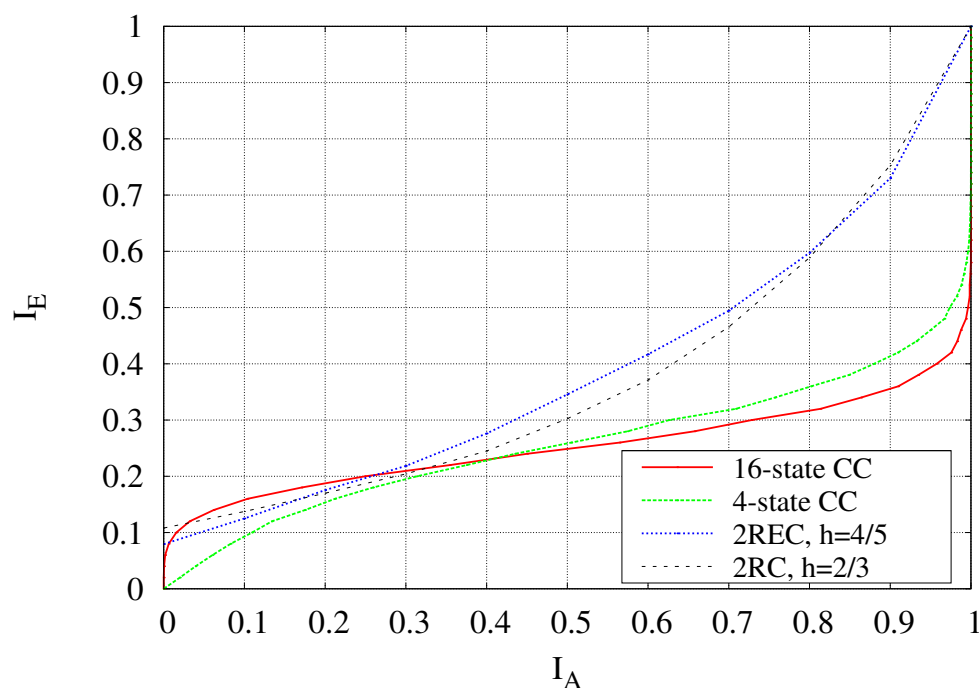


Figure 6.2: EXIT Chart for the two selected CC-CPM schemes with code rate 1/4.

tunnel in the EXIT chart. However, this code can have worse performance in the error floor region with respect to its 16-state counterpart, although EXIT charts investigations are able to only predict the waterfall and not a possible error floor behaviour. Therefore, to cope with this partial unpredictability, PER computer simulations have been carried out, as reported in Fig. 6.3.

Fig. 6.3 shows a comparison between the performance of the CPM waveforms at  $\eta = 0.5$  b/s/Hz spectral efficiency specified in the DVB-RCS2 standard, considered as a reference in this work, and the new waveforms, at  $\eta = 0.25$  b/s/Hz. It can be seen that among the considered waveforms, the best performance is given by the one with the REC pulse and  $h = 4/5$ , by around 0.2 dB both in AWGN and AWGN with ACI. In particular, 6 Adjacent Channel Interferers are considered, with power perfectly balanced with that of the user carrier, i.e., no ACI power unbalance is taken into account. This test has been carried out by considering the code identified by generator polynomials  $[5, 7, 7, 7]$ , that is reported as the optimal code in terms of free distance for that constraint length [71], [72]. On the basis of such results, a further analysis on the selection of the optimal code has been carried out and discussed in detail in the next section.

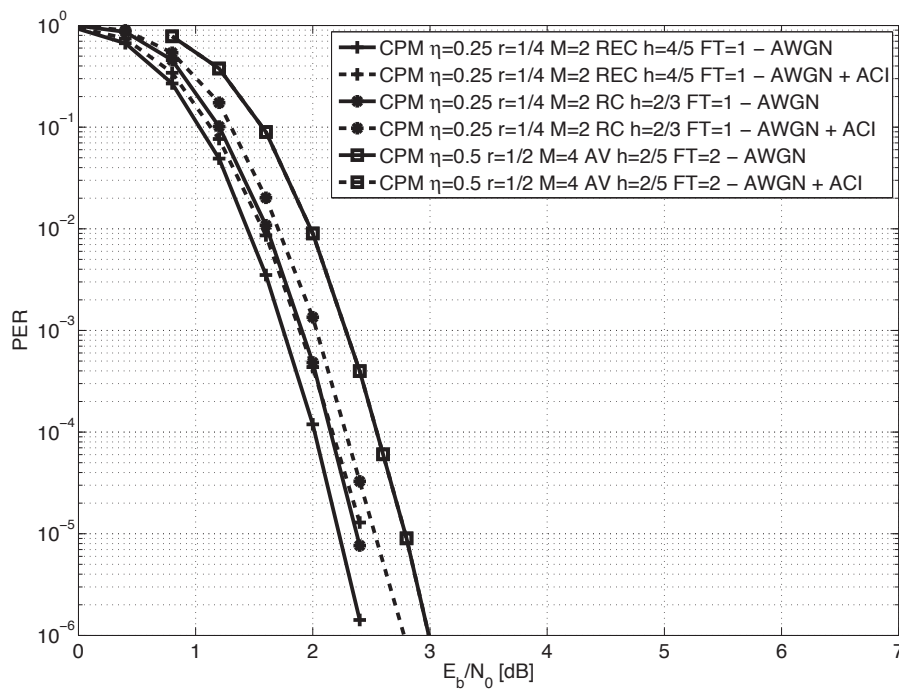


Figure 6.3: Performance comparison between CPM waveforms at  $\eta = 0.5$  b/s/Hz and  $\eta = 0.25$  b/s/Hz in AWGN Channel and AWGN+ACI (PER vs.  $E_b/N_0$ ), Short Traffic Burst ( $k=400$  bits).

## 6.2 Code Selection

CPM waveforms in the DVB-RCS2 standard are designed with a rate-1/2 convolutional code, possibly punctured to achieve a desired code rate, identified by generator polynomials [5, 7] in the case of constraint length  $K = 3$  and [15, 17] in the case of constraint length  $K = 4$ , which are reported in [71] and [72] as the optimal codes in the sense of the free distance ( $d_{min}$ ). When designing the new binary ( $M = 2$ ) CPM waveforms in power-limited environments, thus for lower operating spectral efficiencies ( $\eta = 0.25$  bit/s/Hz) the same criterion, based on the free distance, has been originally followed in order to select the most suitable rate-1/4 code. However, there are multiple suggestions in the literature for this case. For  $K = 3$  both generators [5, 5, 7, 7] and [5, 7, 7, 7] were found to be the best choice (respectively [71], [72]). Preliminary tests have shown that between such two generators, the latter performs better in the considered system and scenario, but the next step has been to evaluate the best convolutional code to be concatenated with the selected CPM formats. More precisely, in a “turbo-like” system, as the Convolutional Code-CPM (CC-CPM) scheme, the  $d_{min}$  optimality criterion plays no more a fundamental role. In fact, aspects such as the iterative behaviour, and the minimum distance between signal trajectories (in the trellis) in the signal space might affect the asymptotic behavior for high  $E_b/N_0$  value (in the so called floor region) whereas the waterfall behavior is determined by the distance spectrum. The minimum Euclidean distance between signal trajectories is also considered in [72]. It must be noted, however, that [72] does not consider bit interleaving nor iterative demodulation and decoding, and that there is no mathematical technique for finding the best codes (in the sense of the minimum Euclidean distance), but rather a series of considerations that can help in dramatically reduce the number of codes (i.e., generators polynomials) to be considered in the optimal code search, which is being still carried out by means of a brute force approach. In [72] it is also shown that optimal codes often share recurring characteristics, regarding the trellis branches labeling. In this analysis, due to the relatively limited number of codes to be generated using the specified parameters, a code search has been performed by means of computer simulations, building on some considerations that can reduce the codes set cardinality: for instance, the “all-zero” code [0, 0, 0, 0] is not considered, as well as the generators with all polynomials set to the same value. Also, generator polynomials which are merely time-reversal of one another have been considered only once.

### 6.3 Performance Analysis

The results of the mentioned code search are reported in Fig. 6.4 where the dotted lines represent the available benchmarks, i.e. the DVB-RCS2 CPM waveform at  $\eta = 0.5$  b/s/Hz and the same waveform considering the adoption of the Burst Repetition technique, which achieves spectral efficiency  $\eta = 0.25$  b/s/Hz but has performance which is indistinguishable in the PER vs.  $E_b/N_0$  plane. Three sets of closely spaced lines summarize the outcome of the code search over the considered set of code generator polynomials, after having removed equivalent polynomials, and other codes as per considerations made in the previous section. It can be seen that there are subsets of codes (here grouped by lines in dashed styles) that perform very close to each other and each of these families shows different performance. Note that, in order to ease the reading of the performance chart, only some representative curves have been reported here from the comprehensive analysis, precisely two for each subset of codes. The gain achieved with the best performing codes with respect to other sets of codes and to the BR technique is significant: at a PER of  $10^{-4}$ , up to more than 1 dB of gain in  $E_b/N_0$  is observed between the waveform adopting the best code and the DVB-RCS2 waveform with Burst Repetition.

Moreover, for the codes set represented by the solid lines, the waterfall region seems to start before that for the codes represented by dashed lines. However, at higher values of  $E_b/N_0$ , the performance of the two families of codes crosses, also because several other codes of the solid lines subset show an error floor.

Finally, Fig. 6.5 shows the same comparison in the PER vs.  $C/N$ , in which is further appreciated the benefit brought by the design of the new waveforms. Indeed, as said, BR yields a gain of exactly 3 dB, due to the fact that each burst is transmitted twice, but the new binary CPM waveforms, along with the selection of the most suitable code, can bring another gain of more than 1dB with respect to the BR solution, up to a total of more than 4 dB with respect to the existing DVB-RCS2 waveform at  $\eta = 0.5$  b/s/Hz.

To the above reported results, which show a significant gain of the new waveforms, a performance assessment in presence of other impairments has been added. For this reason a phase noise process was considered (described by the spectral mask in [73]). This imposes to move to a non-coherent detector [67], that is based on a phase synchronization technique embedded in the BCJR algorithm of the MAP CPM detector, in which a statistical model is assumed for the phase noise process.

The achieved results are reported in Fig. 6.6, in which the focus is on the

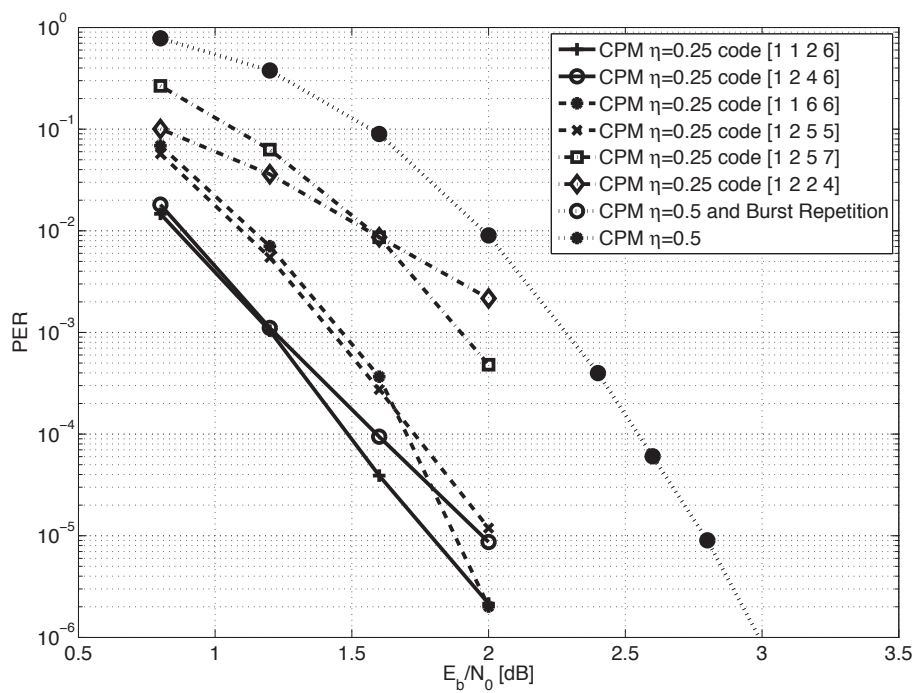


Figure 6.4: Performance comparison between CPM waveforms at  $\eta = 0.5$  b/s/Hz with and without Burst Repetition and  $\eta = 0.25$  b/s/Hz with different convolutional codes (PER vs.  $E_b/N_0$ ).

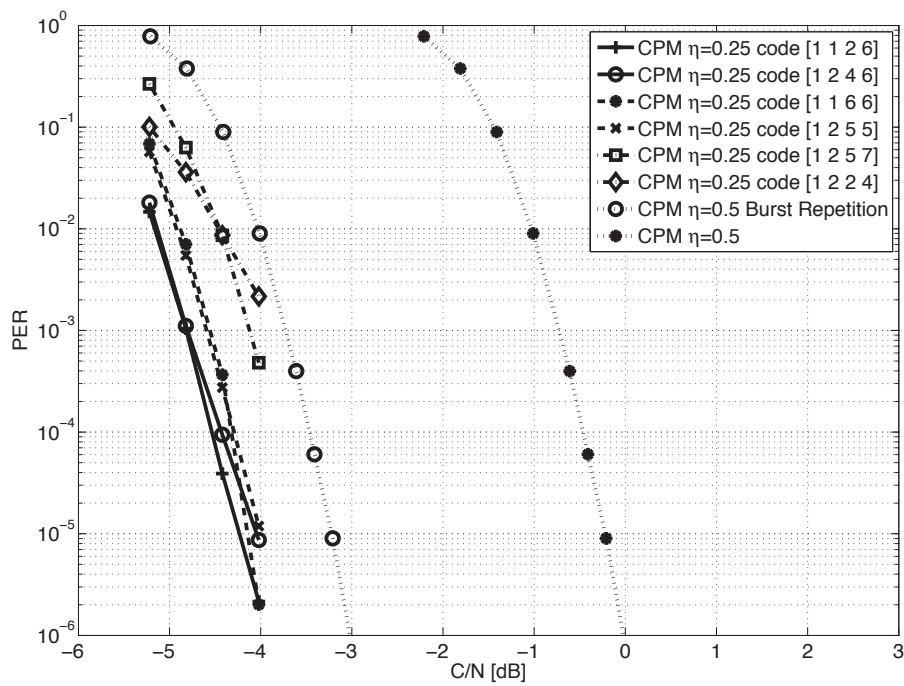


Figure 6.5: Performance comparison between CPM waveforms at  $\eta = 0.5$  b/s/Hz with and without Burst Repetition and  $\eta = 0.25$  b/s/Hz with different convolutional codes (PER vs.  $C/N$ ).

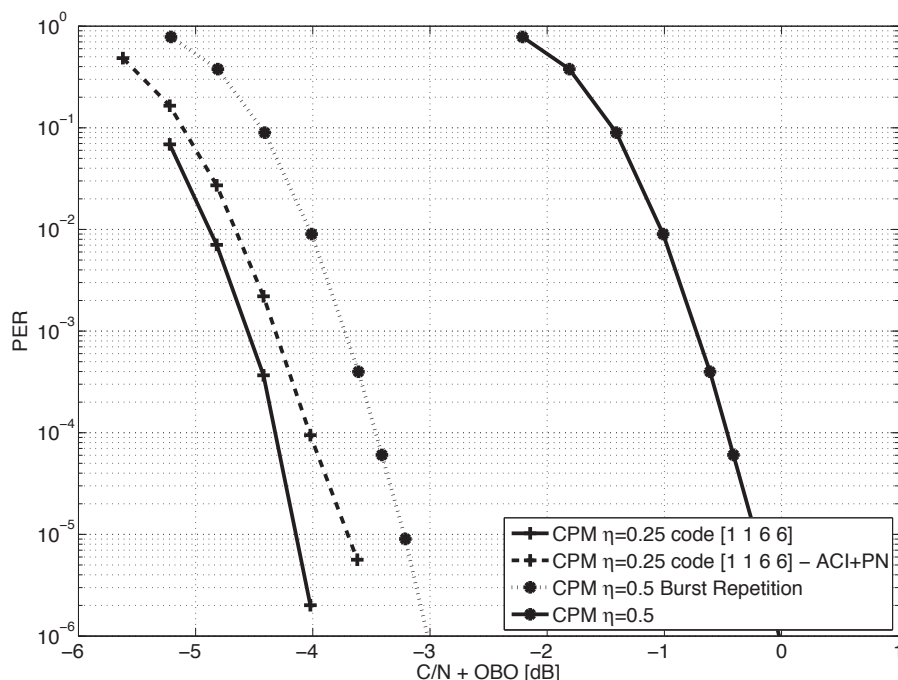


Figure 6.6: Performance comparison between CPM waveforms at  $\eta = 0.5$  b/s/Hz with and without Burst Repetition and  $\eta = 0.25$  b/s/Hz in presence of impairments (PER vs.  $C/N$ ).

behavior of the most promising waveform, the one having generator polynomials for the convolutional code equal to  $[1, 1, 6, 6]$ . The performance of this waveform in presence of AWGN, ACI and phase noise is compared with the performance of the existing CPM DVB-RCS2 waveform at  $\eta = 0.5$  b/s/Hz with burst repetition in AWGN only, i.e. without ACI and phase noise. As it clearly appears, the new waveform impaired by phase noise and ACI outperforms the BR solution even with coherent detection and no impairments, thus further showing the robustness of the proposed solution.

## 6.4 Results Summary

In this chapter, building on the outcomes of chapter 5, an energy efficient waveform design was carried out, particularly oriented to power limited scenarios, in which the main requirements are in available power. In this context, lower spectral efficiencies are considered, and it was performed a selection of the most suitable modulation and

## **110 Energy Efficient CPM Waveform Design for SatCom Mesh Systems**

coding scheme, based on constant envelop modulations. The results show clearly that the proposed waveform outperforms the typical solution for the considered scenario (Burst Repetition technique).

# Appendix **A**

## Satellite Communications: an Introduction

Satellite Communications represent an important part of wireless communications enabling unique applications, both for military and mass market purposes, mainly due to the achievable coverage that satellites link, by nature, allow. Satellite communications date back almost 70 years, from the first visionary publications by Sir Arthur C. Clarke, [74] and have evolved significantly, up to being integrated with terrestrial wireless systems. An overview on the history and evolution from early years to current and future technologies is provided in [75].

In this appendix, a brief introduction on a Satellite Communications System is given, with the purpose of providing definitions and descriptions for the general architecture that is widely referred to throughout this thesis.

### **A.1 Satellite Communications Systems Architecture**

The reference Satellite Communications System architecture, with the main characterizing elements is depicted in Figure A.1

The main elements in the architecture of figure A.1 are:

- the Gateway, or earth-station, which is connected to a Wide Area Network (WAN) on ground, and to other control elements via the feeder-link (i.e., the link between the satellite and the gateway, as opposed to the link between the terminal and the satellite, called user-link)

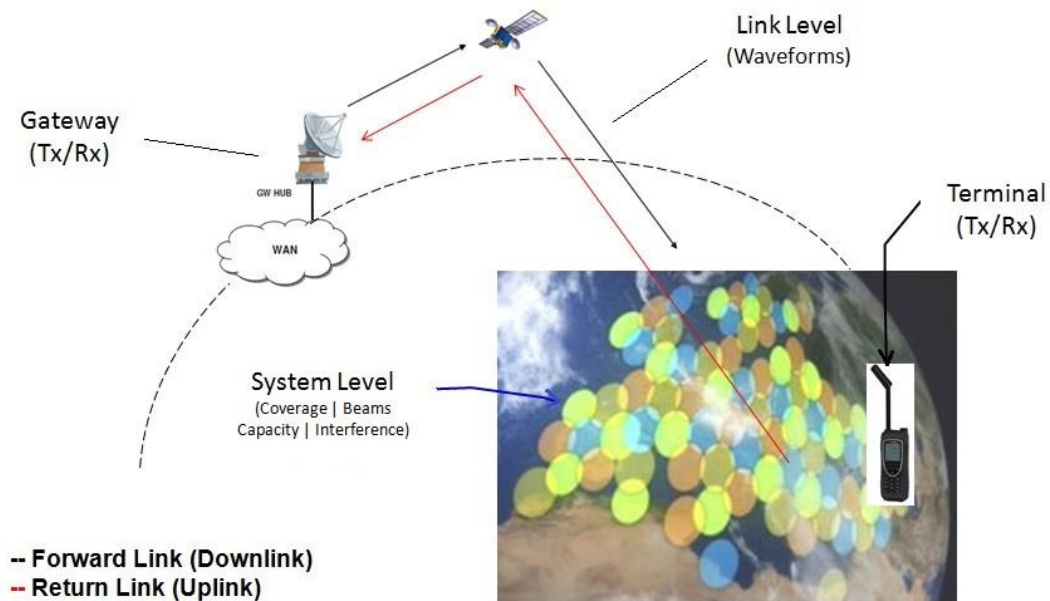


Figure A.1: Reference Satellite Communications System Architecture

- the Satellite, which relays signals transmitted from the ground, with several possibilities in terms of regeneration of the signals
- the Terminal, which is the second end of the communication link, and can be a fixed or a mobile terminal, based on the application, with varying size and weight, ranging from parabolic antennas (diameter in the order of magnitude of 1 meter) to handheld device

The general operation involves communication between the two ends of the transmissions, i.e., the gateway and the terminal, via the Satellite, acting as a relay. The satellite can either be completely transparent, therefore representing what's called a bent-pipe link (in which, thus, the satellite is simply a relay for the communication between gateway and terminal), or have some switching and processing capabilities that can reconstruct or route the signals at the expense of higher complexity.

The most typical satellite link, for instance in reference to broadcast services, is the link in which the gateway operates as the transmitter, and the terminal as a receiver. This is called Forward Link (black line in figure A.1), and it is equivalent in principle to the Uplink of a terrestrial wireless system. More recently, the possibility of allowing a reverse link enabling interactive broadband satellite services, has been conceived. This is referred to as Return Link (red line in figure A.1) and in this

case the terminal is the transmitting side, which generates several considerations with respect to the forward link. For instance transmission power is typically more limited at the terminal side, and also, the terminal is typically equipped with small low-gain antennas, and with cheaper RF components, such as power amplifiers, that impose bespoke designs in this link.

Figure A.1 also highlights the levels of investigation typically involved in the study and design of a satellite system. First the so-called System Level, which overlooks the complete system architecture, thus the coverage area, the overall system capacity and other aspects related to the entire system rather than on the single communication link. The Link Level, on the other hand, involves investigations more related to physical layer and waveforms aspects, such as Error Rate performance, estimation and synchronization aspects and waveform parameters. A more in-depth level of study focusses on intra-receiver (or intra-transmitter, equivalently, although different receiver architectures are possible for the same transmission scheme) aspects, such as modulator/demodulator design and low level signal processing related to a single device.

Satellite Communications Systems were initially based on single coverage region in which users channels were separated in frequency, time and code. The development of Multi-Antenna systems, has had an impact on satellite as well on terrestrial communications, leading to the exploitation of a fourth dimension for the separation of user transmission, which is the spatial dimension. As a result, the coverage area can be divided into several spots of coverage, separated spatially by directive antennas generating narrow beams. This defines the so-called Multi-Beam architecture, which is taken as a reference in this thesis, and that leverages on the concept of beam-forming, and its application to satellite network, which are presented in next sections to introduce the multi-beam architecture on which this thesis is based.

## **A.2 Beam Forming in Satellite Systems**

This chapter introduces the concept of Beam Forming and its applications to satellite systems, which will be used to describe the reference multi-beam scenario for Chapter 1 and Chapter 2, in which interference management strategies will be discussed.

Beam Forming refers to signal processing techniques used to achieve Spatial filtering of signals transmitted by an array of antennas [76]. Physically this is achieved by allowing that each antenna elements in the antenna (array) system is driven by

a coefficient (in amplitude and phase) such that for a certain range of angles with respect to the radiating antennas, signals transmitted by each antenna element interfere constructively and destructively for other angles (i.e., transmission directions). This translates into the possibility of determining by design the spatial selectivity, or directivity of the transmission.

This represents therefore a first way of dealing with interference, since it enables the exploitation of another dimension in which signals can be separated. On top of classical orthogonalization domains, such as Frequency, Time and Code (FDM, TDM and CDM), signals can be also separated in space. Beam Forming is widely used in already existing technologies, such as WiFi (IEEE 802.11n and later revisions, [77]), 3G and 4G terrestrial cellular standards [78, 79].

Beam Forming has been also considered in recent Satellite Systems. The main difference with terrestrial beam forming is the topology of the transmission: due to the position of the satellite with respect to the earth, by means of beam forming it is possible to achieve a tessellation of the coverage area, allowing for frequency reuse and supporting a higher number of active user in the same time-frequency resources.

Beam Forming techniques in Satellite Systems can be broadly distinguished in *on-ground*, *hybrid* and *on-board* beam forming. On-ground beam forming [80] refers to the case of the spatial processing being carried out at the gateway, in which case all signals pertaining to each antenna element (feed) are transmitted to the ground station on the so-called Feeder Link. On-board beam forming is implemented in the payload subsystem of the satellite itself, which means that only the beams signals are transmitted through the feeder link, yielding bandwidth reductions in all the cases in which the beam-forming is operated in a multi-feed per beam fashion. The hybrid beam forming [81, 82] is based on partitioning the beam forming process between the satellite, in which a form of coarse beamforming is carried out, and the gateway, where a fine beamforming is applied. The target of this split processing is the reduction of the feed signal space to a subspace of lower dimension, which translates into reducing the required feeder link bandwidth. The idea is to apply an appropriate transformation to the  $N$  feed signals, in order to project them on a subspace with reduced dimensions, thus frequency multiplexing a number (lower than the number of feeds) of partially-processed signals (beamlets) in order to deliver them to the gateway over the feeder link [10, 11, 14]. Alternative approaches have been proposed [83] for determining the most appropriate weighting to be applied to the feed outputs to obtain the signal from a desired direction in space. The

target is to apply a suitable transformation to the feed signals in order to obtain a reduced set of values, that can still allow the reconstruction of the original signal. For instance, on board solutions based on 2D Butler Matrix or analog FFT [81] can be adopted. Practical implementations of these concepts require a trade-off between the number of beamlets and the performance, since a reduction of the number of signals (semi-processed, or coarsely beamformed) also implies a reduction in the degrees of freedom that the beam forming will leverage on, in terms of beam width precision, placing nulls in the interferers directions and so on. To this extent, different transformations were compared in [11, 14], in which Digital Fourier Transform (DFT) and Karhunen–Loève Transform (KLT) [84] are compared, showing that the latter is better performing, and that savings of up to the 20% can be achieved by compacting the feeder link bandwidth thanks to neglecting less relevant coefficients of the transformed signals, while still being able to recover the original signal on ground.

### **A.3 Multi-Beam Satellite Scenario**

In this section, a practical application of Beam Forming to a satellite system, intended for the coverage of Europe, is reported to introduce the Multi-Beam architecture that will be taken as a reference for the analysis of the Chapter 1 and Chapter 2.

The practical case study hereby considered is based on an antenna model provided by ESA and on the assumption that multiple feeds constitutes each beam, by proper beam forming weights. This will help better depicting the beam forming operation.

The following example is based on a 155 feeds antenna system at the satellite, on top of which a fixed beam forming is applied using 20 weighted feeds signals to shape 100 beams. Figure A.2 reports the radiation pattern in dB of a typical antenna feed (i.e., feed number 10 of the considered antenna). It can be clearly seen that each feed is quite directive even before beam forming, focussing on a narrow region of the coverage area, and the superimposition of all the feeds will be necessary in achieving the intended coverage.

In Figure A.3 the radiation patterns of all of the 155 feeds are represented together, therefore the entire coverage area is depicted. Note that the depicted radiation patterns refer to the value in dB of the antenna gain calculated using the

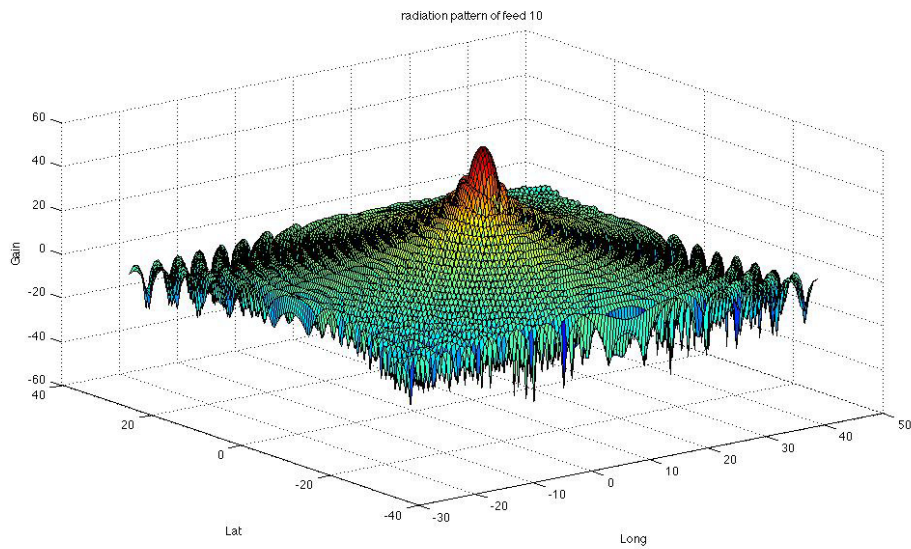


Figure A.2: Radiation Pattern of a single satellite antenna feed

Co-polar component of the antenna, since, although a Cross-polar component is typically present, cross-polarization rejection is usually such that the interference generated is negligible.

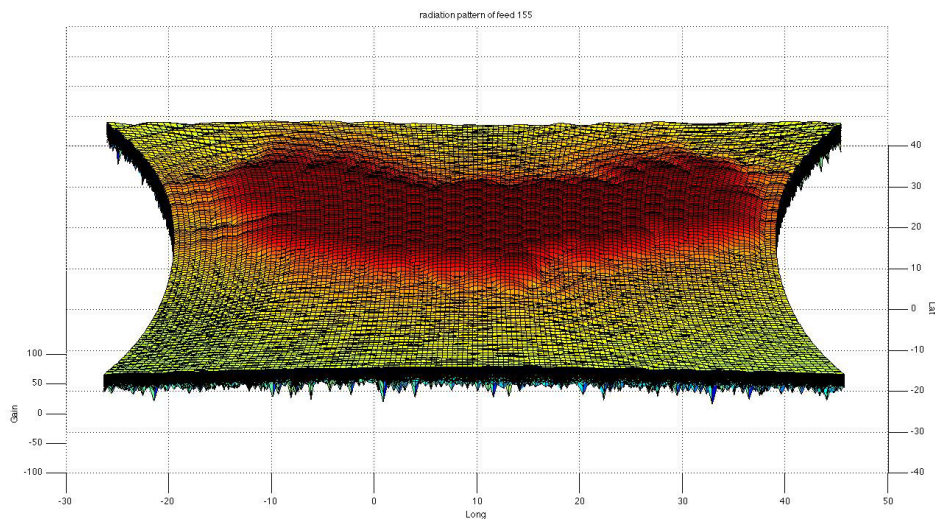


Figure A.3: Radiation Pattern of all the 155 antenna feeds (No Beam Forming)

Even though antenna feeds have already good directivity, beam forming is still very beneficial, as it is aimed at providing uniform coverage by tuning the contributions coming from clusters of feeds so as to close the coverage gaps rather than

only steering the beam radiation pattern towards a specific spatial sector. For each beam, among the feeds used to shape it, there exists typically a single feed weight close to unity, for the most representative feed in that geographical area, and other weights set to much smaller absolute values, and phase corrections defined so as to reduce the interference carried by neighboring locations feeds, that are forced to only superimpose constructively. In turn, this leads to a conveniently shaped beam with coverage extended up to the beam edge without gaps or overlaps. The radiation pattern of one Beam is depicted in Figure A.4.

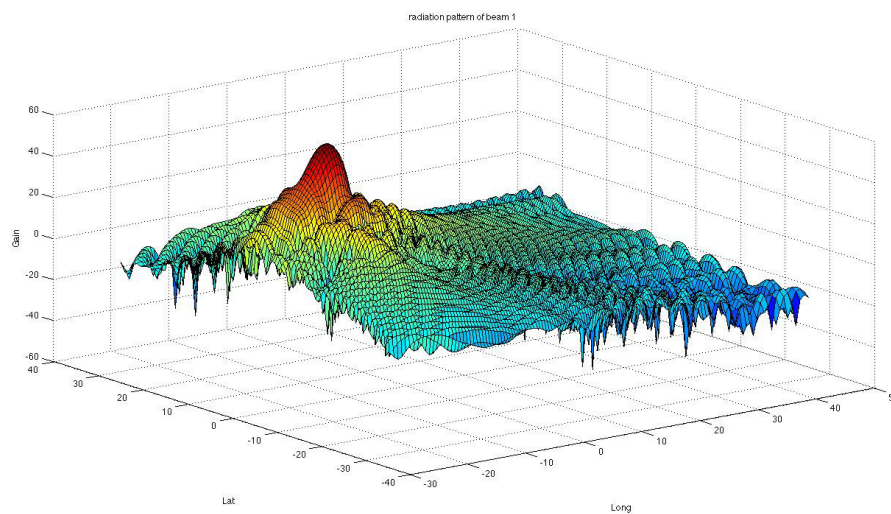


Figure A.4: Radiation Pattern of a single Beam

The overall coverage achieved by beams is shown in Figure A.5. It is easier to appreciate the impact of the beam forming if looking at the C/I distribution over the coverage area before and after beam forming. As clearly shown in Figure A.6, when no BF is performed, the C/I spatial distribution is only acceptable in confined small areas, and it is not uniform over the whole coverage area. Indeed, this is due to radiation pattern generated by the feeds, that although directive, does not provide a uniform tessellation of the coverage area (in part also due to the curvature of the earth). When beam forming is used, as shown in Figure A.7, the C/I spatial distribution is much more uniform, thanks to convenient combinations of feed contributions. Therefore, besides a good coverage, a fair C/I spatial distribution is obtained on the coverage area. Note that in Figure A.6 and in Figure A.7 the whole spatial coverage grid has been considered.

When beam forming is used, as shown in Figure A.7, the C/I spatial distribution

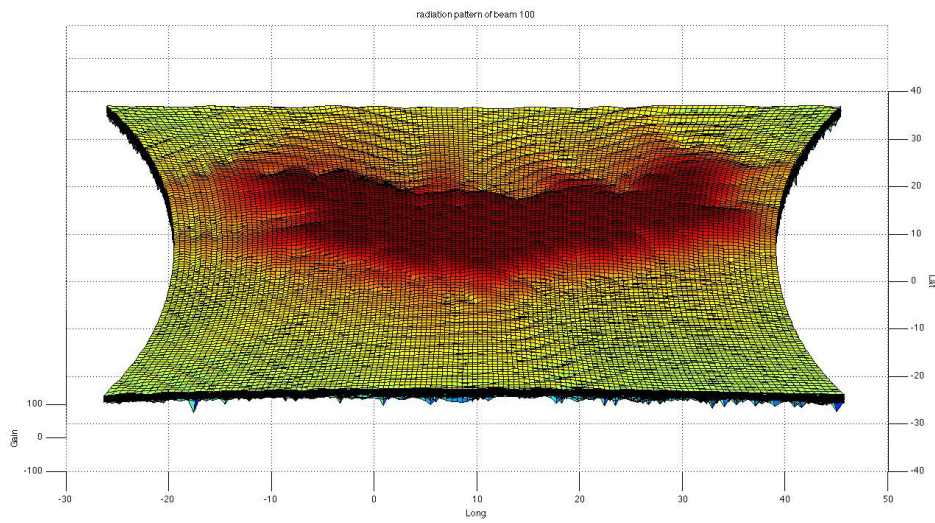


Figure A.5: Radiation Pattern of al the 100 beams

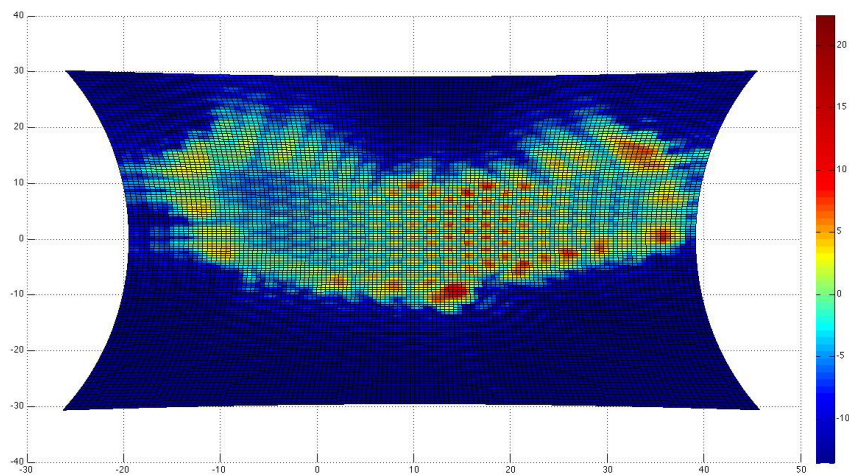


Figure A.6: Distribution of the C/I over the coverage region without beam forming

is much more uniform, thanks to convenient combinations of feed contributions. Therefore, besides a good coverage, a fair C/I spatial distribution is obtained on the coverage area.

The above satellite beam forming example represents a reference for a multi beam scenario, which is adopted throughout this thesis in terms of architecture, although with different numerical parameters if specified.

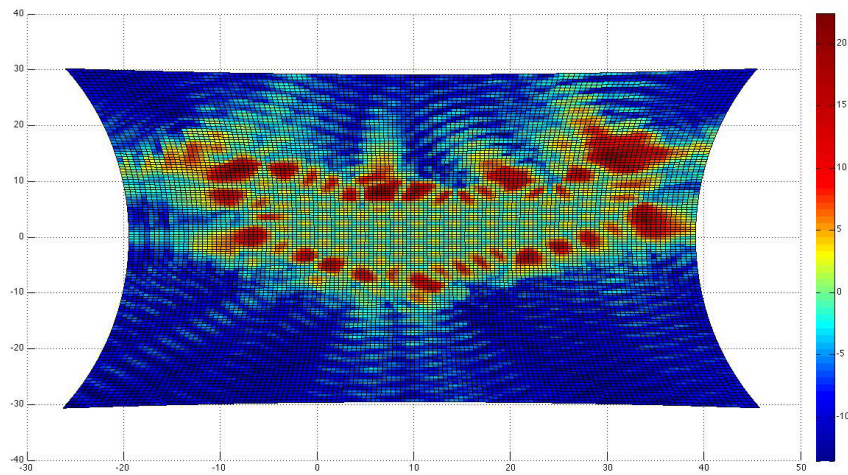


Figure A.7: Distribution of the C/I over the coverage region with beam forming







# Conclusions

This thesis has addressed at several levels the problem of interference in wireless communications, with particular reference to satellite systems, as well as energy efficiency for power limited scenarios. In the first part of this work, the concept of beam forming applied to satellite systems has been presented, in order to introduce the multi-beam satellite scenario, taken as the reference for the following chapters analysis. In Chapter 1 a system architecture was designed, starting from concepts seen in terrestrial wireless counterparts, that is based on the cancellation of co-channel interference. To this extent, first upper and lower bounds for the system capacity were introduced, and then two interference cancellation approaches were presented, with the possibility of leveraging on cooperation between gateways to parallelize the effect of interference cancellation. It was shown that the performance increase in terms of overall system capacity is significant in practically all the considered scenarios, with peak gains in the cases of full frequency reuse, i.e., where there is more interference to be removed. It is also suggested that the design of the interference cancellation based architecture should be done jointly with the design of the antenna system, since the antenna pattern determines the generation of the co-channel interference. In chapter 2 the application of the interference cancellation strategies discussed in chapter 1 to the forward link of a multi-beam satellite system is analysed. Considerations on the forward link scenario lead the analysis to physical layer decodability issues, which are evaluated theoretically and confirmed by computer simulations. The first result shown consists in asserting that conventional interference cancellation strategies, as presented in chapter 1, cannot be adopted in the forward link of a multi-beam satellite system in the practical scenario considered. On top of this, a modified version of the interference cancellation strategy is proposed, based on ModCod (or power) unbalance as a means for distinguishing

the signals transmitted by interfering beams. It is shown that the proposed strategy allows the interference cancellation to be able to decode from a physical layer perspective, whereas the impact on the system capacity depends on the ModCod-to-beam allocation or scheduling. Concluding Part I, in chapter 3 the specific case of the Tracking, Telemetry and Control channel for a satellite system is considered, based on a BFSK-FFH communication scheme, and the issue of intentional interference (jamming) is tackled by designing a novel robust receiver based on a double threshold approach and a logic unit that outperforms existing receivers in terms of resilience to multi-tone jammers.

Part II of this thesis is focussed on efficiency in the power domain. In particular, energy efficiency is considered in reference to the return link of interactive satellite communications by introducing the Mesh architecture in chapter 4 in which there is no infrastructure in the network, therefore allowing a single-hop communication between peers. In this case then, energy efficiency is even more critical than in the return link of a two-hop classical satellite system, since both ends of the transmission are terminals, having limited power resource and small antennas, therefore small antenna gains affecting the link budgets. In chapter 5 a fair comparison between linear and CPM modulation based waveforms for Mesh scenarios is carried out in real-life conditions, accounting for channel impairments and terminals non-idealities, and it is shown that CPM waveforms are a better solution for applications with moderate requirements in terms of transfer rates. This analysis is taken as the starting point for the study in chapter 6 in which the design of new waveforms for power-limited scenarios is carried out, aiming at extending the range of low operating SNR. This is achieved by choosing CPM as the candidate modulation format, as per the analysis in chapter 5, and selecting the most appropriate CPM modulation format and Convolutional Code parameters by means of both theoretical and practical considerations.

Overall, the problem of better exploitation of limited resources in wireless communications has been tackled in this thesis, at different layers, starting from the system level architecture and aiming at increasing the system capacity. The analysis then moved to the link layer, on one hand extending to the forward link of satellite systems the activity carried out for the return link, and on the other hand by considering the design of energy efficient waveforms for power limited scenarios, and then further down to the demodulator design, inside the receiver structure.

This work has been performed within the Digicomm group within ARCES/DEI

at the University of Bologna, led by Professor G.E. Corazza, under the co-tutoring of Professor A. Vanelli-Coralli. Many of the activities were performed in the context of European Space Agency (ESA) studies and international research projects, to which several of the activities reported in this thesis brought valued contribution. Activities related to Part II of this thesis were also carried out in collaboration with Mavigex Srl.



# Personal Contributions

- [1] ESA SatNex III Study Fair Comparison and Combination of Advanced Interference Mitigation Techniques, “Project Technical Report - Multi-User Detection and Precoding techniques for multi-beam satellite systems: Final Results,” 2012.
- [2] F. Lombardo, A. Vanelli-Coralli, E.A. Candreva, and G.E. Corazza, “Multi-Gateway Interference Cancellation techniques for the Return Link of Multi-Beam Broadband Satellite Systems,” *IEEE GLOBECOM 2012 - Selected Areas in Communications Symposium - Satellite and Space Communications Track*, 2012.
- [3] F. Lombardo, E.A. Candreva, I. Thibault, A. Vanelli-Coralli, and G.E. Corazza, “Multi-User Interference Mitigation Techniques for Broadband Multi-Beam Satellite Systems,” *ASILOMAR Conference on Signals, Systems and Computers, November 2011, Session TP6b, Array Processing for Satellite Communications*, 2011.
- [4] F. Lombardo, A. Vanelli-Coralli, E.A. Candreva, and G.E. Corazza, “Throughput Distribution Analysis of Return Link Multi-Gateway Interference Cancellation Strategies for Multi-Beam Broadband Satellite Systems,” *IEEE GLOBECOM 2012 - Broadband Wireless Access Workshop (BWA)*, 2012.
- [5] ESA Study Next Generation Waveforms for Improved Spectral Efficiency, “Project Technical Report: Candidate Techniques for FWD Link Air Interface Enhancements,” 2013-2014.
- [6] R. Baroni, F. Lombardo, E.A. Candreva, R. Pedone, A. Vanelli-Coralli, and G.E. Corazza, “A Robust Interference Mitigation Technique For BFSK Fast

- Frequency Hopped Signals,” *2011 Military Communications Conference - Track 1 - Waveforms and Signal Processing*, 2011.
- [7] R. Suffritti, E.A. Candreva, F. Lombardo, S. Rosati, A. Vanelli-Coralli, G.E. Corazza, and G. Gallinaro, “A Mesh Network over a Semi-Transparent Satellite,” *IEEE GLOBECOM 2011*, 2011.
- [8] R. Baroni, F. Lombardo, R. Suffritti, E.A. Candreva, A. Vanelli-Coralli, G.E. Corazza, G. Colavolpe, G. Gallinaro, and N. Alagha, “Performance Analysis of a Mesh Satellite System based on Linear and Continuous Phase Modulations,” *IEEE ICC 2012 - Selected Areas in Communications Symposium - IEEE ICC 2012 - SAC - Satellite and Space Communications*, 2012.
- [9] R. Suffritti, F. Lombardo, A. Piemontese, A. Vanelli-Coralli, E.A. Candreva, G. Colavolpe, R. Baroni, S. Andrenacci, G.E. Corazza, and N. Alagha, “Energy Efficient CPM Waveforms for Satellite Mesh Networks,” *IEEE GLOBECOM 2012 - Selected Areas in Communications Symposium - Satellite and Space Communications Track*, 2012.
- [10] J. Arnau-Yañez, M. Bergmann, E.A. Candreva, G.E. Corazza, R. de Gaudenzi, B. Devillers, W. Gappmair, F. Lombardo, C. Mosquerax, A. Pérez-Neiraz, I. Thibault, and A. Vanelli-Coralli, “Hybrid Space-Ground Processing for High-Capacity Multi-beam Satellite Systems,” *IEEE GLOBECOM 2011 - Selected Areas in Communications Symposium - Satellite and Space Communications Track*, 2011.
- [11] I. Thibault, F. Lombardo, E.A. Candreva, A. Vanelli-Coralli, and G.E. Corazza, “Coarse Beamforming Techniques for Multi-Beam Satellite Networks,” *IEEE ICC 2012 - Selected Areas in Communications Symposium - IEEE ICC 2012 - SAC - Satellite and Space Communications*, 2012.
- [12] F. Di Cecca, G. Gallinaro, E. Tirro’, S. Cioni, P. Angeletti, E.A. Candreva, F. Lombardo, and A. Vanelli-Coralli, “On-ground Beamforming And Interference Cancellation For Next Generation Mobile Systems,” *18th Ka and Broadband Communication Navigation and earth observation conference, Ottawa – 2012*, 2012.
- [13] F. Di Cecca, G. Gallinaro, E. Tirro, C. Campa, S. Cioni, P. Angeletti, E.A. Candreva, F. Lombardo, and A. Vanelli-Coralli, “Payload Aspects of Mo-

ble Satellite Systems with On-Ground Beamforming and Interference Cancellation,” *2012 IEEE International Conference on Wireless Information Technology and Systems*, 2012.

- [14] I. Thibault, B. Devillers, E.A. Candreva, F. Lombardo, A. Vanelli-Coralli, and G.E. Corazza, “Joint feeder-link bandwidth compaction and interference mitigation based on a hybrid space/ground processing architecture for a broadband multi-beam satellite system,” *International Journal of Satellite Communications and Networking*, doi: 10.1002/sat.1042, 2012.



# Bibliography

- [15] C.E. Shannon, “A mathematical theory of communication,” *Bell System Tech.J.*, vol. 27, pp. 379–423, 623–656, 1948.
- [16] M. K. Simon, J. K. Omura, R.A. Scholtz, and B.K. Levitt, “Spread Spectrum Communications Handbook,” *McGray-Hill*.
- [17] L. Hanzo, L. Yang, E. Kuan, and K. Yen, “Single and Multi-Carrier CDMA,” *Wiley*, 2003.
- [18] G.E. Corazza, “Digital Satellite Communications,” *Information Technology series, Springer Publishing Company, New York*, 2007.
- [19] Caire G, Debbah M, Cottatellucci L, De Gaudenzi R, Rinaldo R, Mueller R, and Gallinaro G, “Perspectives of adopting interference mitigation techniques in the context of broadband multimedia satellite systems,” *Proc. 23rd AIAA Int. Comm. Sat. Sys. Conf. (ICSSC) Rome, Italy*, pp. 1–5, September 2005.
- [20] Cottatellucci L, Debbah M, Gallinaro G, Müller R, Neri M, and Rinaldo R, “Interference mitigation techniques for broadband satellite systems,” *Proc. 24th AIAA Int. Comm. Sat. Syst. Conf. (ICSSC) San Diego, CA*, pp. 1–13, June 2006.
- [21] X. Wang and H.V. Poor, “Iterative (turbo) soft interference cancellation and decoding for coded CDMA,” *IEEE Transaction on Communications*, vol. 47, no. 7, pp. 1046–1061, July 1999.
- [22] S. Verdù, “Multiuser Detection,” *Cambridge University Press*, 1998.

- 
- [23] M.Neri, M.Casadei, A.Vanelli-Coralli, and G.E.Corazza, "Multiuser detection for S-UMTS and GMR-1 mobile systems," *Int. J. Satell. Commun. Networks*, vol. 25, pp. 529–550, 2007.
- [24] J. G. Andrews, "Interference Cancellation for Cellular Systems: A Contemporary Overview," *IEEE Wireless Comm.*, pp. 19–29, April 2005.
- [25] Z. Zvonar and D. Brady, "Multiuser detection in single-path fading channels," *IEEE Trans. Commun.*, vol. 42, no. 2-3-4, pp. 1729–1739, 1994.
- [26] S. J. Grant and J. K. Cavers, "Further analytical results on the joint detection of cochannel signals using diversity arrays," *IEEE Trans. Commun.*, vol. 48, no. 11, pp. 1788–1791, November 2000.
- [27] G. Caire, G. Taricco, J. Ventura-Traveset, and E. Biglieri, "A multiuser approach to narrowband cellular communications," *IEEE Trans. Inf. Theory*, vol. 43, no. 5, pp. 1503–1517, September 1997.
- [28] Moher M. L., "Multiuser decoding for Multibeam system," *IEEE Transaction on Vehicular Technology*, vol. 49, pp. 1226–1234, July 2000.
- [29] B. F. Beidas, H. El Gamal, and Stan Kay, "Iterative Interference Cancellation for High Spectral Efficiency Satellite Communications," *IEEE TRANSACTIONS ON COMMUNICATIONS*, vol. 50, no. 1, January 2002.
- [30] P. D. Alexander, A. J. Grant, and M. C. Reed, "Iterative detection in code division multiple access with error control coding," *European Transactions on Telecommunications*, Sept/Oct 1998.
- [31] S. V. Hanly and P. A. Whiting, "Information-theoretic capacity of multireceiver networks," *Telecommun. Syst.*, vol. 1, 1993.
- [32] I. Emre Telatar, "Capacity of Multi-antenna Gaussian Channels," *European Transactions on Telecommunications*, vol. 10, no. 6, pp. 585–595, Nov/Dec 1999.
- [33] A. Vanelli-Coralli, R. Padovani, J.Hou, and J. Smee, "Capacity of Cell Clusters with Coordinated Processing," *Proc. Information Theory and Applications ITA 2006*, 2006.
- [34] David Tse and Pramod Viswanath, "Fundamentals of Wireless Communication," *Cambridge University Press, New York*, July 2005.

- [35] S. Dolinar, D. Divsalar, and F. Pollara, “Jet Propulsion Laboratory TMO Progress Report 42-133,” May 1998.
- [36] ITU-R, “Recommendation p.1853-0, Tropospheric Attenuation Time Series Synthesis, Geneva, CH,” *Int. J. Satell. Commun. Networks*, 2009.
- [37] DVB TM-S2 Channel Model Group, “DVB SX Channel Models,” January 2013.
- [38] Digital Video Broadcasting (DVB), “Second generation framing structure channel coding and modulation systems for Broadcasting Interactive Services, News Gathering and other broadband satellite applications (DVB-S2),” *ETSI EN 302 307 V1.2.1 (2009-08)*.
- [39] R. Pedone, M. Villanti, A. Vanelli-Coralli, and G.E. Corazza, “Frame synchronization in frequency uncertainty,” *IEEE Transactions on Communications*, vol. 58, no. 4, 2010.
- [40] Digital Video Broadcasting (DVB), “User guidelines for the second generation system for Broadcasting, Interactive Services, News Gathering and other broadband satellite applications (DVB-S2),” *ETSI TR 102 376 V1.1.1 (2005-02)*.
- [41] S. Papaharalabos, M. Papaleo, P. T. Mathiopoulos, M. Neri, A. Vanelli-Coralli, and G. E. Corazza, “DVB-S2 LDPC Decoding Using Robust Check Node Update Approximations,” *IEEE Transactions on Broadcasting*, vol. 54, no. 1, pp. 120–126, March 2008.
- [42] G. Colavolpe, D. Fertonani, and A. Piemontese, “SISO Detection over Linear Channels with Linear Complexity in the Number of Interferers,” *IEEE J. Sel. Top. in Signal Processing*, vol. 5, no. 8, pp. 1475–1485, 2011.
- [43] D.J. Torrieri, “Frequency Hopping with Multiple Frequency-Shift Keying and Hard Decisions,” *IEEE Transactions on Communications*, vol. COM-32, no. 5, pp. 574–582, May 1984.
- [44] C.M. Keller and M.B. Pursley, “Clipped Diversity Combining for Channels with Partial-Band Interference-Part I: Clipped-Linear Combining,” *IEEE Transactions on Communications*, vol. 35, no. 12, December 1987.

- [45] Y. Chen, G. Li, S. Li, and Y. Cheng, "A new anti-jam receiver for MFSK/FFH system with multitone jamming," *11th IEEE Singapore International Conference on Communication Systems, 2008*, pp. 451–455, November 2008.
- [46] Y.C. Chen, "Optimum and joint-suboptimum maximum-likelihood detection for FH/BFSK in multitone jamming," *3rd IEEE Consumer Communications and Networking Conference 2006*, pp. 849–853, January 2006.
- [47] K.C. Teh, A.C. Kot, and K.H. Li, "Performance study of a maximum-likelihood receiver for FFH/BFSK systems with multitone jamming," *IEEE Transactions on Communications*, vol. 47, no. 5, pp. 776–772, May 1999.
- [48] C. Waylan, "Detection of Fast, Noncoherent, Frequency-Hopped FSK," *IEEE Transactions on Communications*, vol. 23, no. 5, pp. 543–546, May 1975.
- [49] T.Ors, Z.Sun, and B.Evans, "A Meshed VSAT Satellite Network Architecture using an On-Board ATM switch," *IEEE International Performance, Computing, and Communications Conference, 1997*, February 1997.
- [50] S. Arnold, A. Noerpel, R. Gopal, and S. Chandrasekharan, "Implementing a mobility architecture for a Regenerative Satellite Mesh Architecture (RSM-A) system a SPACEWAY™ perspective," *IEEE Military Communications Conference, MILCOM 2008, 2008*.
- [51] "The VSAT Report Comsys 2005," *VSAT Industry Status Report to Clients, 2005*, 2005.
- [52] C. Haardt, "Demonstrating Radio Burst Switching by satellite in the ULISS project," *10th International Workshop on Signal Processing for Space Communications, 2008*.
- [53] O. del Rio Herrero and X. Maufroid, "Innovative Hybrid Optical/Digital Ultra-Fast Packet-Switched Processor for Meshed Satellite Networks," *IEEE Journal on Selected Areas in Communications, Feb. 2004.*, February 2004.
- [54] C. Haardt, O. del Rio Herrero, and N. Alagha, "Semi-Transparent Packet Switching by Satellite: migrating existing technologies for new opportunities," *26th International Communications Satellite Systems Conference (ICSSC), 2008, San Diego, CA, 2008*.
- [55] "Dvb-rcs2 lower layer satellite specification," *DVB BlueBook A155-2, 2011*.

- [56] D. Rife and R. Boorstyn, "Single tone parameter estimation from discrete-time observations," *IEEE Trans. on Inform. Th.*, vol.20, no.5, pp. 591- 598, September 1974.
- [57] A. Barbieri and G. Colavolpe, "Simplified Soft-Output Detection of CPM Signals Over Coherent and Phase Noise Channels," *IEEE Trans. on Wireless Comm.*, vol. 6, no. 7, July 2007.
- [58] F. Gardner, "A BPSK/QPSK Timing-Error Detector for Sampled Receivers," *IEEE Trans. on Comm.*, vol.34, no.5, pp. 423- 429, May 1986.
- [59] Y.R. Shayan and T. Le-Ngoc, "All Digital Phase-Locked Loop: Concept, Design and Applications," *IEE Proc.*, vol 136, Pt. F, No. 1, pp 53-56, February 1989.
- [60] G. Albertazzi, S. Cioni, G.E. Corazza, M Neri, R. Pedone, P. Salmi, A. Vanelli-Coralli, and M. Villanti, "On the adaptive DVB-S2 physical layer: design and performance," *IEEE Wireless Comm.*, vol.12, no.6, pp. 62- 68, December 2005.
- [61] A. Barbieri, G.Colavolpe, and G. Caire, "Joint Iterative Detection and Decoding in the Presence of Phase Noise and Frequency Offset," *IEEE Trans. on Comm.*, vol.55, no.1, pp.171-179, January 2007.
- [62] B.E. Rimoldi, "A decomposition approach to CPM," *IEEE Trans. on Inf. Th.*, vol.34, no.2, pp.260-270, March 1988.
- [63] P. Laurent, "Exact and Approximate Construction of Digital Phase Modulations by Superposition of Amplitude Modulated Pulses (AMP)," *IEEE Trans. on Comm.*, vol.34, no.2, pp. 150- 160, February 1986.
- [64] U.Mengali and M.Morelli, "Decomposition of M-ary CPM Signals into PAM Waveforms," *IEEE Trans. on Inform. Th.*,pp 1265-1275, 1995.
- [65] A.N. D'Andrea, U. Mengali, and M. Morelli, "Symbol timing estimation with CPM modulation," *IEEE Trans. on Comm.*, vol.44, no.10, pp.1362-1372, October 1996.
- [66] A. Barbieri, D. Fertoni, and G. Colavolpe, "Spectrally-efficient continuous phase modulations," *IEEE Trans. Wireless Commun.*, vol. 8, no.3, pp. 1564-1572, March 2009.

- [67] A. Barbieri and G. Colavolpe, "Simplified Soft-Output Detection of CPM Signals Over Coherent and Phase Noise Channels," *IEEE Trans. on Wireless Comm.*, vol. 6, no. 7, July 2007.
- [68] S. ten Brink, "Convergence Behavior of Iteratively Decoded Parallel Concatenated Codes," *IEEE TRANSACTIONS ON COMMUNICATIONS*, vol. 49, no. 10, October 2001.
- [69] J. Hagenauer, "The EXIT Chart - Introduction to Extrinsic Information Transfer," *Iterative Processing, In Proc. 12th Europ. Signal Proc. Conf (EUSIPCO)*, 2004.
- [70] A. Ashikhmin, G. Kramer, and S. ten Brink, "Extrinsic information transfer functions: Model and erasure channel properties," *IEEE Transactions on Information Theory*, vol. 50, no. 11, pp. 2657–2673, 2004.
- [71] J.G. Proakis, "Digital Communications," *McGraw-Hill, New York*, 2001.
- [72] S. Pizzi and S. Wilson, "Convolutional Coding Combined with Continuous Phase Modulation," *IEEE Transactions on Communications*, January 1985.
- [73] "Digital Video Broadcasting (DVB); Second Generation DVB Interactive Satellite System (DVB-RCS2); Guidelines for Implementation and Use of LLS: EN 301 545-2," .
- [74] A. C. Clarke, "Extra-terrestrial relays," *Wireless World*, pp. 305–308, October 1945.
- [75] B. Evans, P.T. Thompson, G.E. Corazza, A. Vanelli-Coralli, and E.A. Candrea, "1945-2010: 65 Years of Satellite History From Early Visions to Latest Missions," *Proceedings of the IEEE*, vol. 99, no. 11, pp. 305–308, November 2011.
- [76] B.D. Van Veen and K.M. Buckley, "Beam-Forming: A Versatile Approach to Spatial Filtering," *IEEE ASSP Magazine*, April 1988.
- [77] IEEE, "802.11n-2009—Amendment 5: Enhancements for Higher Throughput. IEEE-SA," October 2009.
- [78] 3GPP, "High Speed Packet Access (HSPA) evolution; Frequency Division Duplex (FDD) 3GPP TR 25.999," .

- [79] 3GPP, “Requirements for further advancements for Evolved Universal Terrestrial Radio Access (E-UTRA) (LTE-Advanced) 3GPP TR 36.913,” .
- [80] P. Angeletti, G. Gallinaro, M. Lisi, and A. Vernucci, “On-ground digital beamforming techniques for satellite smart antennas,” *Proc. 19th AIAA, Toulouse, France*, pp. 1–8, April 2001.
- [81] P. Angeletti and N. Alagha, “Space/Ground Beamforming Techniques for Emerging Hybrid Satellite Terrestrial Networks,” *Proc. 27th AIAA, Edinburgh, UK*, pp. 1–6, June 2009.
- [82] V.S. Reinhardt, “Hybridized Space/Ground Beamforming,” *US patent 6571081, 2003*, 2003.
- [83] J. Livta and T. Know-Yeung Lo, “Digital Beamforming in Wireless Communications,” *Artech House, Norwood, MA*, 1996.
- [84] H. C. Andrews and T. S. Huang, “Two-dimensional transforms,” *Picture Processing and Digital Filtering, Springer-Verlag*, pp. 21–68, 1979.



# Acknowledgements

This thesis reports the scientific outcomes of a 3 years program, throughout which I had the chance of making a huge amount of experience, at all levels. I had the chance of working with extraordinary people, that have taught me more than a lot, on a professional as well as on a human level. I will always be ever so grateful.

Warm thanks are in particular for Prof. Giovanni Emanuele Corazza, on one hand for inspiring me towards research and scientific investigation, and more importantly for tutoring and educating me, not only scientifically, but on a human level as well, making a real difference in what I have become. It has been a joy to be a part of the Digicomm group, which is a true family to me.

All my gratitude and admiration are also for Prof. Alessandro Vanelli-Coralli, who has given me the example and shown me the way, sharing his experience and knowledge to teach me, building a professional and personal relationship based on respect, friendship and trust, which is a key feature of this group.

Many thanks to the colleagues that have shared day-by-day professional and personal experiences with me, and have played a significant role in making this journey a lot easier. In particular, thanks to Alberto, Lina, Giulio, Roberta, Sergio, Valentina and all the people in *our* open space.

Thanks to Alessandro and Stefano, my *associates* inside and outside the office, for countless *best moments* and for the feeling that, thanks to each other, we are really growing into better persons (although some might argue that some week-end mutual influences have not exactly been educational..).

Thanks to my brother Paolo, because just like universal constants, he does not seem to be really affected in its value by space and time (although I must confess, I never really tested him for compliance with relativity and string theories).

Thanks to Beatrice, my source of strength every single day, however close of far we are, whatever our mood, whatever the weather, whatever.. always. Thank you for bearing up with me (I'm told it's not that straightforward). I love you, but I kind of hope you already know at this point..

Thanks to my parents for always supporting and sustaining my ambitions, my hopes and my dreams, thank you.